Institute of Electrical Engineering
Slovak Academy of Sciences
841 04 Bratislava, Dúbravská cesta 9, Slovak Republic

Final Report

Superconducting Coils for AC currents Using YBCO Coated Conductors

Award No: FA8655-05-1-3062, Effective date: 30. September 2005
Item 0003

Bratislava, October 2006

REPORT DOCUMENTATION PAGE

Form Approved OMB No. 0704-0188

1. REPORT DATE *(DD-MM-YYYY)*	2. REPORT TYPE	3. DATES COVERED *(From – To)*
20-10-2006	Final Report	30 September 2005 - 02-Apr-07

4. TITLE AND SUBTITLE

Superconducting Coils for AC Currents using YBCO Coated Conductors

5a. CONTRACT NUMBER
FA8655-05-1-3062

5b. GRANT NUMBER

5c. PROGRAM ELEMENT NUMBER

6. AUTHOR(S)

Dr. Milan Polak

5d. PROJECT NUMBER

5d. TASK NUMBER

5e. WORK UNIT NUMBER

7. PERFORMING ORGANIZATION NAME(S) AND ADDRESS(ES)
Institute of Electrical Engineering
Dubravska 9
Bratislava 84104
Slovak Republic

8. PERFORMING ORGANIZATION REPORT NUMBER

N/A

9. SPONSORING/MONITORING AGENCY NAME(S) AND ADDRESS(ES)

EOARD
Unit 4515 BOX 14
APO AE 09421

10. SPONSOR/MONITOR'S ACRONYM(S)

11. SPONSOR/MONITOR'S REPORT NUMBER(S)
Grant 05-3062

12. DISTRIBUTION/AVAILABILITY STATEMENT

Approved for public release; distribution is unlimited.

13. SUPPLEMENTARY NOTES

14. ABSTRACT

This report results from a contract tasking Institute of Electrical Engineering as follows: The Grantee will investigate experimental studies of superconducting coils wound with the second generation of superconductors (II G), which have YBCO superconducting layer deposited on a metallic substrate. The behavior of coils carrying AC (alternating) currents with frequencies of the order of 100 Hz will be studied. Short sample experiments and those with test coils using AC tolerant (filamentary) conductor under development and experiments with saddle type winding will also be performed.

15. SUBJECT TERMS
EOARD, Aircraft Subsystem, Power, Superconductivity

16. SECURITY CLASSIFICATION OF:			17. LIMITATION OF ABSTRACT	18, NUMBER OF PAGES	19a. NAME OF RESPONSIBLE PERSON
a. REPORT	b. ABSTRACT	c. THIS PAGE			GEORGE W YORK, Lt Col, USAF
UNCLAS	UNCLAS	UNCLAS	UL	73	**19b. TELEPHONE NUMBER** *(Include area code)* +44 (0)1895 616163

Principal investigator: Milan Polák

This work was done in collaboration with:

Eduard Demenčík
Lubomil Janšák
Jozef Kvitkovič
Elemir Ušák
Pavol Ušák
Pavol Mozola

Technicians: Dagmar Erbenová
Jana Ryzá
Jozef Talapa

The research programme was proposed and realized in collaboration with Dr. P. Barnes and Dr. G. Levin, WPAFB.

Content

1 Introduction and goals

The project is focused on experimental studies of superconducting coils wound with the second generation of HTC superconductors (II G), which have YBCO superconducting layer deposited on a metallic substrate.

The work is concentrated on the electromagnetic behavior of coils carrying alternating (AC) current with frequencies of the order of 100 Hz. The coils, or material for coil winding, were be provided by Wright Patterson Air Force Base, Dayton, Ohio.

The experimental coil is wound with ~ 5 m of the tape (tape Super Power [1]). The tape was provided by the Wright Patterson Air Force Base (Dr. P. Barnes). New samples of filamentary YBCO were prepared by WPAFB. Following experiment were done:

- Additional tests of the coil 13_2m, publication of the results in APL
- Electromagnetic characterization of the tape Super Power including tests with tape strained by torsion
- Design of the coils wound with 5 meters of the tape Super Power
- Determination of the coil characteristics (I-V curve, critical current, inductance) at 77 K. Comparison with the theory.
- Measurements of AC losses in the new coil (Super Power Coil-SPC) as a function of frequency and current, determination of the coil inductance and its dependence on the current and frequency.
- Measurements of coil heating in AC regime

2 Electromagnetic characterization of the tape Super

2.1 I-V curves with DC current at 77 K in external magnetic fields

The E-I curves measured in magnetic field perpendicular to the tape plane on a short sample at 77 K are shown in Figure 1

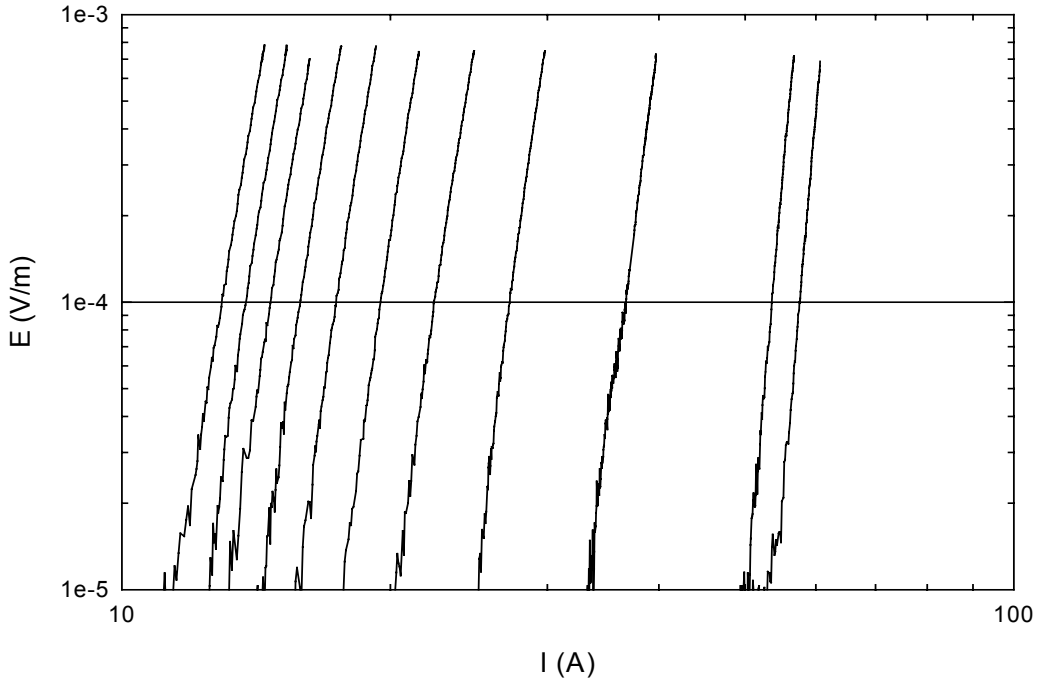

Figure 1.: E-I curves of the short sample, tape Super Power at 77 K: Magnetic fields from the right to the left: (mT) 0, 9.297, 27.9, 46.5, 65.1, 83.7, 102.3, 120.9, 139.5, 158.1, 176.6

From these curves we determined I_c vs. B dependence for two criteria of I_c (Figure 2.) and n-factor vs. magnetic field (see Figure 3).
The observed drop off at lower magnetic fields is quite surprising, but it is proved by magnetic measurements, as it can be seen later in Figure 15. The width of the hysteresis loop decreases visibly at even small external field, too.

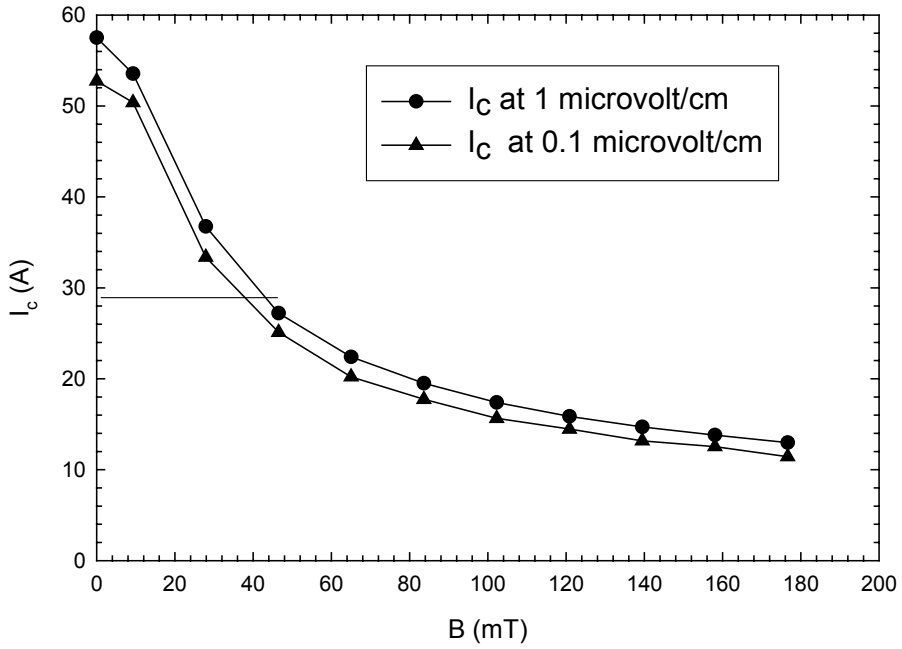

Figure 2.: I_c(B) for short sample Super Power determined at 0.1 μV/cm and 1μV/cm

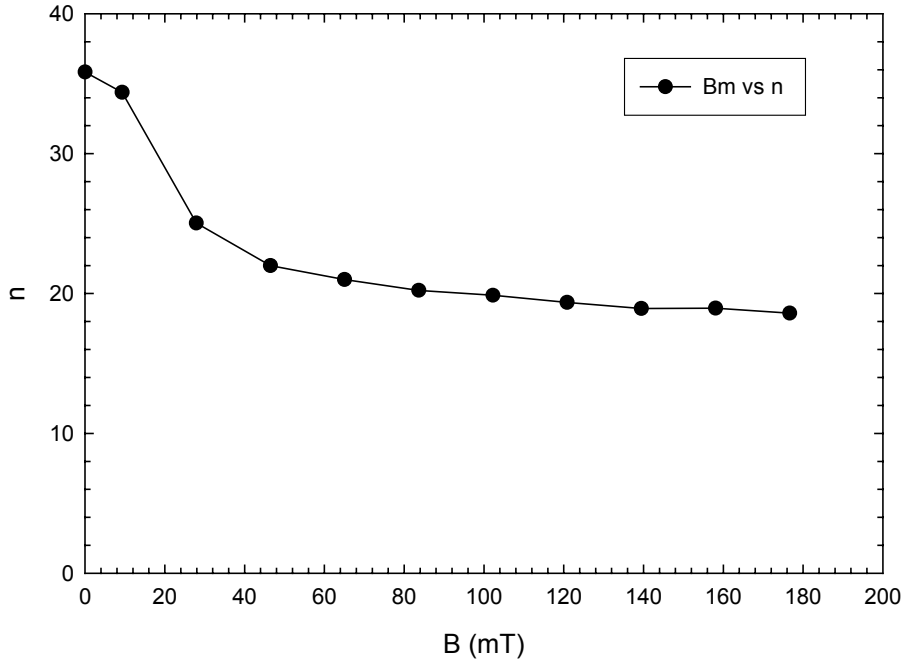

Figure 3.: n-factor vs.B for a short sample Super Power determined at 77 K

2.2 I-V curves of the tape exposed to torsion strain

The aim of this test is to get information on the uniformity of tape damage due to torsion at 77 K and to determine the torsion causing a reduction of the critical current by more than 5 % of its original value.

For the torsion tests we prepared a simple device shown in Figure 4. The length of the measured tape is about 100 mm.

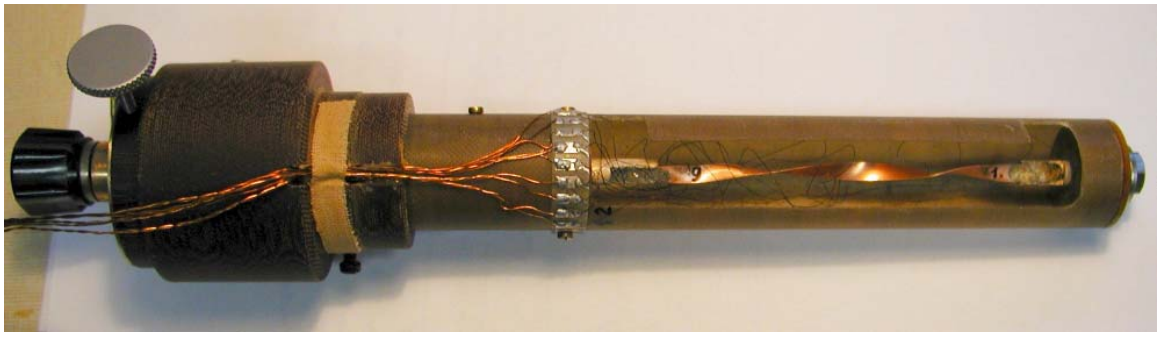

Figure 4.: The device for the measurements of I-V curves with sample twisted around its axis (torsion). The tape was twisted by up to 420 degrees

The original position of the sample with potential taps attached to the sample by soldering is shown in Figure 5.

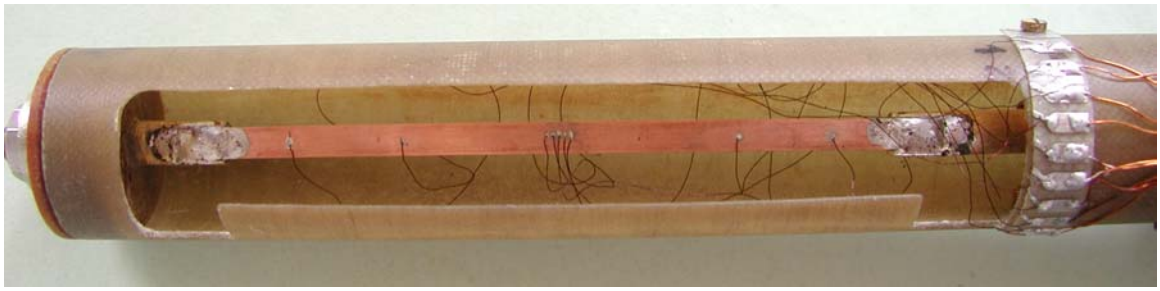

Figure 5.: The sample (tape) with the potential taps in the original, not twisted position

Results

The I-V curves measured between taps 1 and 9 distanced by ~ 70 mm vs. torsion angle are shown in Figure 6.

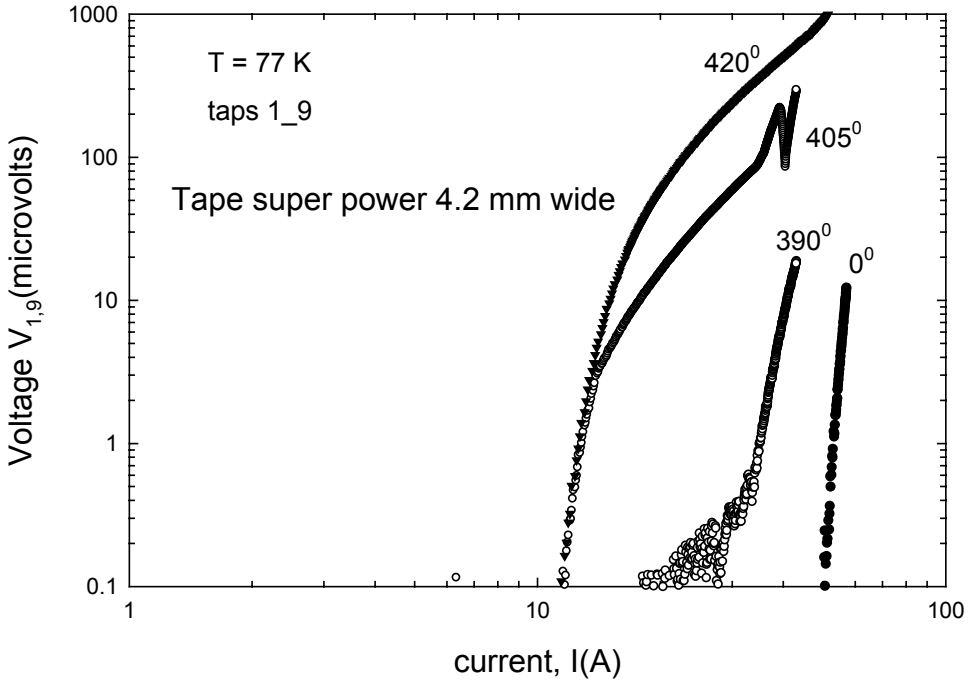

Figure 6.: I-V curves measured between taps 1 and 9 vs. current for torsion angles 0, 390^0, 405^0 and 420^0 (the curves for angles below 390^0 are not shown)

The dependence of the critical current vs. torsion angle is shown in Figure 7.

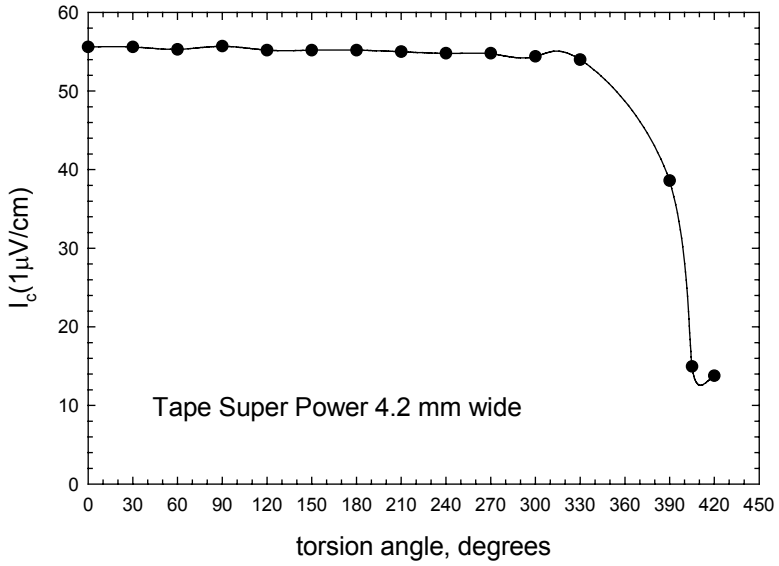

Figure 7.: I_c at 1 μV/cm vs. torsion angle at 77K

As we see in Figure 7, the degradation of I_c starts at torsion angles above 330 degrees.

Using several potential taps we localized the section in which the tape is degraded. It is very interesting to note that the degradation is not uniform along the tape, but it is strongly localized. We have found the tape section in which the tape is damaged and used the Hall Probe mapping to see the defect shape and its position more exactly. The result is seen in Figure 8. The defect seems to have a shape of a crack inclined with respect to the tape axis.

The piece was sent to Dr. P. Barnes for structural analysis.

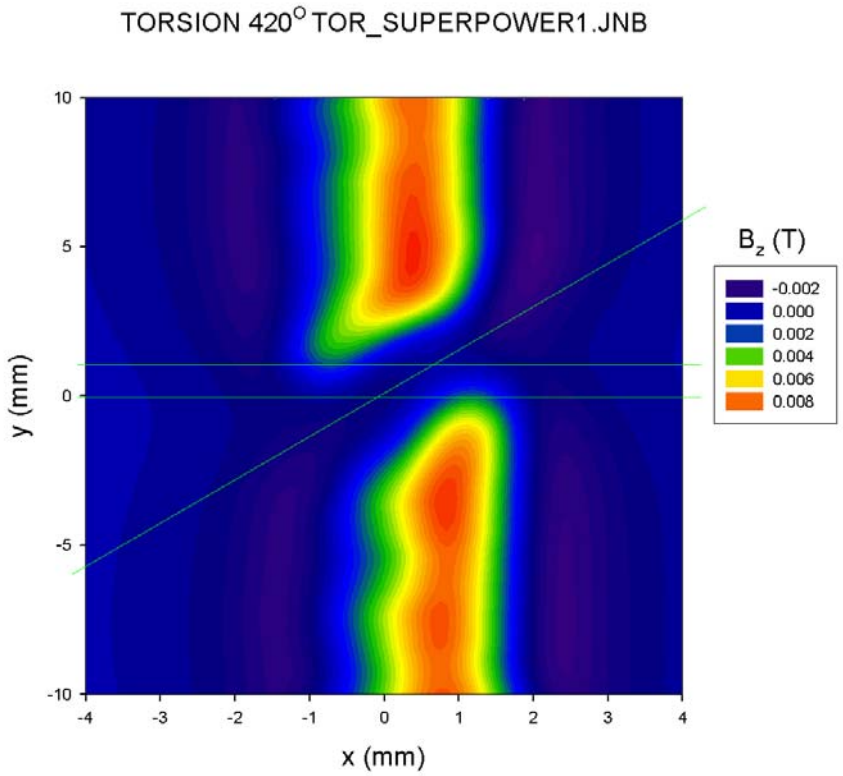

Figure 8.: The magnetic field map due to magnetization currents, showing the position of the defect created by torsion damage

2.3 AC losses due to transport current without external field

We have measured the frequency dependence of the transport current loss of YBCO tape (Super Power) at 77 K and also the temperature dependence of the transport current loss at lower temperatures.

Dimensions of the sample :	Length	7 cm
	Width	4 mm
	Thickness	0.15 mm

The sample was covered from both sides by electrolytically deposited Cu layer with thickness about 20 μm. The measured critical current of the measured tape was 58 A.

The sample tape was supplied using 200 A AC power source.

The loss measurement was done using the standard technique using lock-in amplifier. Distance of the voltage taps was 4 cm.

Frequency dependence of transport current loss measured at temperature 77.3 K.

The frequencies used in experiments were 23 Hz, 43 Hz, 57 Hz, 103 Hz, 203 Hz, 503 Hz and 703 Hz. The results are shown in Figure 9.

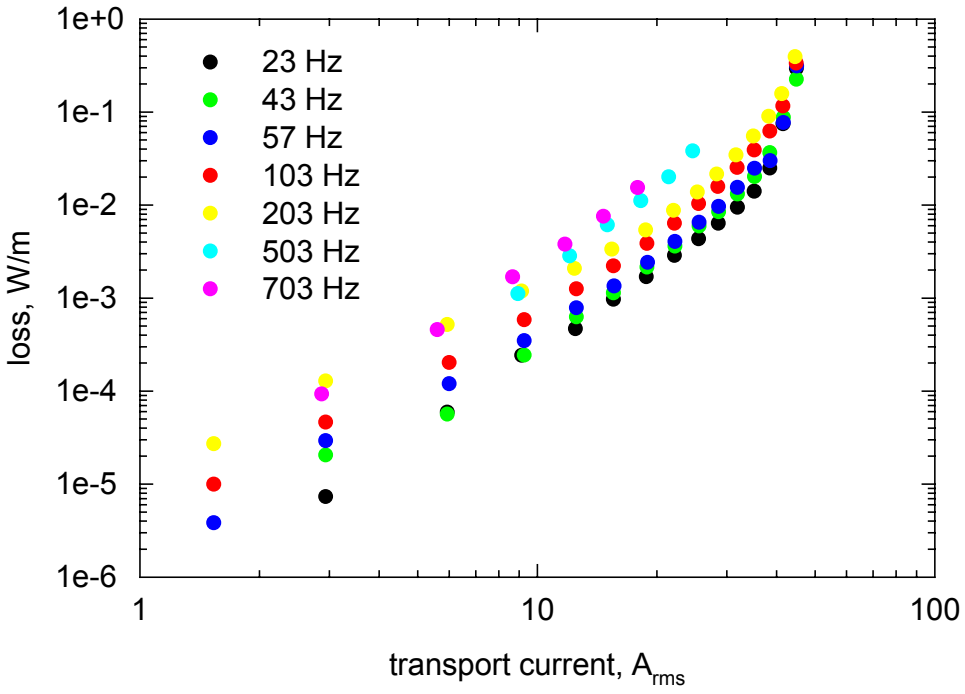

Figure 9.: Frequency dependence of transport current loss – YBCO Super Power, W/m

The loss per cycle vs. transport current curves are shown in Figure 10. It is interesting to note that the loss per cycle at a given value of the transport current decreases with increasing frequency.

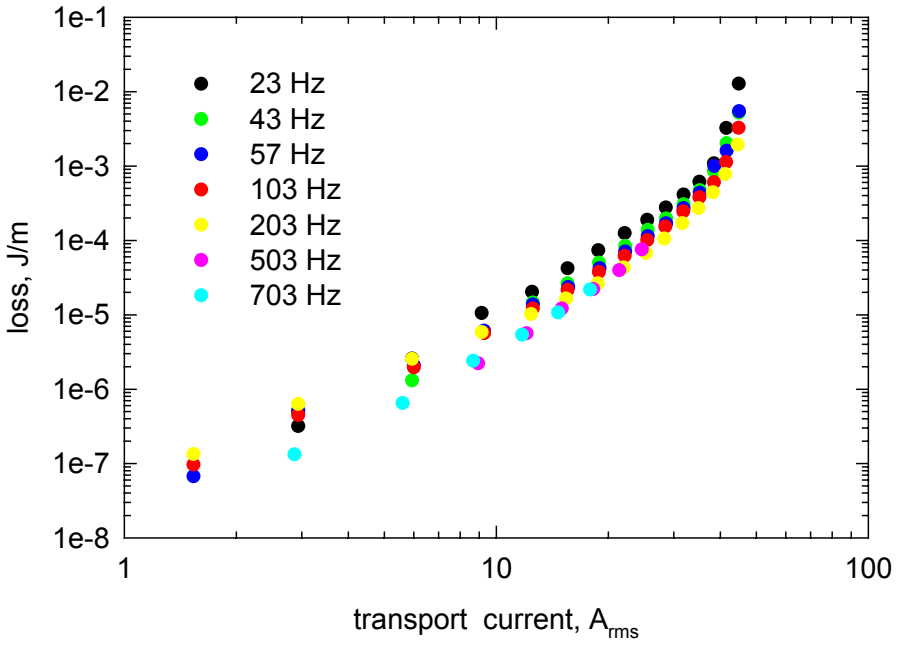

Figure 10.: Frequency dependence of transport current loss per cycle at 77.3 K– YBCO Super Power, J/m

We have measured also transport current loss by YBCO tape covered from both sizes by thin glass fiber tissue, glued to the tape by Epoxy ChS 2000.

The result of the measurements were practically identical. This result indicates that the tape heating is probably not affecting the tape temperature.

We also compared the measurement loss with Norris model, see Figure 11.

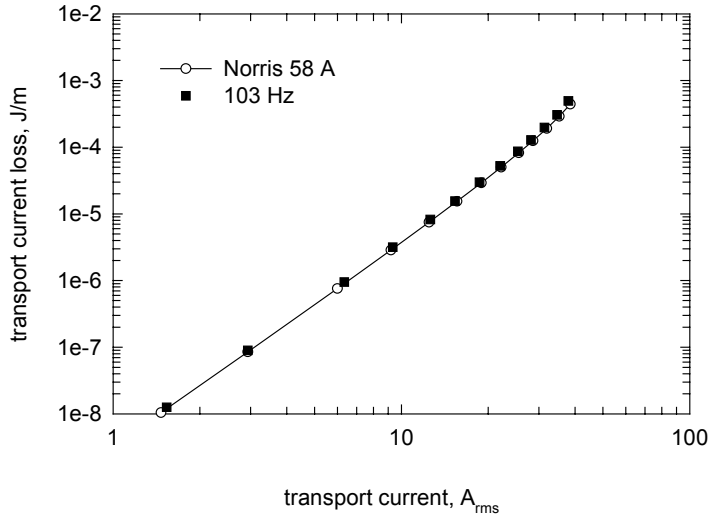

Figure 11.: The comparison of the measured transport current loss with Norris model

Temperature dependence of transport current loss.

The temperature dependence of transport current loss was measured in plastic cryostat. The temperature was reduced by pumping the nitrogen gas.

The real temperature of the liquid nitrogen bath was measured by calibrated Pt thermometer (excitation current 0.1 mA). The results are in Figure 12.

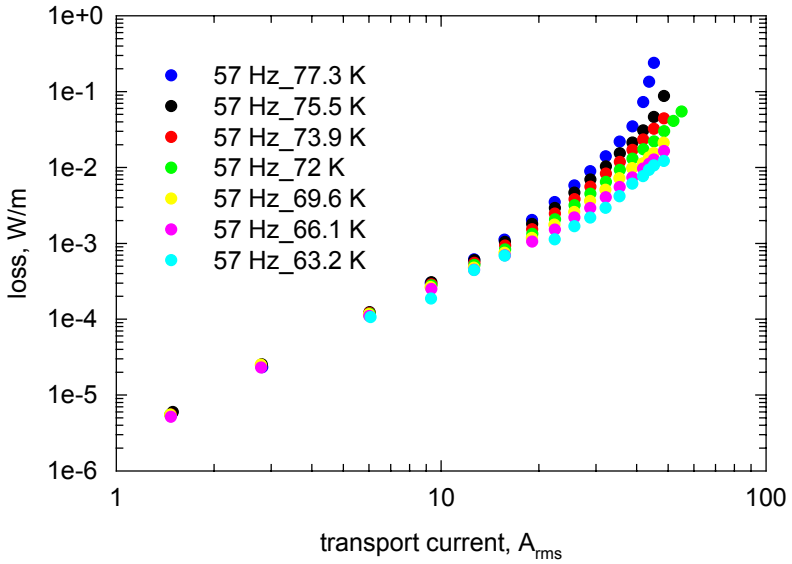

Figure 12.: The temperature dependence of transport current loss, 57 Hz, W/m

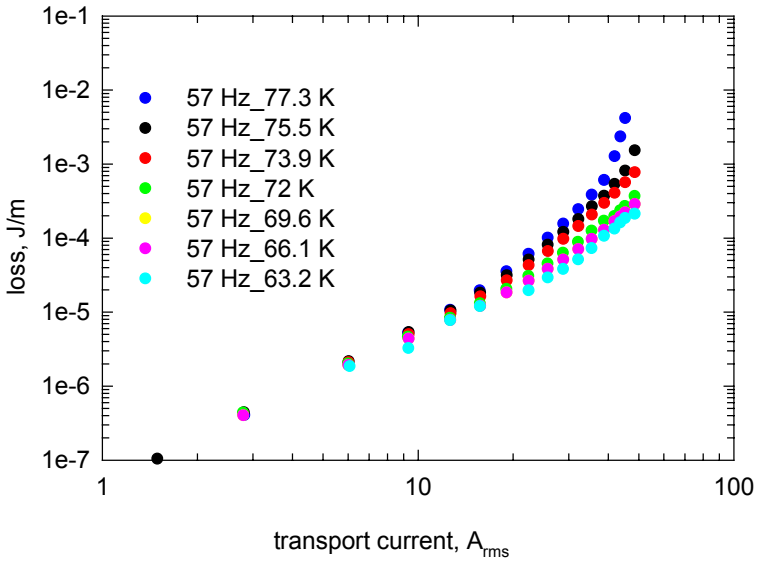

Figure 13.: Temperature dependence of transport current loss, 57 Hz, J/m

As expected, the lowering of temperature T causes a reduction of losses measured at the same transport current, as the critical current increases with decreasing temperature. This tendency is also illustrated in Figure 14.

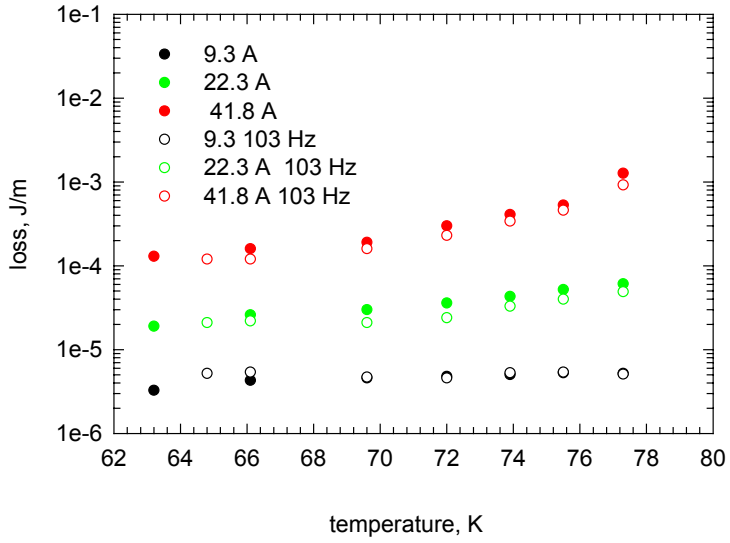

Figure 14.: Temperature dependence of the transport current loss for different transport currents (9.3 A, 22.3 A and 41.8 A) and two frequencies (57 Hz and 103 Hz)

At low transport current the temperature dependence of transport current loss is practically constant, for higher current (42 A) and lower temperature the loss is smaller.

Concluding we can say that the reduction of the operating temperature which can be reached by simple pumping the nitrogen gas can considerably reduced the transport current losses at a given operating current.

2.4 AC losses in external magnetic field without transport current

We measured the loss per cycle at low frequency (100 mHz) in the magnetic field perpendicular to the tape plane using the Hall probe method described in [2]. The hysteresis loops B_{sz} vs. external field B are shown in Figure 15. The losses determined from the hysteresis loops at 77 K are shown in Figure 16.

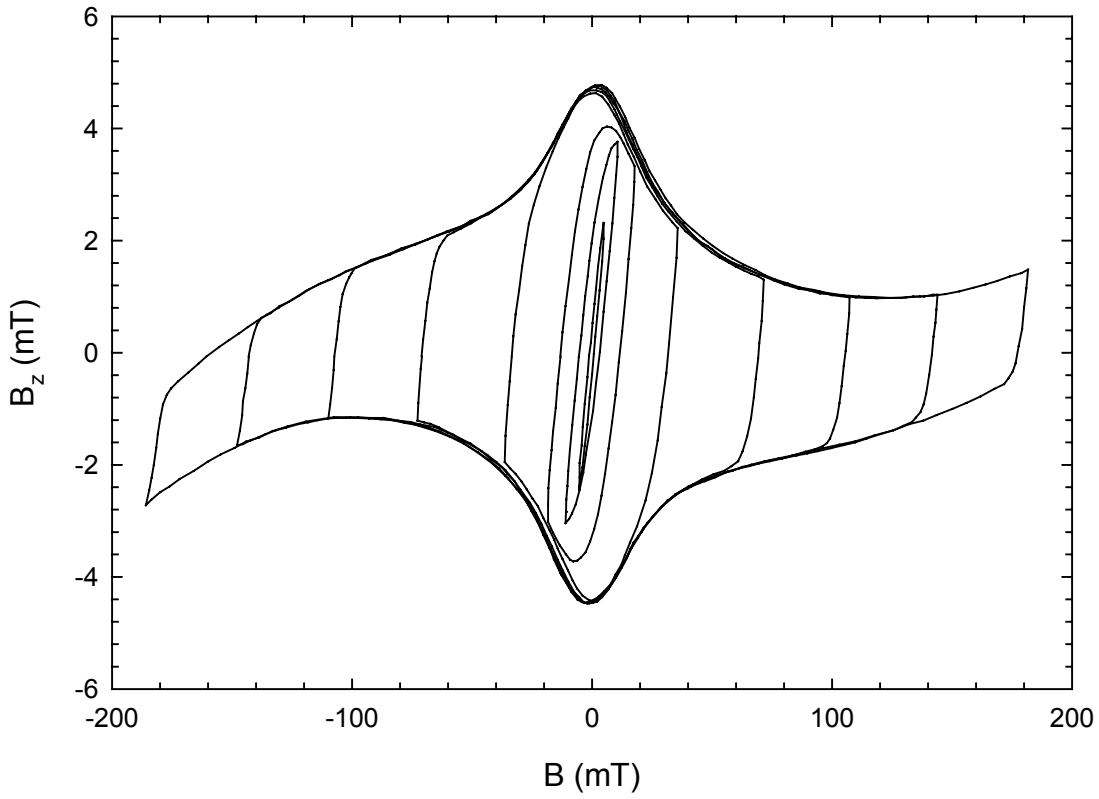

Figure 15.: The magnetic field in the vicinity of the sample, B_{sz}, as a function of the external field measured at f = 50 mHz

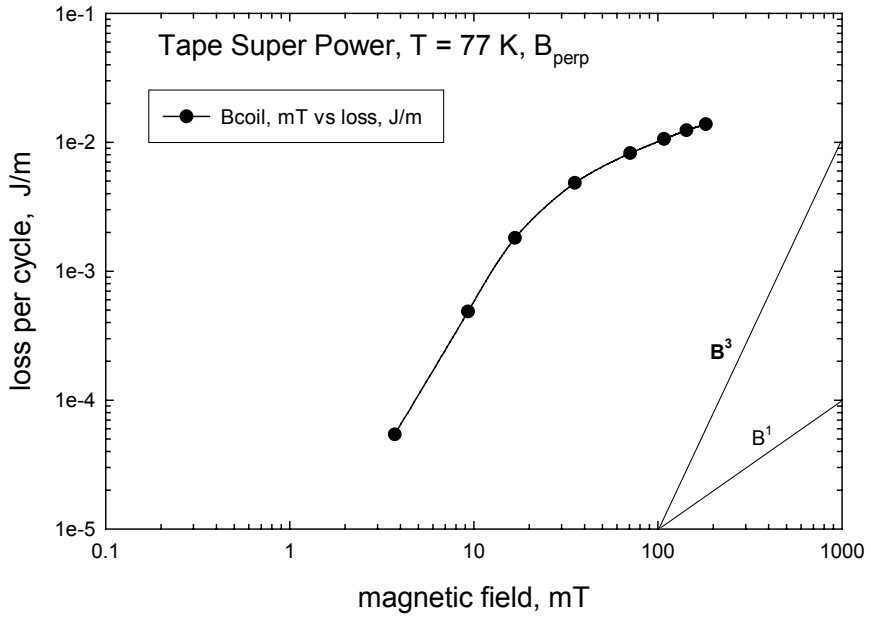

Figure 16.: The loss per cycle of the tape Super Power

In low fields the losses are proportional to B^3 and in fields close to 0.1 T the losses are proportional to B, as predicted by theories.

Supposing that the effect of frequency on AC losses in YBCO layers is small we plotted the loss in W/m at frequencies 100 Hz and 500 Hz (see Figure 17).

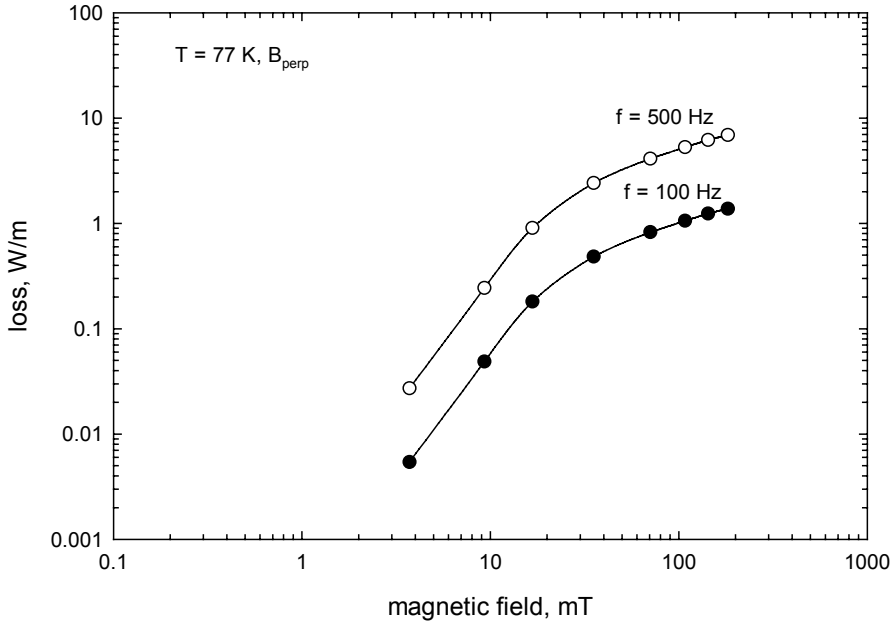

Figure 17.: Loss vs. B for tape Super power at 100 Hz and 500 Hz

As seen in the previous graphs, the AC losses of the non-striated tape Super Power are unacceptably large.

3 Study of the current distribution in tape Super Power

The Hall probe magnetometry was applied to self-field of the YBCO superconducting tape with gradually increasing transport current. After reaching the maximum at the vicinity of full critical current, the gradual decrease of transport current ending with zero value followed. The mapped data of magnetic field component B_z perpendicular to tape plane were used in inverse calculation of the lateral current distribution across the width of the tape (x direction). The concept of longitudinal invariance of current distribution present in the calculation was preserved at least on local scale (several millimeters wide band in longitudinal y direction).

Comparison of magnetic self field data and corresponding calculated current distributions for transport current 30A during the increase and decrease illustrates the sensitivity of the field profile to the transport current distribution. The results are shown in Figure 18, and Figure 19.

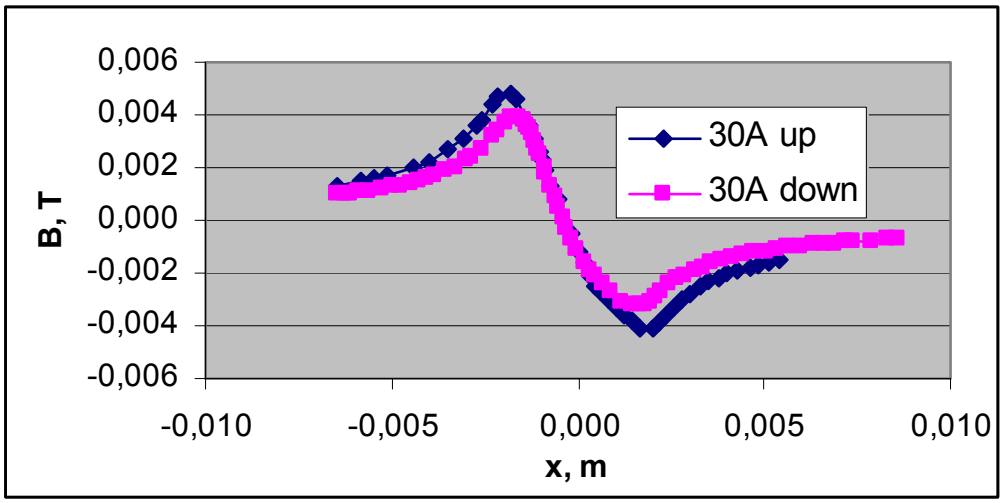

Figure 18.: Field profiles measured in the vicinity of the sample carrying the current of 30 A

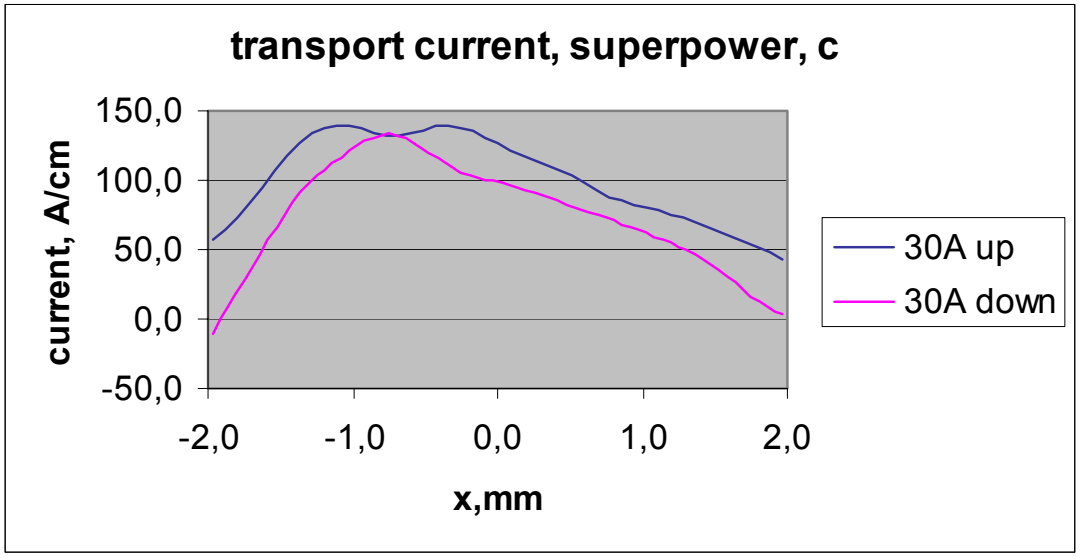

Figure 19.: The sheet current distribution across the tape Super Power

The change of lateral current distribution during gradual increase of the transport current is in Figure 20. Analogical picture of the current distribution during gradual transport current decrease is on Figure 21.

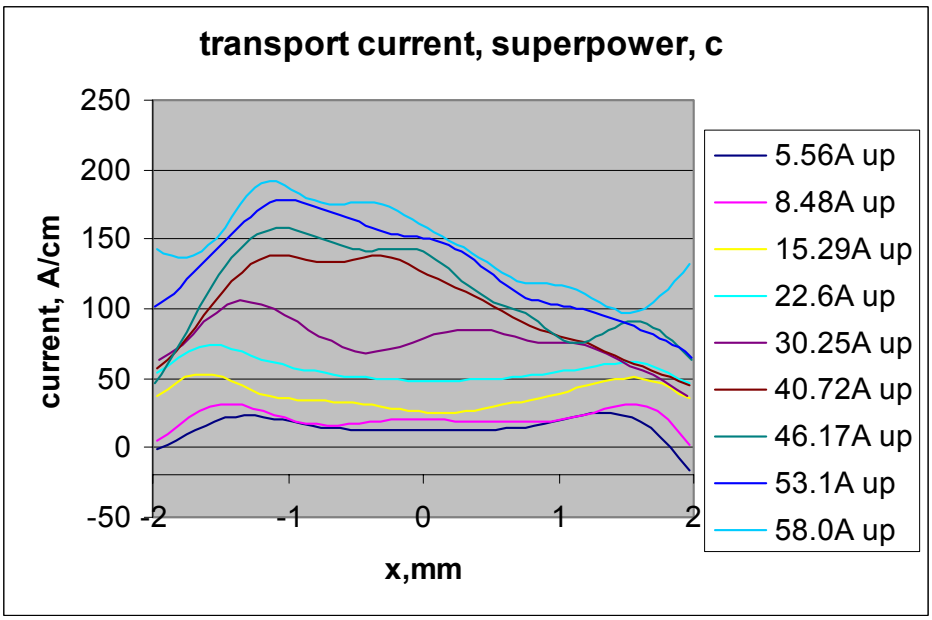

Figure 20.: The sheet current distribution at various currents increased stepwise

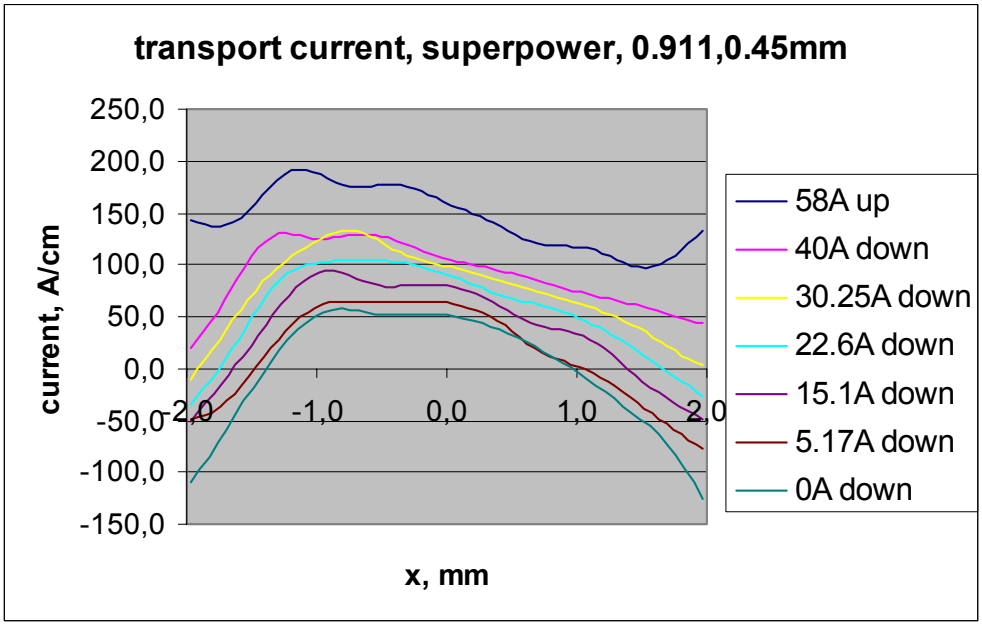

Figure 21.: The sheet current distribution at various currents decreased stepwise

In summary, the study showed that the distribution of the sheet current in tape Super Power in not completely uniform.

Also measurement of magnetic field due to persistent magnetization currents, which are not presented here, showed that the profile of the magnetic field across the tape is not completely symmetrical, which also indicates a non-perfect current distribution.

4 Design of the coils wound with 4 meters of the tape SuperPower

We designed a double pancake coil with resistive joints between the pancakes.

It was epoxy impregnated during the winding. The cross section of the coil is shown in Figure 22.

The coil formers 1A and 1B (material G10) support the winding of pancakes A and B.

The pancakes are separated by 1.2 mm thick separating disk. The flanges (4) were used during the winding only, after finishing the winding they were be removed.

The photograph of the coil former with the removable flanges is shown in Figure 23.

As insulation we use about 0.06 mm thick paper. For soldering of the current contacts and potential taps pure indium solder was used.

To test the behavior of the coil we used potential taps, thermocouples and heaters, which allow to measure the coil heating due to AC losses, I-V curves of the whole coil and also I-V curves of turns exposed to various radial magnetic fields. The sketch of the location of potential taps, sensors and heaters are shown in Figure 24.

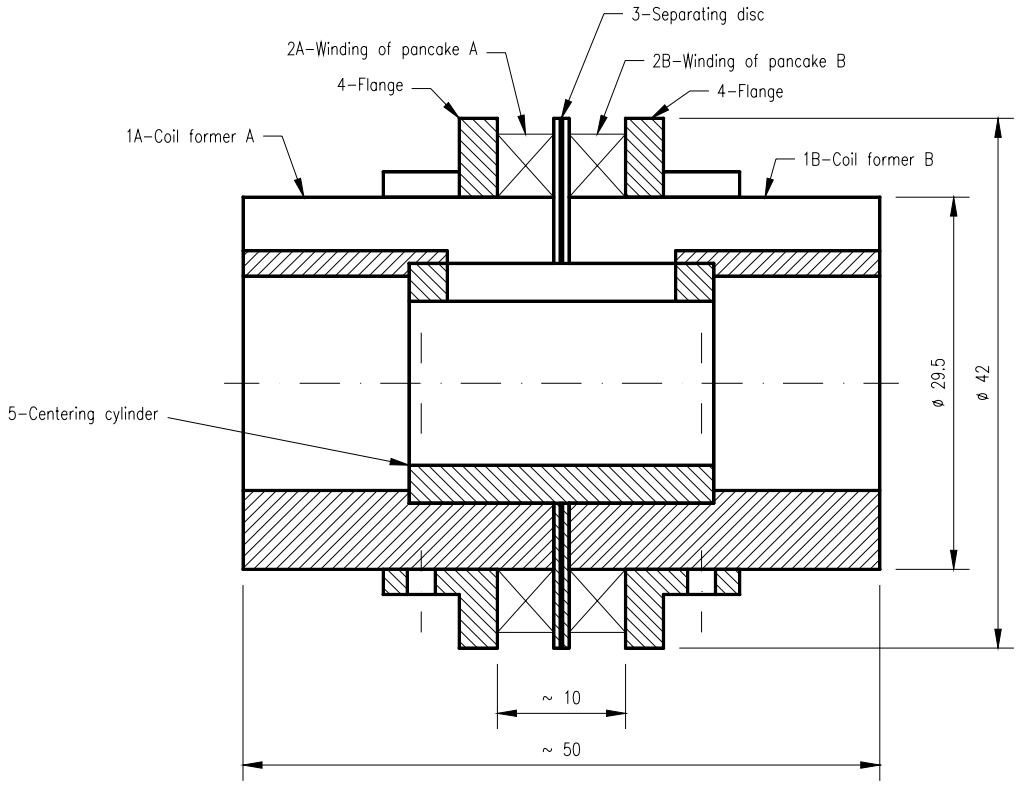

Figure 22.: Cross-section of the YBCO double pancake coil

Figure 23.: Photograph of the coil former with flanges and separating disk

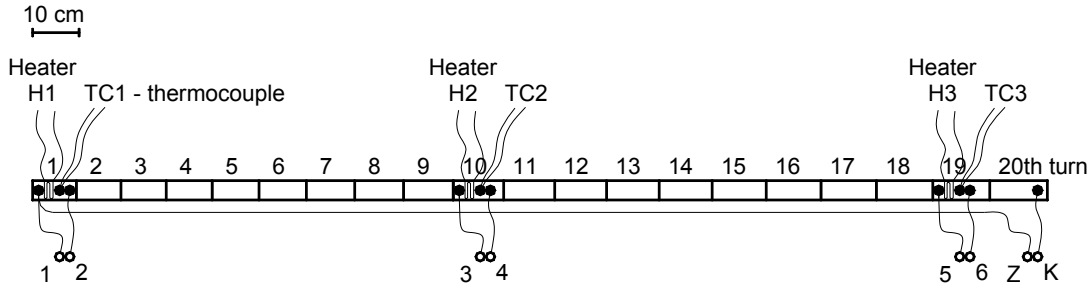

Figure 24.: Location of potential taps, sensors and heaters in the coil winding

A photograph of one heater installed in the coil is shown in Figure 25. The heater is made from a thin constantan wire.

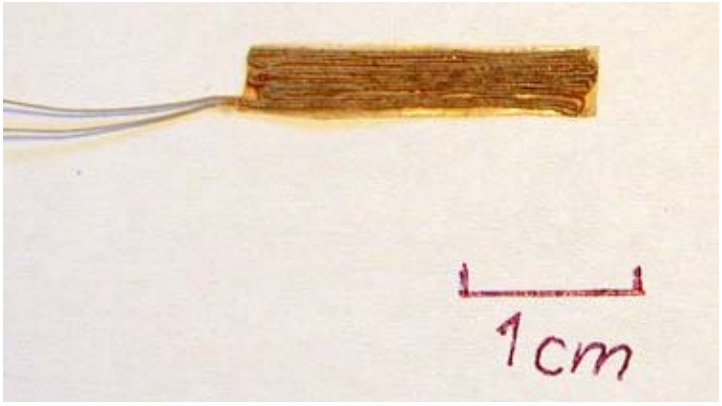

Figure 25.: A heater wound with Constantan wire

5 I-V curves of the coil heating in DC regime

Current-voltage curves of the pancake coil A measured with low frequency current at 77 K is shown in Figure 26. The coil critical current at 1μV/cm is ~ 29 A at 77 K.

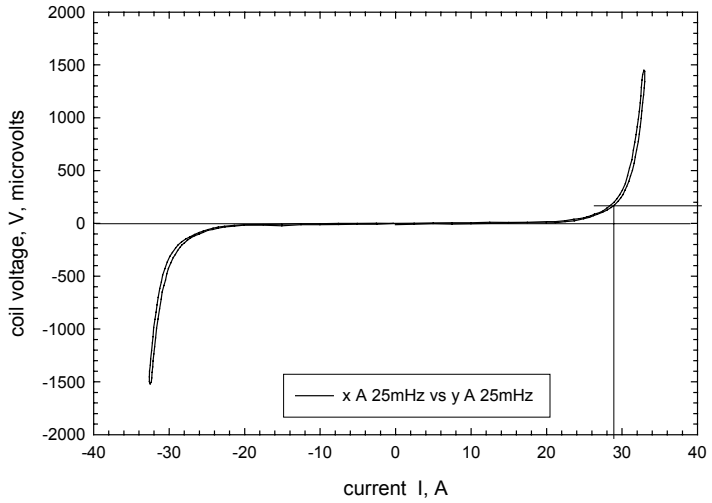

Figure 26.: I-V curves of the pancake coil A measured at 25 mHz and 77 K

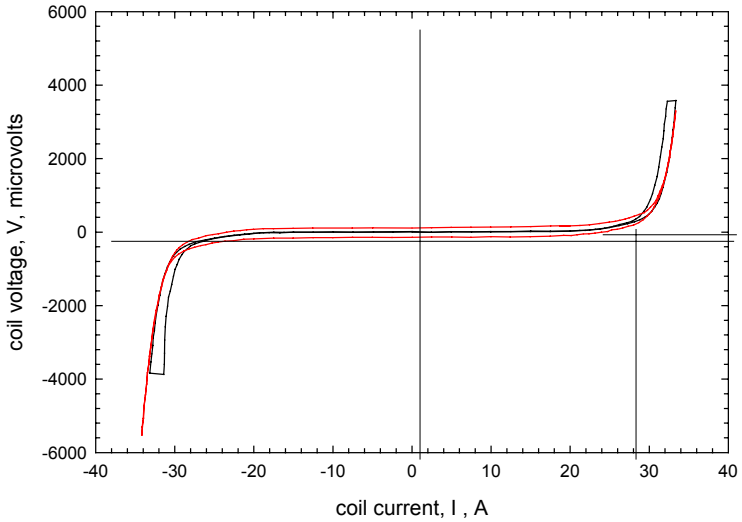

Figure 27.: I-V curves of pancake B

The I-V curves measured on the whole coil (pancakes A and B in series) are shown in Figure 28.

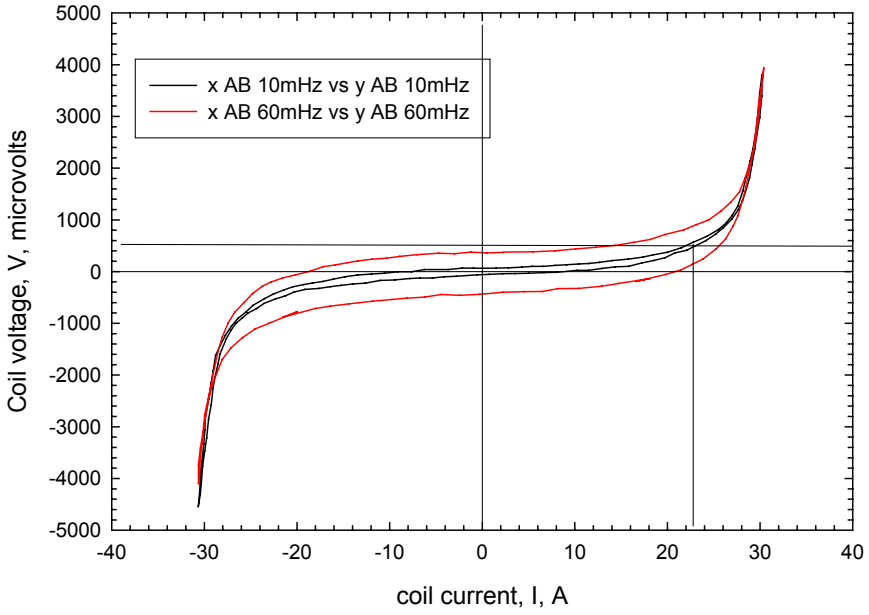

Figure 28.: I-V curves of the whole coil (A+B) measured at 2 frequencies. The critical current in this configuration at the mean electric field of 1μV/cm (V~400 μV) is about 23 A. This is by 6 A smaller current then that of the pancakes measured separately. It is the result of the increase of the radial field component

In Figure 29 we plotted $I_c(B)$ curves of the short sample of the tape Super power together with load line of the complete coil (pancakes A and B in series). The load line represents the dependence of the radial component B_r measured at the coil edge on radius r at which its value is maximal. The cross point between this line and $I_c(B)$ characteristics yields current I = 25.5 A. This is a value very close to the critical current of the coil, which is 23 A.

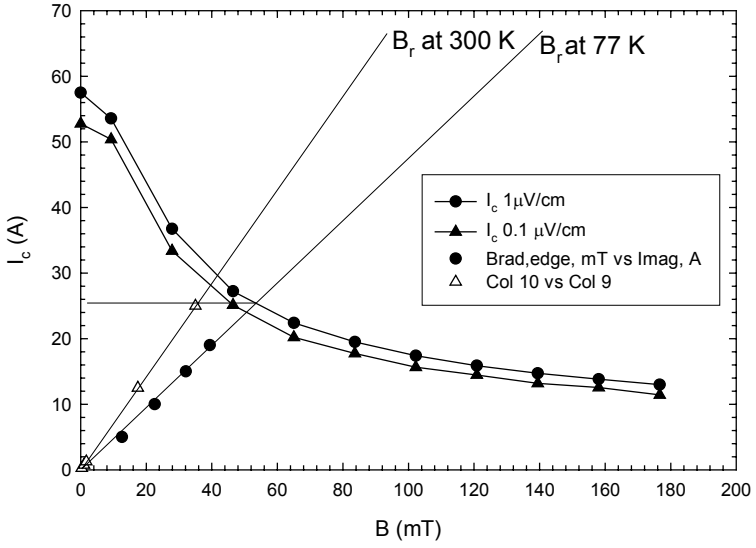

Figure 29.: The load line of the complete coil at 300K and 77 K

Coil heating

Using the thermometer T/2 in the pancake A we measured the heating in this pancake supplied separately by DC current. The time dependence of the temperature measured by T/2 is shown in Figure 30. As seen, the heating at the maximal current 33.15 A is quite small in spite of the fact that the coil critical current is about 29 A. However, we note that the tape critical current was not ideally uniform and probably T/2 is not located in the point where the heating is maximal.

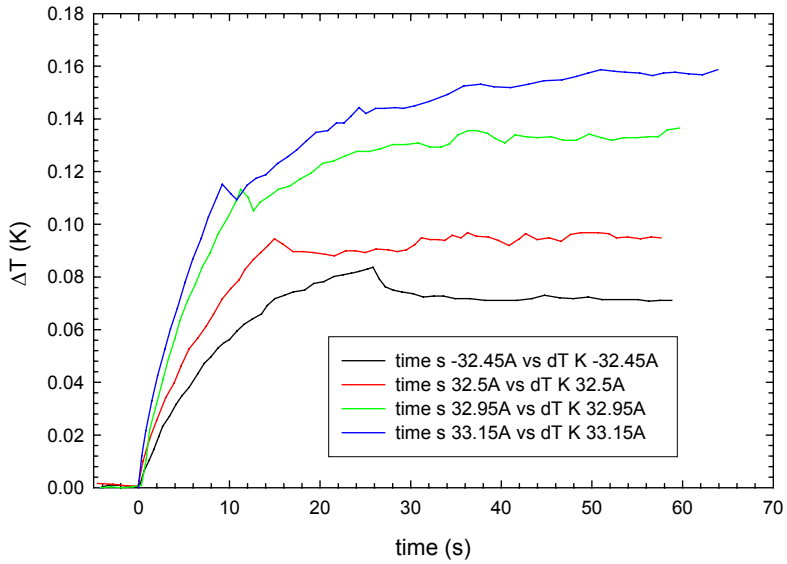

Figure 30.: The time dependence of the coil temperature measured by T/2. The pancake A was supplied separately

6 Measurement of the thermal runaway current for pancake A

The thermal runaway current, I_{trc}, characterizes the behavior of a coil made from HTC superconducting tapes better than the critical current I_c , determined using the mean value of the electric field $E = V_{coil}/L_{tape} = 1\ \mu V/cm$ along the whole tape length L_{tape} used in the winding.

For Bi-2223/Ag coil I_{trc} is usually larger than I [1]. We can expect that for YBCO coils the value of I_{trc} will be above I_c, but the difference could be smaller because of smaller amount of normal metal.

The measurement procedure was the same as that in [1]. We set certain coil current and recorded the coil voltage as function of time.

The results for the pancake A are shown in Figure 31.

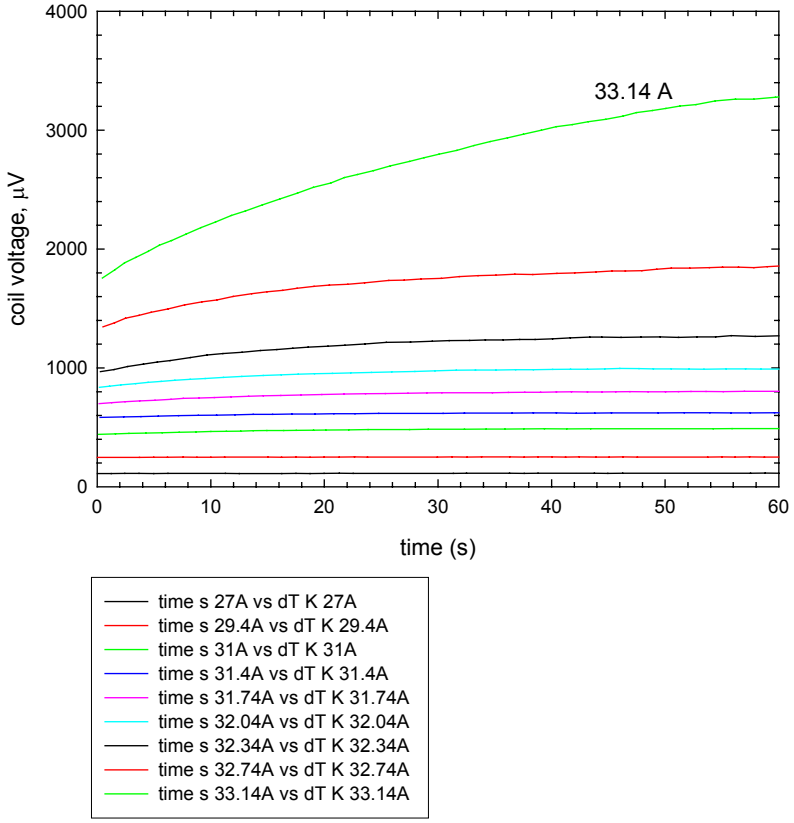

Figure 31.: The time dependence of the voltage across the pancake A measured at various constant coil currents

7 AC losses of the coil

7.1 pancake coil A

The AC losses measured in pancake A at 3 frequencies, 54 Hz, 432 Hz and 864 Hz are shown in Figure 32. As see, the losses are proportional to I^3 at medium currents. At low currents (below 5A) we observed a deviation from this dependence. We believe this is the consequence of the non-uniformity of the tape properties. The loss per cycle increases slowly with increasing frequency (from 0.227 mJ/cycle at 54 Hz to 0.232 mJ/cycle at 864 Hz and 10 A_{rms})

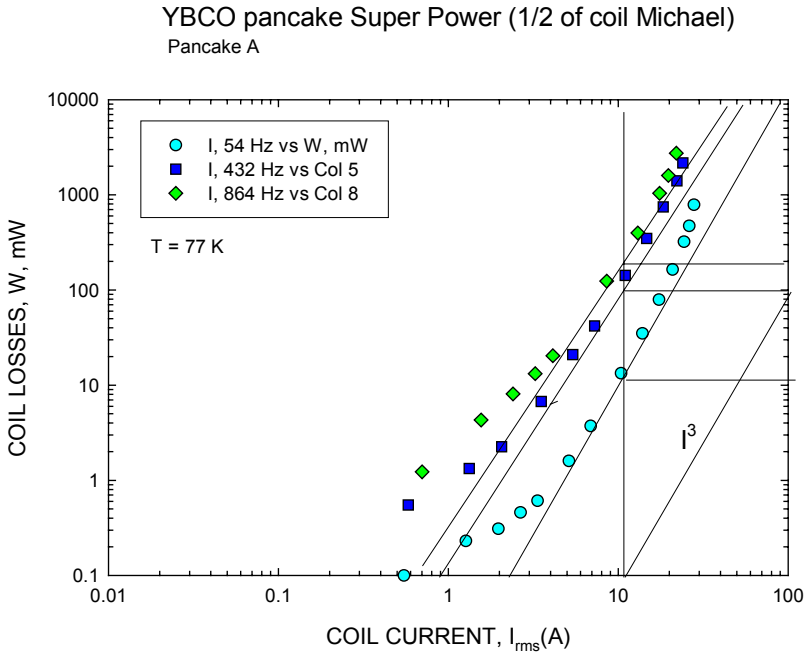

Losses per cycle at 10A (rms value)

54 Hz: 12.3 mW/54 = 0.227 mJ/cycle
432 Hz: 100 mW/432 = 0.230 mJ/cycle
864 Hz: 200 mW/864 = 0.232 mL/cycle

Figure 32.: The measured AC losses of the pancake A (not connected with B) at 3 different frequencies

7.2 Pancake coil B

This pancake had a short circuit between 2 turns, which we detected and localized. After we removed it, the losses were practically the same as those of pancake A. The measured losses are shown in Figure 33.

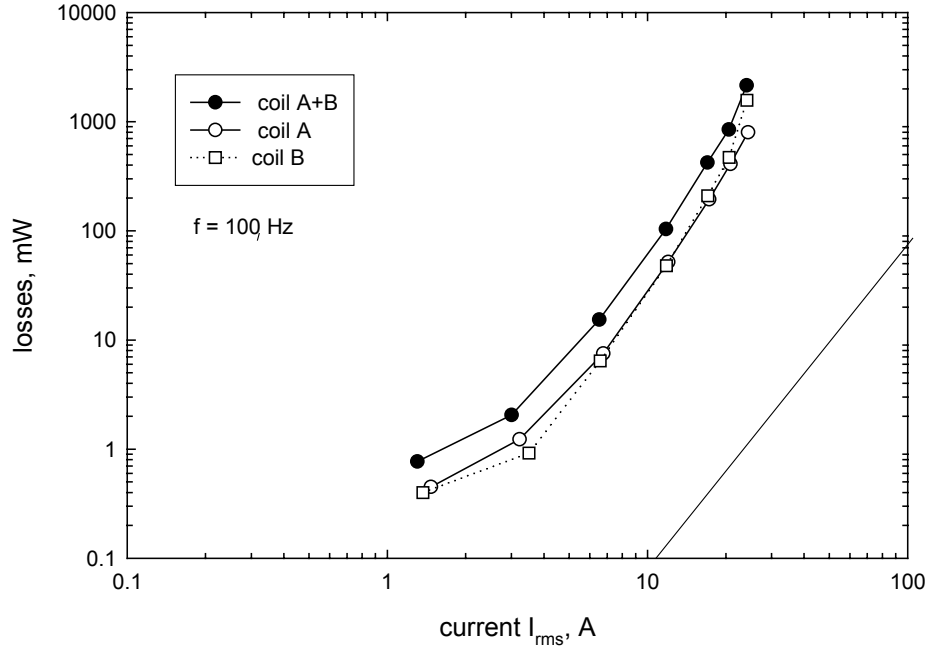

Figure 33.: Losses in pancake B and A separately and A+B in series, f = 100 Hz

7.3 Complete coil A + B in series

The losses measured in the complete coil (pancakes A and B in series) are shown in Figure 34.

The loss per cycle in the complete coil at I = 10 A and f = 54 Hz and 432 Hz is 20 mW/54 Hz = 0.3705 mJ/cycle and 200 mW/432 = 0.463 mJ/cycle. These values are approximately the double of the losses of one pancake (A).

At the current I_{rms} = 16.2 A, which corresponds to the critical current of the whole coil, 23 A, the losses per cycle are:

f = 54 Hz	coil loss	130 mW	loss/cycle	2.4 mJ
f = 108 Hz		270 mW		2.50 mJ
f = 216 Hz		500 mW		2.31 mJ
f = 432 Hz		900 mW		2.08 mJ

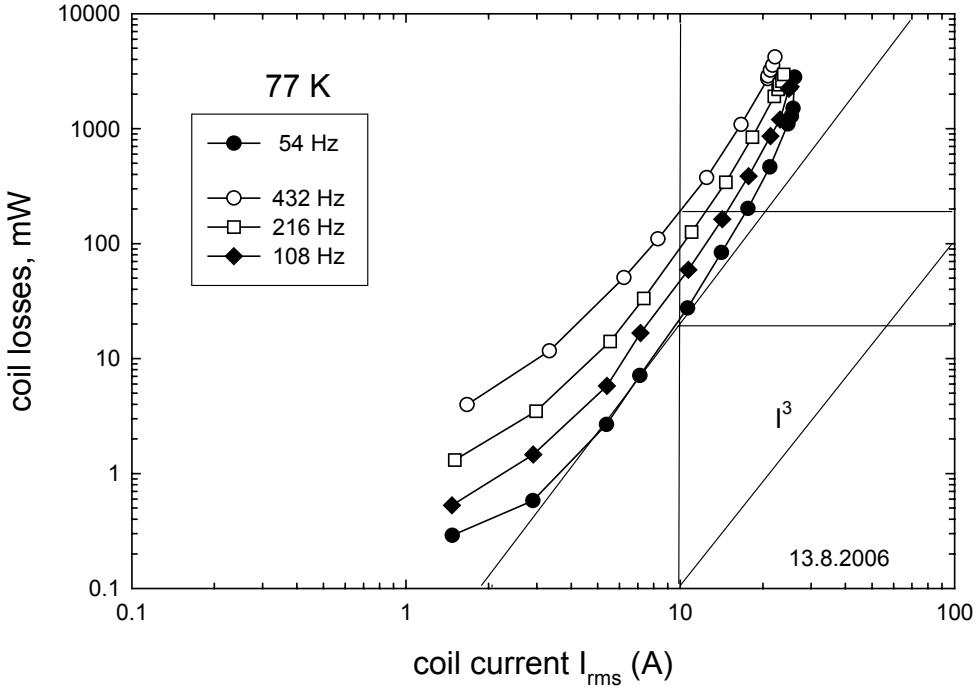

Figure 34.: The losses in the complete coil (A+B)

8 Radial components of magnetic field in the vicinity of the coil

8.1 Measuring devices

As generally accepted, the loss and critical current behavior of anisotropic tapes like Bi-2223 and YBCO is controlled by the magnetic field component perpendicular to the tape plane. In the frame of our project we carefully studied the behavior of the radial field component which is perpendicular to the YBCO tape in the winding, as well as the field component parallel to the tape plane (B_z).

For the measurements of $B_r(z)$ and $B_z(z)$ we developed a special sensor formed by two Hall probes fixed to the sensor holder (see Figure 35). For the measurements of $B_r = f(r)$ we used another measuring set-up which is shown in Figure 36.

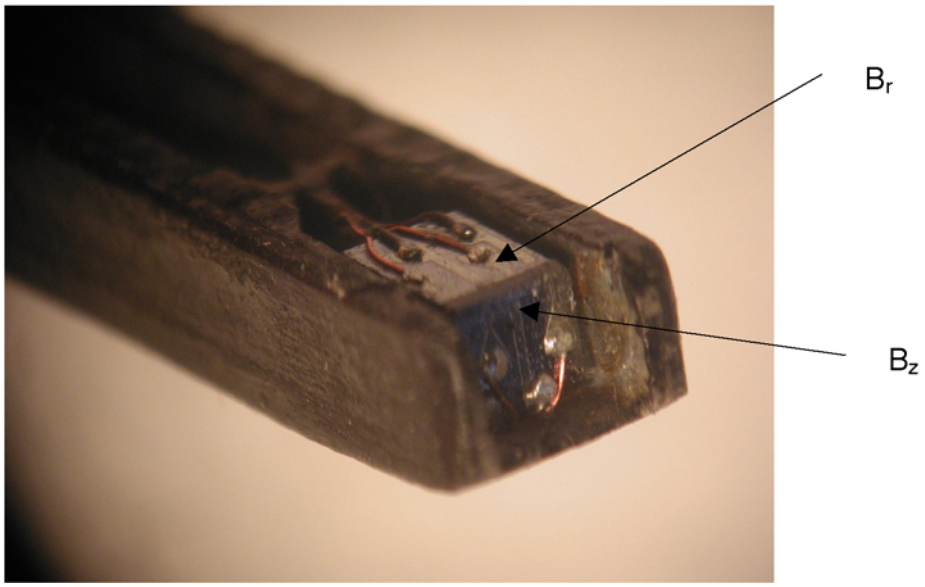

Figure 35.: Holder of two Hall probes measuring 2 field components as a function of z

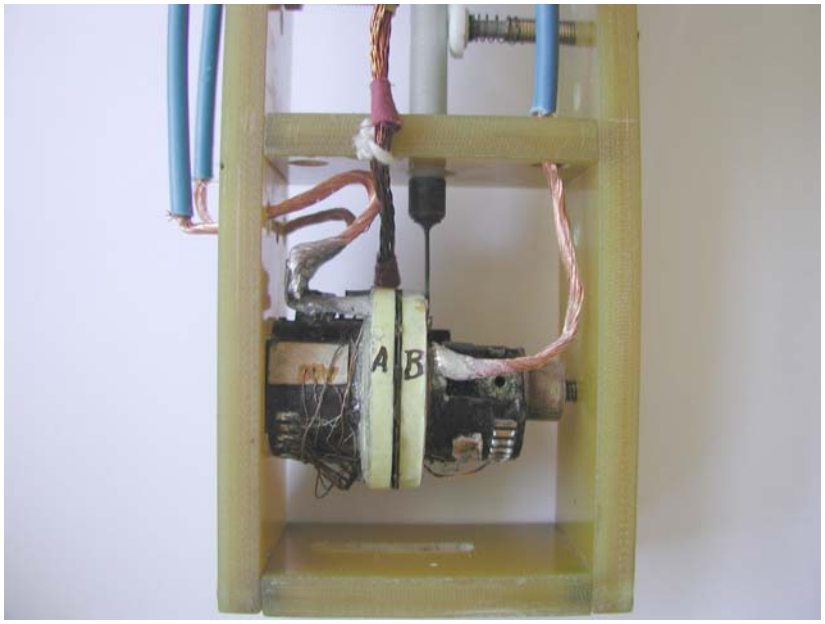

Figure 36.: The measuring set-up used to measure the radial field component at the edge of a coil or in the gap between the coils

8.2 Pancake coil A measured individually

At first, we measured the radial field components close to the inner winding diameter, B_r(r= 14 mm) = f(z) and B_r(r=0) = f(r) at room temperature. In this case the current density is uniformly distributed across the tape. The results are shown in Figure 37.

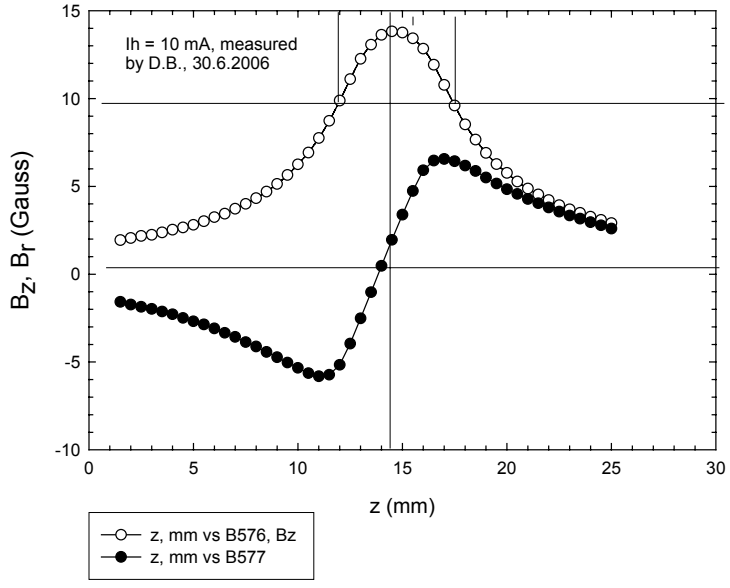

Figure 37.: The components B_z and B_r measured vs. the coordinate z at room temperature

The longitudinal field component of the pancake A measured individually, B_z, as a function of z for various currents increased stepwise is shown in Figure 38.

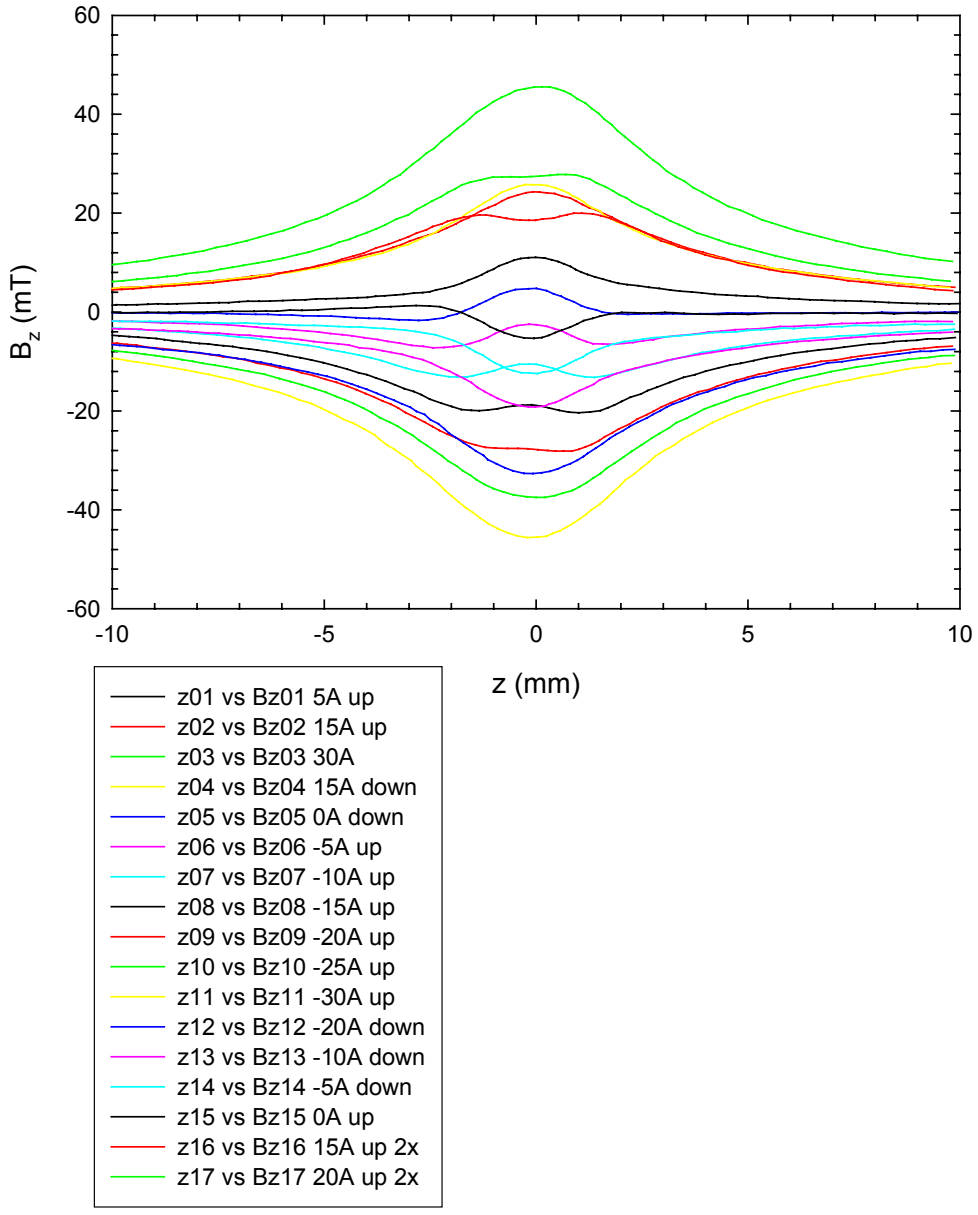

Figure 38.: The measured curves of $B_z = f(z)$, pancake A, 77 K. The current increased from 0 to 30 A, then it decreased to zero, and after reversal it increased to –30 A and decreased to 0

The results of the measurements of the radial field components on pancake A for increasing and decreasing current are shown in Figure 39, Figure 40.

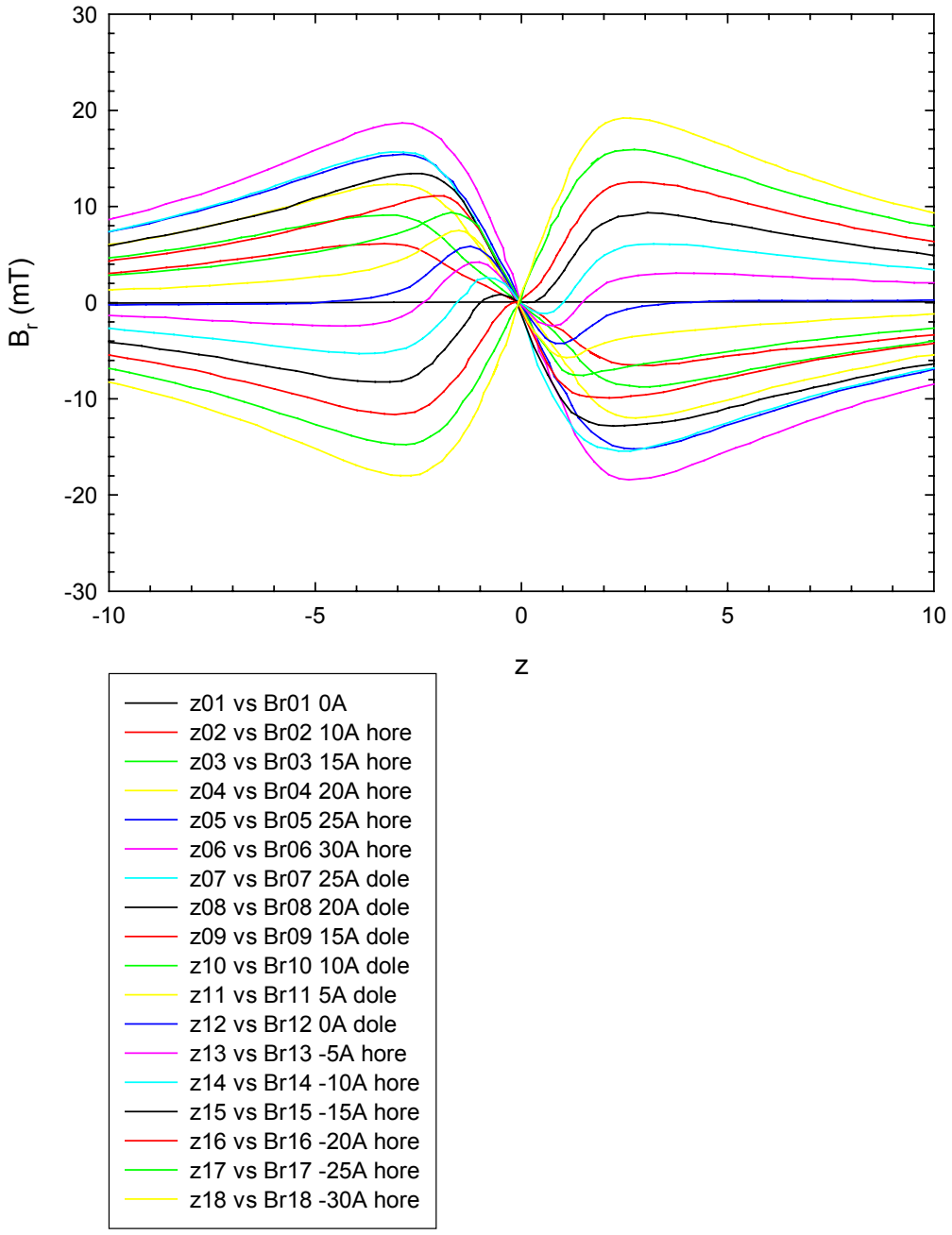

Figure 39.: The maximal radial component at the coil edge (in the middle of the winding thicknes) measured at various currents and 77 K

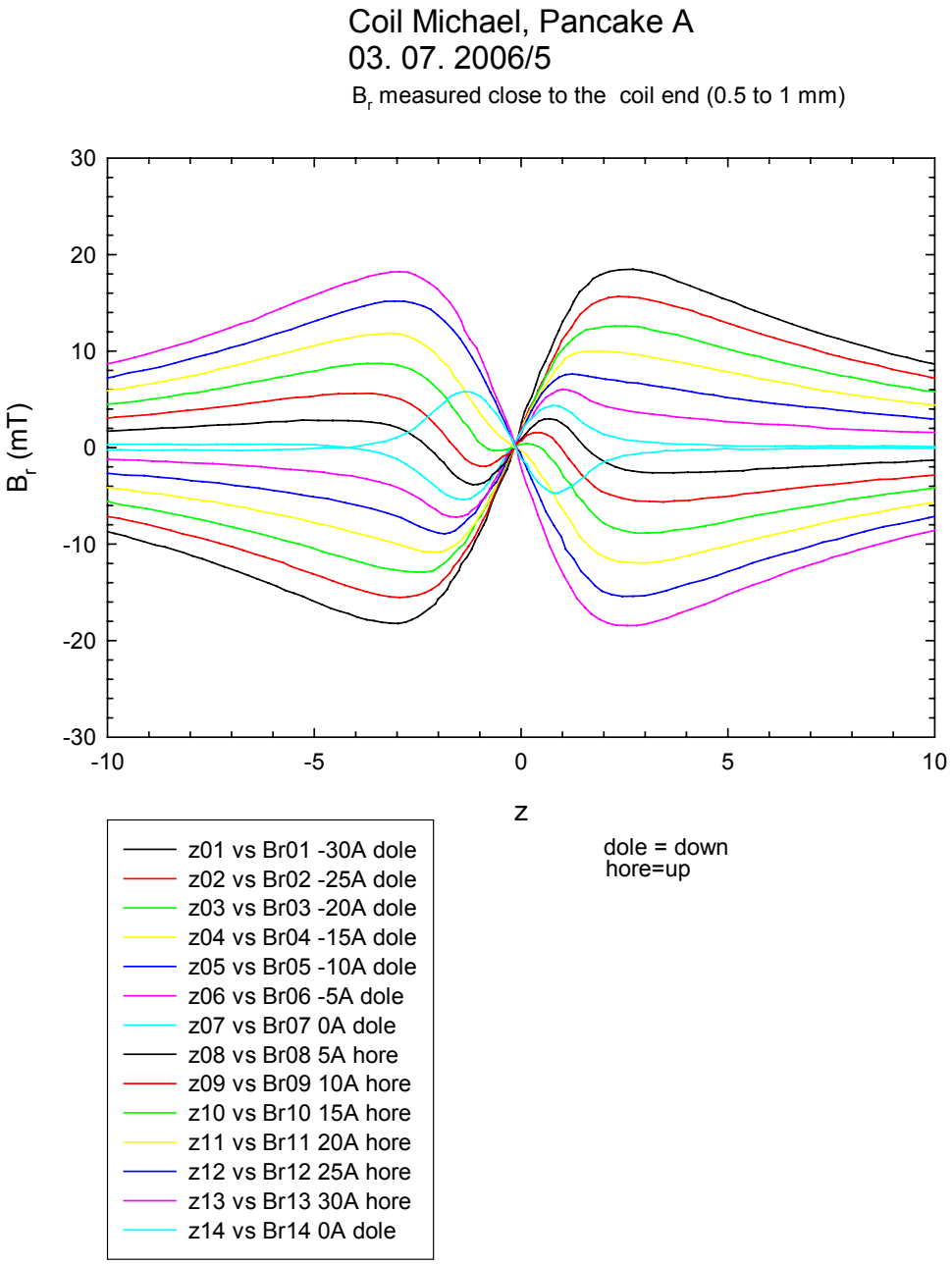

Figure 40.: The radial field component measured at r = 14 mm vs. the coordinate z at various currents and 77 K

8.3 Complete coil

The radial field component measured at the edge of the whole double pancake coil at 300 K is shown in Figure 41.

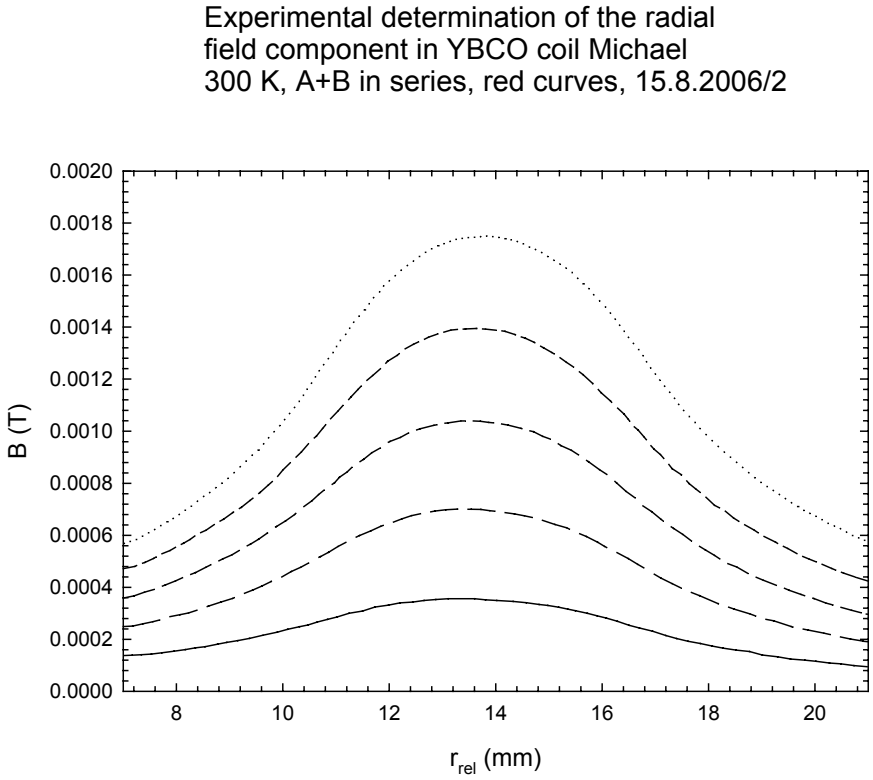

Figure 41.: The radial field component at 300 K, pancake A and B in series. Coil currents (from the bottom to the top curve) 0.25 A, 0.5 A, 0.75 A, 1 A, 1.25 A

In the following Figure 42 we plotted the radial field component measured at the outer edge of pancake B for the coil supplied by

- blue curves: only pancake A supplied
- black curves: only pancake B supplied
- red curves: A and B supplied in series

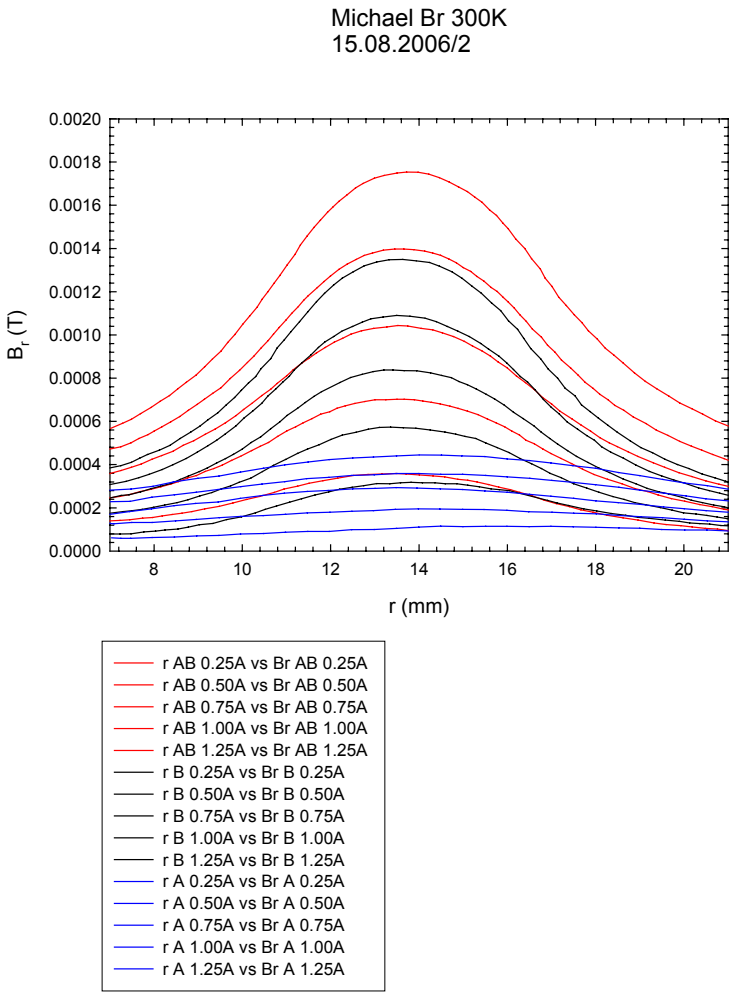

Figure 42.: Radial field component vs. r measured at 300 K

9 Radial component of the magnetic field inside the winding of a model coil wound with Bi-2223/Ag

The distribution of the transport current across a HTC tape in pancake coils is still an unsolved problem. Recently a possible approach to this problem was published [4]. However, the results must be verified experimentally.

To contribute to this problem, we prepared a small BSCCO coil wound with 4 mm wide Bi-2223/Ag tape. The ASC tape (4 mm x 0.25 mm) was wound on ϕ 58 mm former, Figure 43. The coil has 7 turns with slot between 3rd and 4th turn. The width of the slot was 0.6 mm. We measured radial components of magnetic field inside the slot by the Hall probe at room and 77K temperatures. The Hall probe was placed on very thin fiberglass plate which was attached to the end of rod. The rod was precisely moved by xyz positioning system, Figure 44. The results of the measurements at various coil currents are presented in Figure 45 to Figure 50. The critical current of the coil was 41 A.

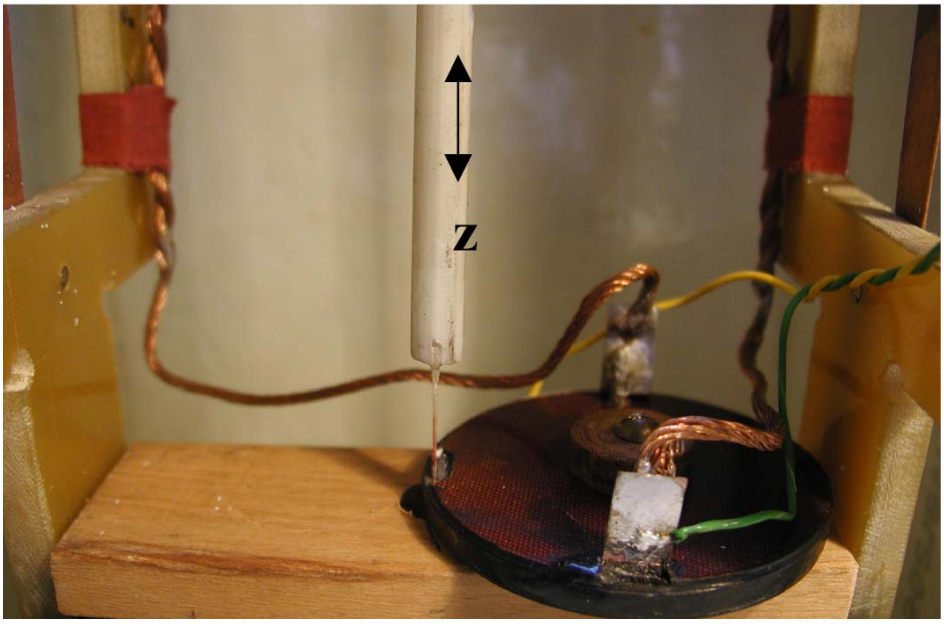

Figure 43.: BSCCO model coil with current leads and Hall probe on fiberglass rod

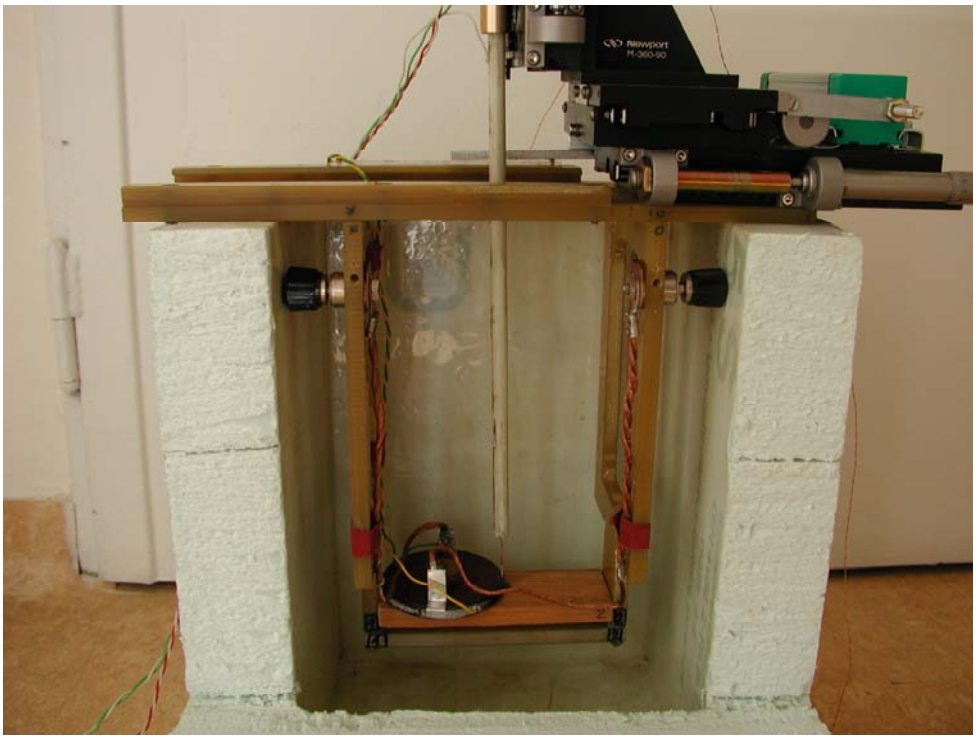

Figure 44.: Global view of the system for measurement of radial components of the magnetic field in the slot of BSCCO model coil

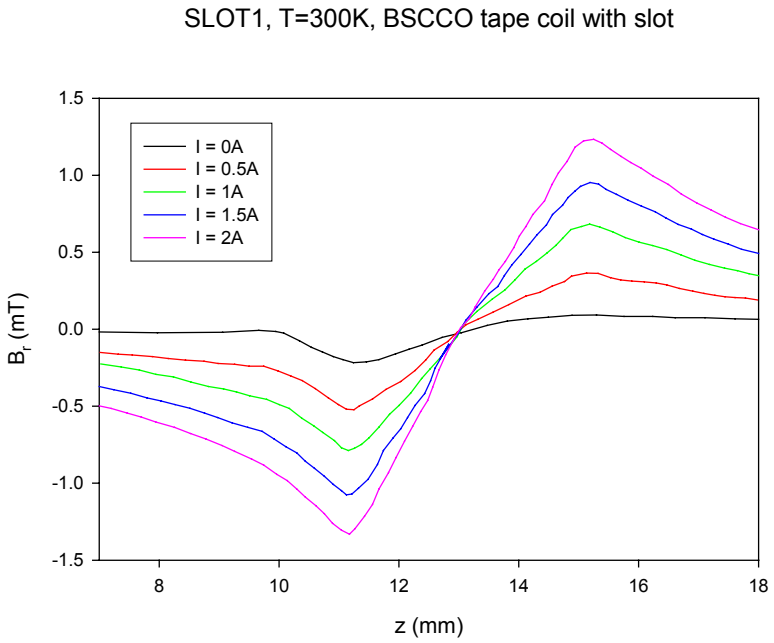

Figure 45.: Magnetic field profiles of radial component in the slot of BSCCO coil at room temperature at various transport currents. The profile at I = 0 A represents remanent magnetic field measured after coil current I = 2 A

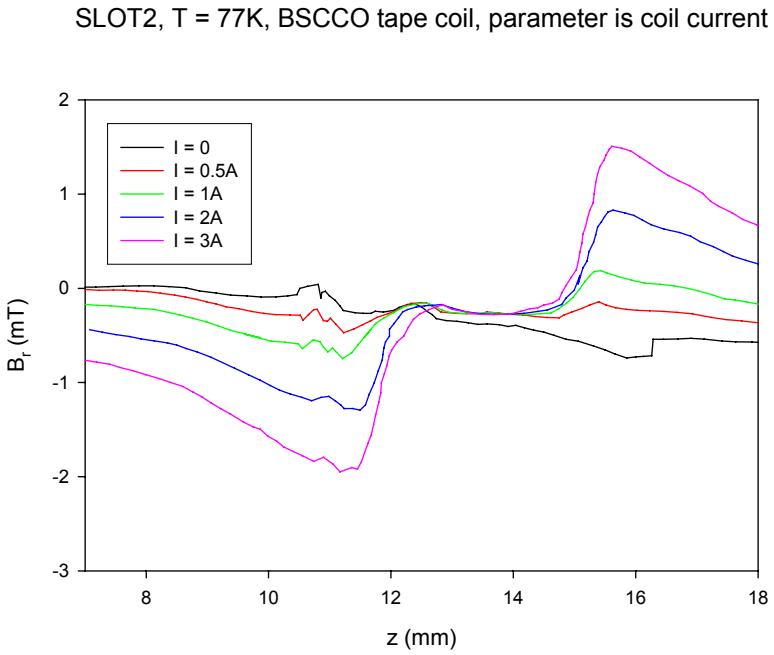

Figure 46.: Magnetic field profiles of radial component in the slot of BSCCO coil at temperature of 77 K at various transport currents. The profile at I = 0 A represents remanent magnetic field measured after coil current I = 3 A

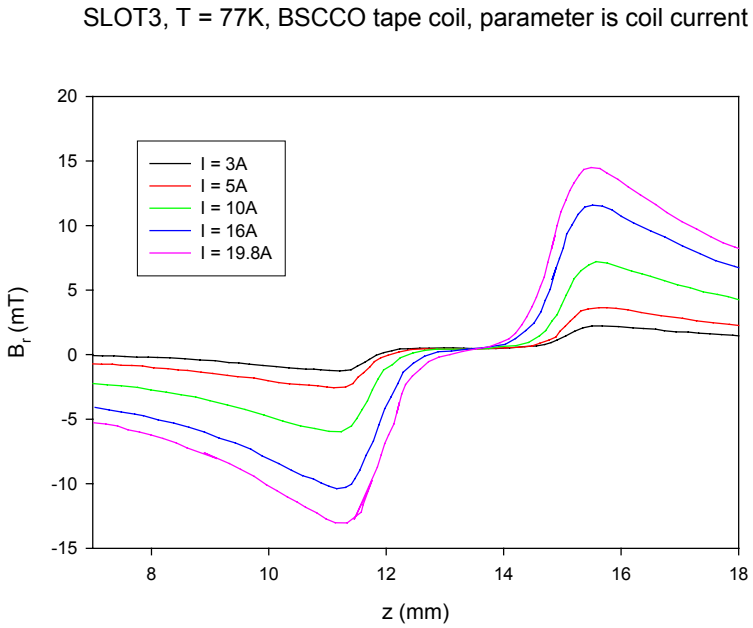

Figure 47.: Profiles of radial component in the slot of BSCCO coil at 77 K. Coil current was increased from 3 A up to 19.8 A

SLOT4, T = 77 K, BSCCO coil with slot, parameter is decreasing current

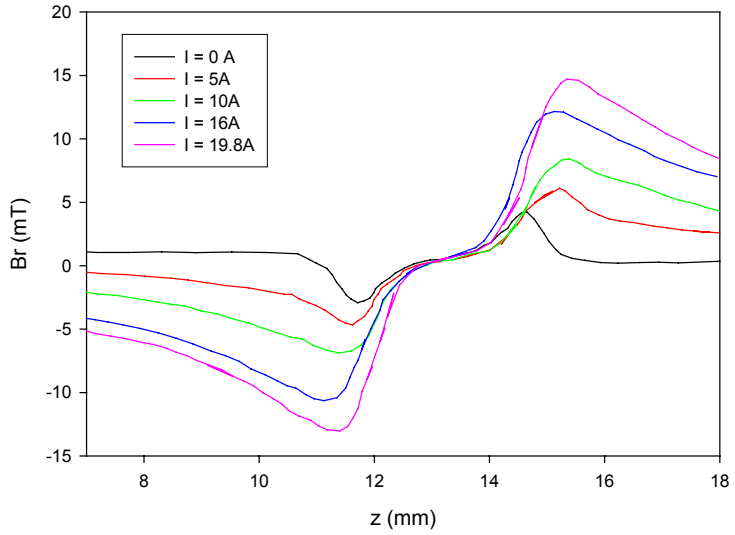

Figure 48.: Profiles of radial component in the slot of BSCCO coil at 77 K. Coil current was decreased from 19.8 A to 0

SLOT5, T = 77 K, BSCCO coil with slot

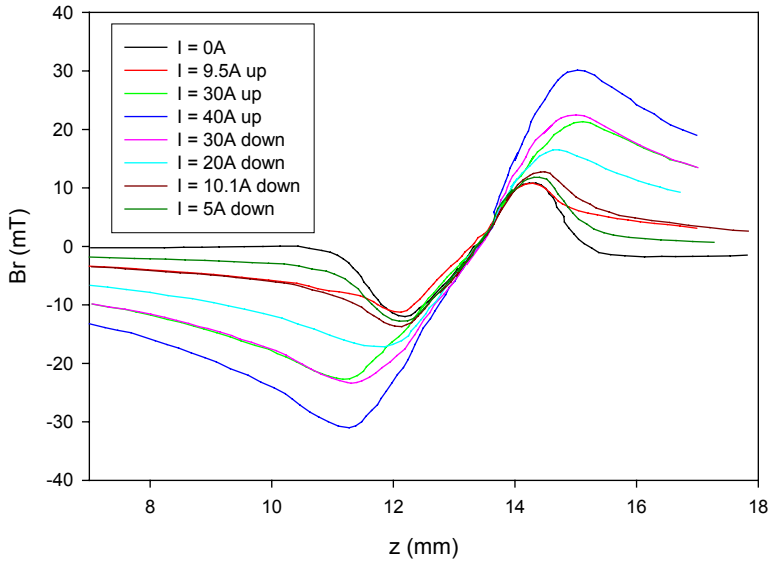

Figure 49.: Profiles of radial component in the slot of BSCCO coil at 77 K. Coil current was increased from 0 up to 40 A and then decreased to 5 A current

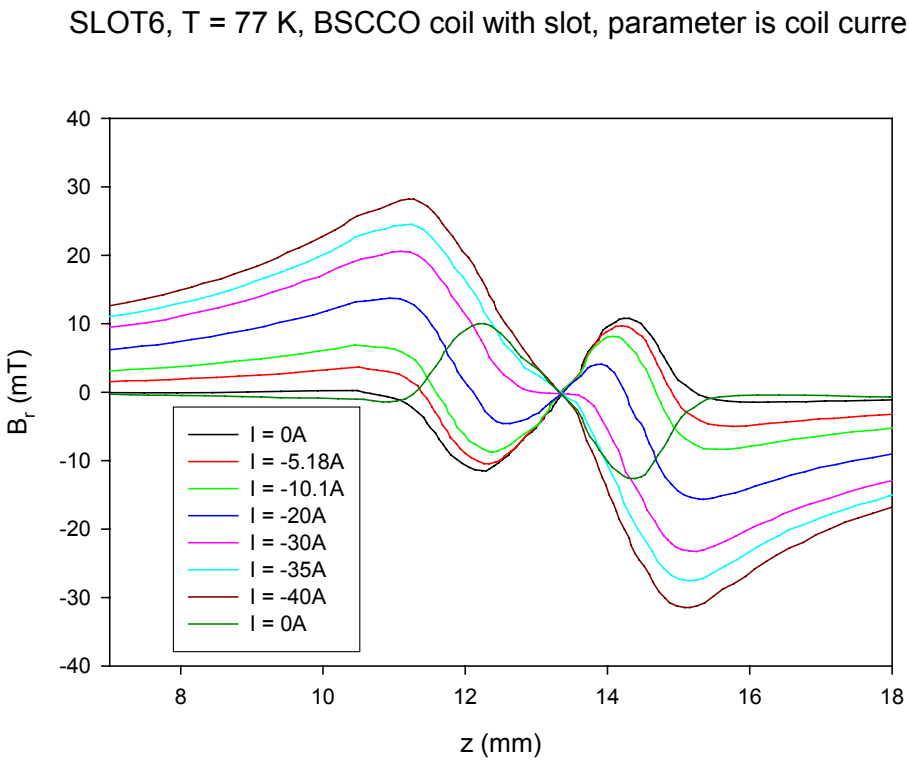

Figure 50.: Profiles of radial component in the slot of BSCCO coil at 77 K. Coil current was reversed and increased from 0 to –40 A

From the experiments we can say that the radial field component measured with coil in the superconducting state is very different from that in the normal state at room temperature. Due to magnetization currents the radial component at lower currents is small in the tape central area. With increasing transport currents the role of magnetization currents becomes smaller.

10 Identification and localization of short-circuits in the coil winding and their effect on the coil behavior

As the measured inductance of pancake 2 was frequency dependent, we supposed that the coil had a short circuit, as observed in several of our previous experiments. To identify and localize the short circuit, we measured the voltage between the current contact and a movable contact n (a needle) at constant coil current. This voltage should linearly depend on the distance between the current contact and the movable contact.

As shown in the following Figure 51, this was not the case.

A careful observation of the winding showed that there was probably a short-circuit between the first and second turn caused by a potential contact, which short circuited these turns.

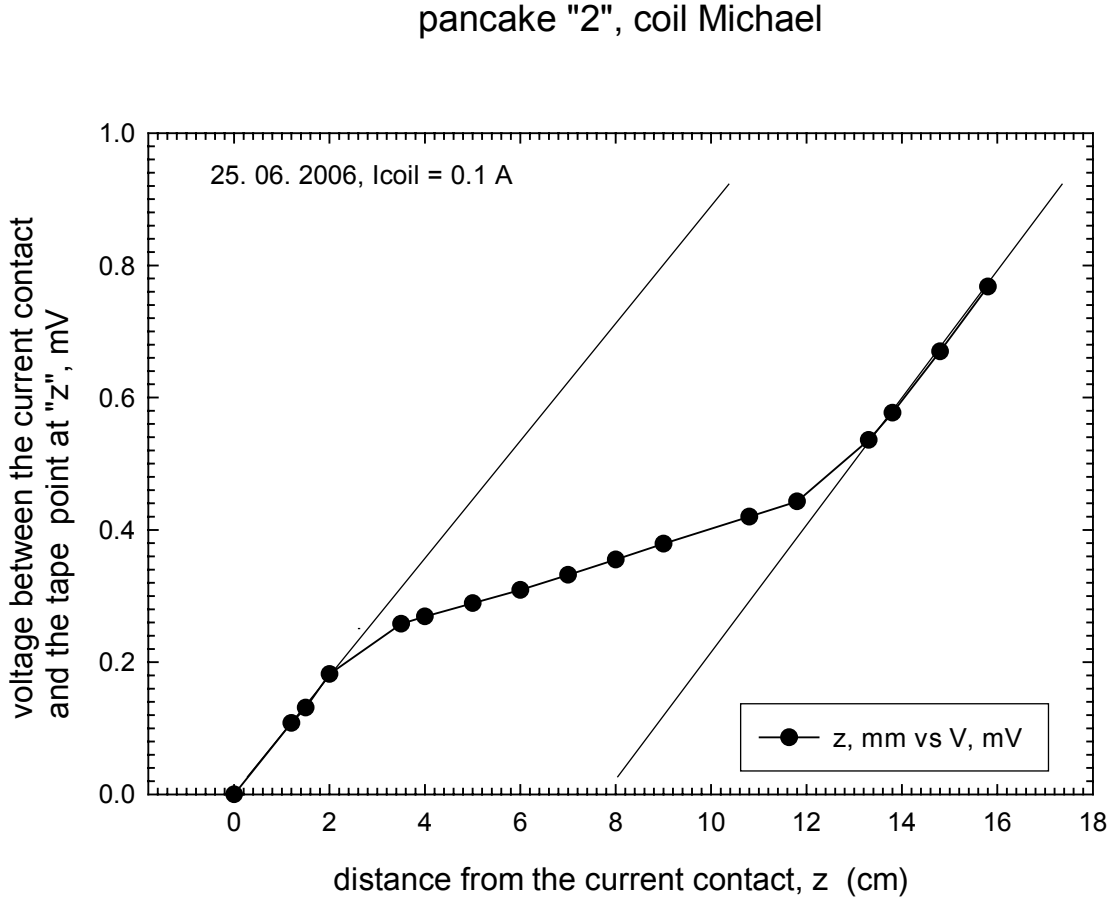

Figure 51.: The voltage between the current contact and the movable contact vs. their distance measured at 300 K and current 0.1 A

We removed this short-circuit successfully.

11 Studies of some problems important for the development of YBCO AC conductor

11.1 Visualization of the coupling current path in filamentary YBCO tapes

The coupling currents in filamentary tapes YBCO are usually small because of large transverse resistivity. Our idea was to amplify the amplitude of the coupling currents by soldering thin copper foil on the top of the filamentary sample. By this way the coupling currents become much larger and their path could be studied by Hall probe magnetometry.

The results of our investigations are presented in a paper which was sent to SUST (see Appendix I)

11.2 Current transfer length

The current transfer length is an important parameter characterizing the quality of the tape. The metallic layer (usually silver) serves as a protecting layer. It also allows soldering the current contact to the tape. High contact resistance may cause heating of the contact and can affect the behavior of samples or coils.

One of possible technology developments is based on the idea of conducting buffer layer. In the case of filamentary YBCO tapes the contact resistivity would affect also the transverse resistivity and coupling losses.

Our actual results are presented in a paper published in the scientific journal Superconductor Science and Technology, see Appendix VI.

12 Conclusions

A small YBCO coil wound with 4 mm wide YBCO tape super power was prepared and experimentally tested. We determined I-V curves, AC losses at frequencies up to Hz, the thermal runaway current and the coil heating in the resistive state.

The experiments showed that the not striated tape can be successfully operated at frequencies of several hundreds of Hz. However, the AC losses are quite large.

The critical current of the coil is 23 A. This current is nearly identical with the current at which the short sample $I_c(B)$ and the load line of the coil, $B_{r,max} = f(I)$ cross. $B_{r,max}$ is the radial component of the coil field measured close to the coil edge. It is quite interesting, as the radial component linearly decreases towards the tape axis and linearly increases in the opposite direction towards the other tape edge.

We also obtained results which are of importance for the development of low loss AC YBCO conductor. We determined the resistivity of YBCO/Ag boundary of the tape used to wind the coil, $\sim 5 \times 10^{-12}\ \Omega m^2$ at 77 K.

The study of the individual filaments of a multifilamentary tape showed that the filaments are visibly not uniform.

For the first time to our knowledge, we visualized the paths of coupling and hysteresis current in an model YBCO filamentary tape, where the coupling currents were amplified by reducing the transverse resistivity.

The obtained results were presented at important international conferences (ASC 06, Eucas 05) and published in scientific journals.

13 List of papers published in the frame of this contract

Appendix II:
Polák, M., Demenčík, E., Janšák, L., Ušák, E., Mozola, P., Thieme, C.L.H., Aized, D., Levin, G.A., and Barnes, P.N.: *Properties of a YBCO pancake coil operating with AC current at frequencies up to 1000 Hz*, IEEE Trans. Applied Supercond. **16** (2006) 1423-1426.

Appendix III:
Polák, M., Ušák, E., Janšák, L., Demenčík, E., Levin, G.A., Barnes, P.N., Wehler, D., and Moenter, B.: *Coupling losses and transverse resistivity of multifilament YBCO coated superconductors*, J. Phys.: Conf. Ser. **43** (2006) 591-594.

Appendix IV:
Polák, M., Demenčík, E., Janšák, L., Mozola, P., Aized, D., Thieme, C.L.H., Levin, G.A., and Barnes, P.N.: *AC losses in a $YBa_2Cu_3O_{7-x}$ coil*, Applied Phys. Lett. **88** (2006) 23501-1-3.

Appendix V:
M. Polak, J. Kvitkovic, P. Mozola, P. N. Barnes, G. A. Levin: *Characterization of Individual Filaments in a Multifilamentary YBCO Coated Conductor*, presented at ASC 2006 conference, to be published at IEEE Trans. on Appl. Supercond.

Appendix VI:
Polák, M., Barnes, P.N., and Levin, G.A.: *YBCO/Ag boundary resistivity in YBCO tapes with metallic substrates*, Supercond. Sci Technol. **19** (2006) 817-820.

14 References

[1] Y.-Y. Xie, A. Knoll, Y. Chen, Y. Li, X. Xiong, Y. Qiao, P. Hou, J. Reeves, T. Salagaj, K. Lenseth, L. Civale, B. Maiorov, Y. Ywasa, V. Slovyov, M. Suenaga, N. Cheggour, C. Clickner, J. W. Ekin, C. Weber, V. Selvamanickam, Physica C 426-431, 849 (2005)

[2] **Polák**, **M**., Krempaský, L., Chromik, Š., Wehler, D., and Moenter, B.: *Magnetic field in the vicinity of YBCO thin film strip and strip with filamentary structure*, Physica C **372-376** (2002) 1830-1834.

[3] Polák, M., Kvitkovič, J., Janšák, L., and Mozola, P.: *The effect of epoxy impregnation on the behaviour of a Bi-2223/Ag coil carrying DC or AC current*, Supercond. Sci. Technol. **19** (2006) 256-262.
[4]

15 Appendix I

Visualization of coupling current paths in striated YBCO coated conductors at frequencies up to 400 Hz

E. Demencik, P. Usak, S. Takacs, I. Vavra and M. Polak
Institute of Electrical Engineering, Slovak Academy of Sciences, 841 04 Bratislava, Slovakia
G.A. Levin, P.N. Barnes
Air Force Research Laboratory, Wright-Patterson Air Force Base, OH 45433

Corresponding author:

Eduard Demenčík, Institute of Electrical Engineering, Slovak Academy of Sciences, Dúbravská cesta 9, 841 04 Bratislava, Slovakia, tel.: +421 2 5477 3545, fax.: +421 2 54775816, E-mail.: eduard.demencik@savba.sk

The magnetic flux density component perpendicular to the broad tape face was mapped by miniature Hall probes in the vicinity of the striated YBCO coated tape at frequencies of external magnetic field from 21 to 400Hz, applied perpendicularly to the tape surface. For reasons of modeling the coupling currents behavior in tapes with conductive substrate, we amplified the coupling current-amplitude by soldering 25μm thick copper foil on the top of the filaments. The aim of this procedure was to decrease the transverse resistivity of the tape. The longitudinal components of the total currents flowing in the tape were calculated by inverse method from the field map corresponding to the zero phase of the applied field. The diffusion lengths, characterizing the flux penetration into the tape, were determined for the respective frequencies. The experimentally determined diffusion length is in good accordance with theoretical models. While at 21Hz both weak coupling currents and distinctive hysteretic currents of individual filaments are observed; at 400Hz the coupling currents are predominant in this YBCO tape.

A significant amount of development has occurred for high temperature superconducting (HTS) wires and more recently for the second generation (2G) $YBa_2Cu_3O_{7-x}$ (YBCO) coated conductor especially. In order to make these HTS tapes suitable for AC applications, a part of this developmental effort has gone toward studies leading to a more ac-tolerant architecture for the conductor[1]. As part of this, a variety of techniques are widely used for characterization of the electromagnetic properties of the HTS tapes, such as AC loss, current density vs. electric field (E-J), resistivity vs. temperature (R-T) measurements, etc. However, these techniques are typically integral methods describing the tapes as a whole on the scale of several millimeters or more. Much less is known about the behavior of these tapes on a sub-millimeter scale when exposed to an external AC magnetic field, where local variations of the critical current or the magnetic self-field may occur.

As already determined, the sample length plays an important role in AC loss measurements. While the total hysteresis power loss is proportional to the sample length, the total coupling loss in a twisted multifilament conductor increases as the square of the twist pitch length l_t^2. A linear, not twisted multifilament tape with the length of L behaves like the twisted one with twist pitch $l_t = 2L$.To reduce the coupling losses in an application, the multifilament HTS tape must be either physically twisted or have a "twist" of the filaments incorporated into the conductor's architecture[3,4]. In a rectangular non-twisted multifilament sample, the coupling currents at the end of the tape will flow in a direction perpendicular to the filaments. In the central section of the tape, however, the coupling currents flow in the direction parallel to the

filaments' axis. The measurement techniques, such as the time integration of the pick-up coil voltage[5], the temperature increase of the sample due to the self heating[6], or a technique based on AC susceptibility measurements[7], provide only the total loss value. Due to the complex current paths in an actual filamentary tape, it is important to verify the simplified theoretical predictions by an appropriate experiment giving information also on the local scale. Magneto-optical imaging (MOI) and Hall probe mapping (HPM) are useful tools in this respect. MOI was already used in experiments focused on the current density distribution in YBCO at frequencies up to 1 kHz[8]. The advantages of HPM compared to MOI are the higher sensitivity of the Hall probe sensors to the magnetic field, higher versatility, and a lower cost of the experimental device. In this work, we focused on the visualization of both the magnetization and the coupling currents in a special filamentary sample of YBCO coated conductor.

A multifilamentary YBCO-coated conductor sample with the dimensions 4×40 mm^2 was prepared for this investigation from a uniform 12 mm wide coated conductor provided by SuperPower Inc.[9] In this conductor, the ~1 μm thick YBCO layer is deposited on 50 μm thick IBAD buffered Hastelloy substrate and covered with the silver cap layer about 3 μm thick. The non superconducting grooves segregating the superconducting stripes were cut by laser ablation as described in reference[10] and the sample was annealed in flowing oxygen afterwards[11]. The distance between the grooves is 0.5 mm and their width is about 30 μm. Before striation the critical current of the 12 mm wide conductor was about 160 A. The AC loss measurements in the frequency range from 28.5 Hz to 203 Hz indicate that the coupling loss in the sample is quite small, as the loss per cycle at given amplitude of the external magnetic field, B_{ext}, was practically frequency independent. This is the result of post-ablation oxygenation that leads to formation of high resistivity oxides (NiO, Cr_2O_3, etc.) in the grooves[11]. For the purpose of this investigation the coupling currents were amplified to allow their spatial determination by deliberate reduction of the interfilamentary resistance. A 25 μm thick Cu foil was soldered to the surface of the silver cap layer (see Fig. 1). Thus, the coupling currents were able to flow between the superconducting filaments through the copper overlayer[12].

Miniature Hall probes (developed in our laboratory, HHP-VU) with a sensitivity of ~150mV/T and an active area of 50 by 50 μm were used for the field mapping. The experimental system used to perform the HPM measurements is described elsewhere[13]. The system provided a harmonic signal $B_e = B_{max} \sin(\omega t)$ with B_{max} = 33.5 mT. By using a triggered-signal data acquisition technique for the selected phase of the AC field[13], we measured a series of lateral magnetic self-field profiles $B_{sf,z} = f(x)$, where x- is the direction perpendicular to the superconducting stripes. The measurements were repeated by shifting the Hall sensors along the stripes with a spatial step of Δy = 1 mm from one tape end to the other, Fig. 2. At the tape ends, the step Δy was reduced to Δy = 0.5 mm to track changes of the self-field. The distance of the Hall probe sensor from the tape's surface was Δz = 0.35 mm. The AC magnetic profiles were measured at the fixed phase of the external field $\phi = \omega t = 0$; they correspond to zero value of the external field, when the coupling current is at its maximum. The maps of $B_{sf,z}(x, y)$ measured at frequencies 21 Hz, 165 Hz and 400 Hz are shown in Fig. 3.

From these results we calculated the lateral distribution of the local sheet current values, $I_{s,y}(x)$, at each position y by solving the inverse problem. The details of the method used, are described in reference[14]. The number of elements used to calculate $I_{s,y}(x)$ was 85. The paths of the magnetization currents determined by the calculations using the data from Figs. 3a), b) and c) are shown in Figs. 4a), b) and c). The current profiles $I_{s,y}(x)$ at the position y = 16 mm are shown in Figs. 5a) and b). The magnetization current paths deduced from the calculations in Figs. 4a), b)

and c) are schematically shown in Figs. 4d), e) and f). For y values close to the sample center $\sum_i I_{s,y}(x_i) = 0$, as no transport current flows in the sample. The mean of lateral sum of absolute values, $1/n \sum^{n}_{i=1} \left| I_{s,y}(x_i) \right| = I_y$, equals to the total induced sheet current's longitudinal component at longitudinal position y. This value is supposed to be maximum in the center of the tape and decreasing to the ends in favour of the complementary transversal sheet current component. This one is supposed to be maximum at the tape's ends, with amplitude equal to the longitudinal component I_y at the tape's center.

The magnetic flux penetration into the tape can be quantitatively described by means of the diffusion length which is the length characterizing the exponential decay of the complementary transversal component of coupling current amplitude from the tape ends[15]:

$$l_d = \frac{1}{\sqrt{\mu_0 \omega n_p \ln(1 + 2n_\perp)/2\pi\rho_{tr}}}, \qquad (1)$$

where ω is the angular frequency, $\omega = 2\pi f$; n_p and $n_\perp$ stand for number of filaments parallel or perpendicular to the broad tape side, respectively; and ρ_{tr} is the transverse resistivity. The amplitude of the transverse component of the coupling currents for a given distance from the tape end can be deduced from the decrease in the longitudinal component of the current. While in the tape's central region the longitudinal current component is maximal and essentially equals the net coupling current, it continuously decreases to zero value at tape's ends, ($I_y \rightarrow 0$). This decrease is compensated with an increase in the transversal component $I_x = f(y)$ towards the tape ends. The I_x (y) component (complementary to I_y) decays from tape ends following the exponential function:

$$I_x = k \cdot \exp\{-y/l_d\}, \qquad (2)$$

where l_d is the diffusion length.

The diffusion lengths (l_d) were determined from the HPM experiments based on Eq. (2). Based on curve fitting of the data shown in the figures, we determined the diffusion lengths l_d to be 8.7 mm, 3.5 mm and 2.1mm for 21Hz, 165Hz and 400Hz, respectively. As expected from Eq. (1), the diffusion length decreases with increasing frequency. Using the expression $R = l_d(f)/l_d$ (21Hz), the ratios of the diffusion length for each frequency with respect to the diffusion length at the lowest frequency, i.e. 21 Hz, are $R_{165\text{Hz}} = 0.40$ and $R_{400\text{Hz}} = 0.24$. This is in good agreement with the theoretical square root frequency dependence suggested by Eq. (1), namely $R_{165\text{Hz}} = 0.36$ and $R_{400\text{Hz}} = 0.23$.

From the experimentally determined diffusion lengths, we calculated the transverse resistivity using equation (1), taking n_p and $n_\perp$ to be 6 and 1, respectively, for our sample. The mean value of the transverse resistivity determined from the measurements was $\rho_{tr\_mean} = 5.66 \times 10^{-9} \Omega.\text{m}$. This value compares favorably with the copper foil resistivity measured at LN_2 temperature, ρ (77K) = $2.48 \times 10^{-9} \Omega\text{m}$.

In conclusion, we have reconstructed the current paths of the longitudinal (I_y) component of coupling currents in a striated YBCO conductor with non-striated copper stabilizer. This was accomplished by solving the inverse problem and thus determining the induced coupling currents from the measured magnetic field. The results obtained for three particular frequencies (21 Hz, 165 Hz and 400 Hz) confirm the theoretical prediction of the $f^{1/2}$ frequency dependence of the diffusion length. For the lowest frequency of 21 Hz, we observed weak coupling currents between the filaments with dominant hysteretic currents. At higher frequencies of 165 Hz and 400 Hz the superconducting filaments are almost fully re-coupled by the currents flowing

through the copper stabilizer. The resistivity of the coupling medium obtained from the values of the diffusion length by inverting Eq. (2) is close to that of copper.

This work was supported by the AFOSR grant, number FA8655-05-1-3062. The work was partially supported also by projects VEGA 2/5089/25, CENG and APVV-51-002305.

References:

[1]P.N. Barnes, M.D. Sumption, and G.L. Rhoads, Cryogenics **45** (2005) 670-686.
[2]K. Kwasnitza and St. Clerc, Physica C **233** (1994) 423.
[3]M.D. Sumption, P.N. Barnes, and E.W. Collings, IEEE Trans. on Appl. Supercond. **15** (2005) 2815-2818.
[4]P.N. Barnes, G.A. Levin, C. Varanasi, and M.D. Sumption, IEEE Trans. on Appl. Supercond. **15** (2005) 2827-2830.
[5]M D Sumption, E W Collings and P N Barnes, Supercond. Sci. Technol. **18** (2005) 122-134.
[6]Nguyen, D.N., Sastry, P.V.P.S.S., Zhang, G.M., Knoll, D.C., Schwartz, J., IEEE Trans. Applied Supercond. **15** (2005) 2831-2834.
[7]F. Gomory, Supercond. Sci. Technol. **10** (1997) 523-542.
[8]A. Lucarelli, G. Lupke, T.J. Hauqan, G.A. Levin, P.N. Barnes, Supercond. Sci. Technol. **19** (2006) 667-670.
[9]Y.-Y. Xie, A. Knoll, Y. Chen, Y. Li, X. Xiong, Y. Qiao, P. Hou, J. Reeves, T. Salagaj, K. Lenseth, L. Civale, B. Maiorov, Y. Iwasa, V. Solovyov, M. Suenaga, N. Cheggour, C. Clickner, J.W. Ekin, C. Weber and V. Selvamanickam, *Physica C* **426-431,** 849-857 (2005).
[10]G. A. Levin, P. N. Barnes, N. Amemiya, S. Kasai, K. Yoda, Z. Jiang, and A. Polyanskii, J. Appl. Phys. **98**, 113909 (2005) and references therein.
[11]G.A. Levin, P.N. Barnes, J.W. Kell, N. Amemiya, Z. Jiang, K. Yoda, and F. Kimura, Appl. Phys. Lett. **89** (2006) 012506.
[12]M. Polak, P.N. Barnes, and G.A. Levin, Supercond. Sci. Technol. **19** (2006) 817-820.
[13] L. Frolek, E. Demenčík, IEEE Trans. Applied Supercond. **15** (2005) 3660-3663.
[14]P. Usak, Physica C **384** (2003) 93.
[15]S. Takacs, F. Gomory, Inst. Phys. Conf. Ser. No. 167 2000 IOP Publishing Ltd., 611-614.

Figure captions

Fig.1 Electron microscope microphotograph of the YBCO coated conductor tape in lateral cross-section showing the layer structure of the original tape, as well as the additional copper layer soldered with Indium sold and reducing thus the transverse resistivity; approximate layer thicknesses are as following: substrate 50 μm, YBCO 2 μm, silver cap layer 3 μm, Cu foil 25μm, indium sold 15μm.

Fig.2 HPM measurement of the *z*-component of the magnetic self field due to magnetization currents induced in the tape by AC external magnetic field, perpendicular to the broad tape face.

Fig.3 Magnetic self field map $B_{sf,z}(x, y)$ generated by magnetization currents induced in the tape exposed to external AC field; measurement by Hall probe in the distance z = 0.35mm above the tape. The *x* is the coordinate across the tape (in millimeters), *y* axis (at the left side of the figures) is coordinate in the direction along tape in millimeters, color bar represents amplitude of the *z*-component's magnetic flux density B_z in [mT]. Phase of the external field $\phi = \omega t = 0$.
Lateral self field profiles along the horizontal lines for y = 16mm are shown in fig. 5a).
a) frequency 21Hz
b) frequency 165Hz
c) frequency 400Hz

Fig.4 Inversely calculated map showing longitudinal component of coupling currents. Axis *x* and *y* are spatial coordinates in [mm], color bar represents the amplitude of the coupling current y -component per unit width I_y in [$A.cm^{-1}$]. Note that at the tape ends the longitudinal (I_y) component decreases to zero, it is due to the increase of the transverse (I_x) component of the current loops.
One can see in b), e) and in c), f) that at frequencies 165Hz and 400Hz, the coupling currents predominate over hysteretic currents, while at 21Hz, see a), d), the coupling currents play only a minor role.
Lateral current profiles along the horizontal lines y = 16mm are shown on fig. 5b).
a), b), c) - calculation for frequencies 21, 165 and 400Hz, respectively
d), e), f) - schematic magnetization currents paths deduced from a), b) and c) calculations

Fig.5 The measured lateral self magnetic field profiles $B_{sf,z}(x)$ and corresponding lateral current profiles $I_y(x)$ along the horizontal line y=16mm from fig.3a), b) and c) and fig.4a), b) and c) for the frequencies 21Hz, 165Hz and 400Hz, respectively.

Fig.6 Measured data of frequency dependence of the diffusion length compared to the theory, calculated for the following value of transverse resistivity: $\rho_{tr} = 5.66.10^{-9}\Omega.m$.

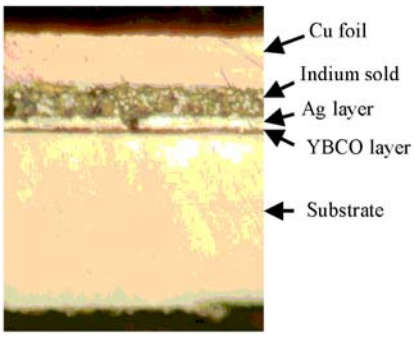

Fig. 1

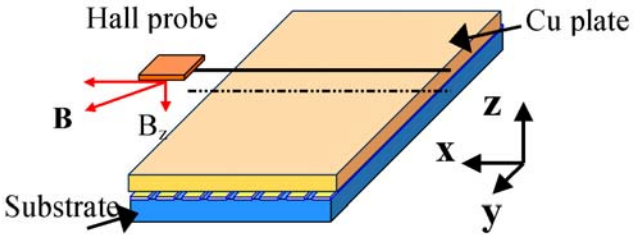

Fig. 2

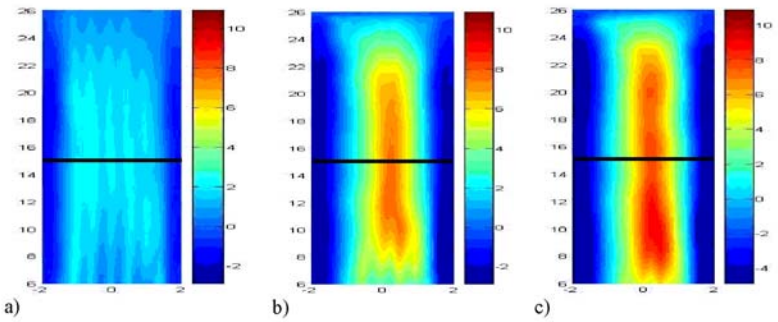

Fig. 3

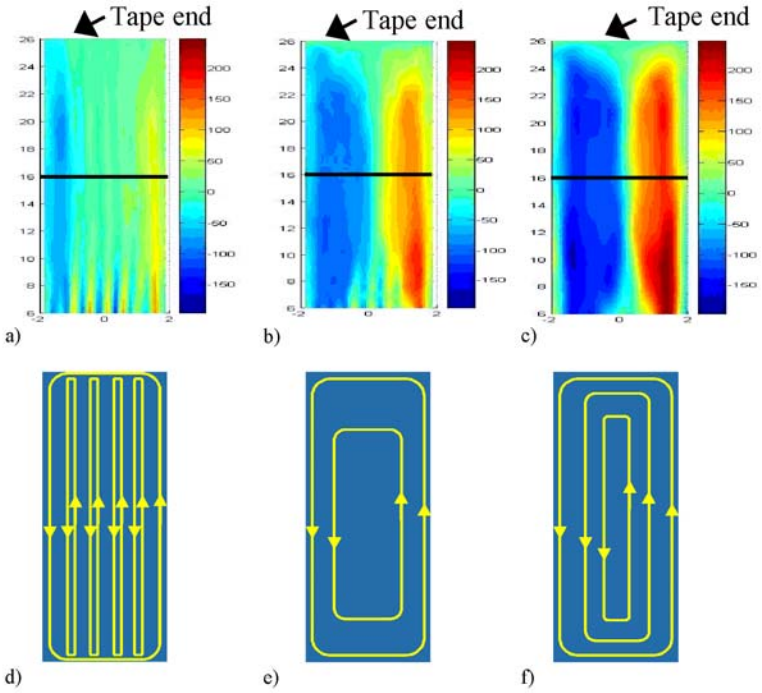

Fig. 4

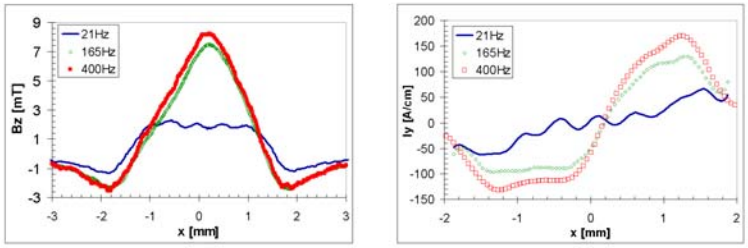
21Hz
165Hz
400Hz
Bz [mT]
x [mm]
21Hz
165Hz
400Hz
Iy [A/cm]
x [mm]

a) b)

Fig. 5

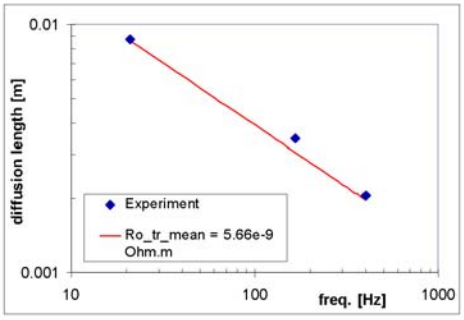
0.01
0.001
diffusion length [m]
Experiment
Ro_tr_mean = 5.66e-9 Ohm.m
10
100
1000
freq. [Hz]

Fig. 6

16 Appendix II

Properties of a YBCO pancake coil operating with AC current at frequencies up to 1000 Hz

Milan Polak, Eduard Demencik, Lubomil Jansak, Elo Usak, Pavol Mozola, Cees L. H. Thieme, D. Aized, Paul N. Barnes, George A. Levin

Abstract— **A small pancake coil was wound using 1.2 m long, 10 mm wide YBCO coated superconductor tape with impregnation by epoxy resin. The coil was tested in several regimes. In the DC regime, we measured the I-V curve, the hysteresis of the magnetic field-current curve at liquid nitrogen temperature and the radial component of the coil field at the coil edges. The AC losses were measured in the frequency range from 100 Hz to 1000 Hz. The coil was immersed in liquid nitrogen at atmospheric pressure and the coil heating due to AC losses was monitored. The frequency dependence of the power loss and the critical currents of a short sample at 77 K were also measured and compared with those of the coil.**

***Index Terms*—Losses, Magnetic fields, Superconducting Magnets**

I. INTRODUCTION

The applications of YBCO coated conductors in AC devices are often considered, but the main effort of the industry is still focused on the improvement of DC properties like the critical current density and the current carrying capacity. The conductors have the shape of a tape several millimeters wide (typically 10) with thickness of the order of 0.1 mm [1]. For technology reasons a stack of pancake type coils is preferred to make coils when using wide tapes. For Bi-2223/Ag coils it was shown that the magnetic anisotropy strongly and by a complicated way affects the distribution of the current density inside the tapes [2]. The critical current of the coil is limited by the largest magnetic field component perpendicular to the tape plane [3]. The tape in the pancakes located at the ends of the coil and close to them is exposed to an inhomogeneous magnetic field and it is not a straightforward procedure to determine the critical current in this case [4]. Similar problems appear in coils wound with YBCO coated conductors.

For AC operation the direction of the magnetic field with respect to the tape plane and the tape width play an important role. According to Brandt and Indenbom [5], the hysteresis losses in YBCO in the transverse magnetic field are directly proportional to the tape width. Amemyia et al. have shown that in the case of an arbitrary orientation of the magnetic field AC loss are proportional to the transverse component of the field [6].

To our opinion it is interesting to have information on AC behavior of coils made of wide, non striated YBCO coated conductor. It is of particular interest to get data on coil AC losses in wide interval of frequencies. In this work, we compare AC behavior of a pancake coil wound with YBCO coated conductor with a similar coil wound of copper tape, both of them were cooled by liquid nitrogen.

Manuscript received September 20, 2005. This work was supported by AFOSR, grant number FA8655-03-1-3082. We also acknowledge the partial support of the Center of Excellence CENG, Slovak Academy of Sciences. M.P. thanks the Alexander von Humboldt Foundation for the support.

M. P., E. D., L. J., E. U, are with the Institute of Electrical Engineering, Slovak Academy of Sciences, 841 04 Bratislava, Slovakia. Corresponding author M. P.: phone ++421 2 54773545, fax ++421 2 54775816, email elekpola@savba.sk)

C. T., D. A. are with the American Superconductors, Westborough, MA 01581, USA (e-mail CThieme@amsuper.com

P. B., G. L. are with Wright Patterson Air Force Base, OH 45433, USA (e-mail paul.barnes@wpafb.af.mil).

II. EXPERIMENTAL

A. Description of YBCO coil and Cu coil

The 2G YBCO coil was made using a 1.2 m length of copper-stabilized YBCO coated conductor. It was co-wound with wet, epoxy-saturated fiberglass cloth on a G10 coil form, and had an inner and outer diameter of 25.8 mm and 33.8 mm after completion. The number of windings was 13.

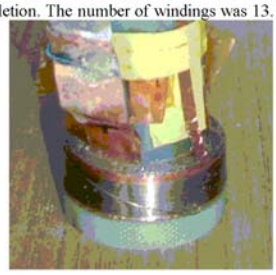

Fig.1. The photograph of the YBCO coil

The conductor was made using a RABITs type Ni-5at% W substrate with a sputtered Y_2O_3 seed layer, a YSZ barrier layer, and a CeO_2 cap layer [6]-[7]. The substrate had a Curie temperature of ~60°C and is ferromagnetic at 77 K [8].

This ferromagnetism is expected to contribute to the coil's inductance. The 0.8 μm YBCO layer was deposited using a TFA-based solution process and subsequently capped with a 3 μm Ag layer to which a 50 μm thick Cu 110 foil was laminated. The copper coil was made using a ~110 μm thick, 1.26 m long copper tape, 10 mm wide, with a resistivity of 1.8 x 10^{-7} Ωcm at 77 K. The number of turns, the inner and outer coil diameter, and insulation were the same as those of the YBCO coil. NORMA Power Analyzer 4000D was used to measure the losses of the coil.

III. Results and Discussion

The DC critical current of the coil with slowly increasing transport current was 154 A at which the coil voltage was 12μV (see Fig. 2), which corresponds to the mean electric field of 0.1 μV/cm and to the mean current density in the winding cross-section of 5000 A/cm^2.

At coil current 154 A the axial field in the coil center, $B_z(r=0)$ and at the inner turn of the coil, $B_z(r=20$ mm) calculated assuming a constant current density in the tape is

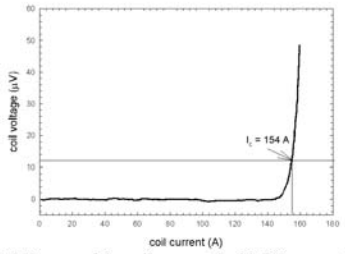

Fig.2. I-V curve of the coil measured with DC current, 77 K

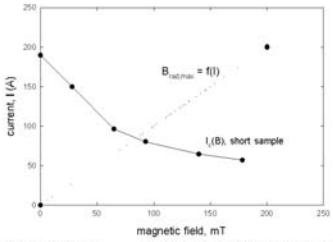

Fig.3. The load line $B_{r,max} = f(I)$ and $I_c(B)$ curve of the YBCO tape used in the coil.

As we see, the real critical current of the coil was The load line $B_{r,max} = f(I)$ intersects $I_c(B)$ curve of the tape used for coil winding at 80 A is considerably higher (154 A) This discrepancy clearly shows that the critical current of a tape exposed to non-uniform radial field component with the maximum $B_{r,max}$ at the tape edges is not equal to the critical current determined in the uniform external field $B = B_{r,max}$.

Using a small active area Hall probe we measured the radial field component, $B_r(r)$, close to the longitudinal edge of the coil (z = 5.5 mm).

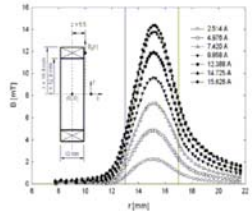

Fig.4 The radial field component, B_r, as a function of the radial position, r, measured at various current (rms) at 500 Hz

In Fig.3 we show the typical set of $B_r(r)$ curves measured at 500 Hz. The radial component of the coil field measured at z = 5.5 mm has a maximum, $B_{r,max}$, at $r_m \cong 15$ mm (in the middle of the winding thickness). The measurements were repeated with the coil in the normal state (300 K) carrying a DC current and at 77 K with a DC and then an AC current with frequencies 100 Hz and 1000 Hz. $B_{r,max}$ is plotted vs. coil current in Fig.4.

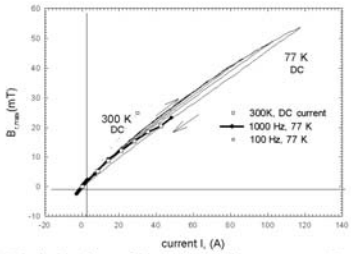

Fig. 5: Maximal values of the radial field component, $B_{r,max}$ (at r = 15 mm) as the function of current I (peak values) measured at DC current and 77 K (full lines) for 4 different runs $0 \rightarrow I_{max} \rightarrow 0$. The dotted line is the extrapolation of the $B_{r,max}(I)$ curve at 300 K. The curves with AC current were measured at 100 Hz (•) and 1000 Hz (□).

The values of $B_{r,max}$ increase linearly with increasing current at 300 K, but at 77 K they have a hysteretic character and are considerably lower. This behavior clearly indicates an inhomogeneous current distribution in the tape. The observed behavior of B_r and its non-uniformity demonstrate the need for new procedures to determine ac losses other than simple extrapolation from short sample data.

To determine the coil inductance, L, we recorded the coil voltage, V, while applying triangular transport current waves with the amplitude of 50 A at frequencies of 50, 100, and 200 mHz (Fig.5). With V = L dI/dt, the shape of the curves shows that L depends on the current at low current values, ranging from ~7 μH at I = 0 to ~5 μH with increasing currents. At higher currents, L is current independent which independence tends to shift to higher current levels as dI/dt increases.

Loss measurements for the YBCO coil at frequencies from 60 to 1000 Hz are shown in Fig.4. We also show the losses of the Cu coil with a DC current and AC currents of 100 and 1000 Hz. There is little difference in losses of the Cu coil between the DC and AC 100 Hz currents. At 1000 Hz, the losses also contain a measurable eddy current contribution. The total losses of both coils increase proportional to I^n, where $n \cong 1.7$ at a frequency of 60 Hz and $n \cong 1.9$ at 1000 Hz. The losses of the copper coil are proportional to I^2 as predicted by theory. However, considerable heating of the Cu coil was observed at larger currents as deduced from the V-I curve, 8.9 K at I=100 A.

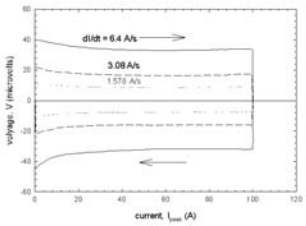

Fig.6 Coil voltage measured vs. current for triangular current waves with dI/dt = 6.4 A/s (•), 3.08 A/s (o) and 1.578 A/s (◊).

Loss measurements for the YBCO coil at frequencies from 60 to 1000 Hz are shown in Fig.6. We also show the losses of the Cu coil with a DC current and AC currents of 100 and 1000 Hz. There is little difference in losses of the Cu coil between the DC and AC 100 Hz currents. At 1000 Hz, the losses also contain a measurable eddy current contribution. The total losses of both coils increase proportional to I^n, where $n \cong 1.7$ at a frequency of 60 Hz and $n \cong 1.9$ at 1000 Hz. The losses of the copper coil are proportional to I^2 as predicted by theory. However, considerable heating of the Cu coil was observed at larger currents as deduced from the V-I curve, 8.9 K at I=100 A.

At 60 Hz, the losses in the YBCO coil are nearly 2 orders of magnitude lower than the Cu coil. With increasing frequency, the YBCO coil losses increase and approach the Cu coil losses, but are still smaller at 1000 Hz. The main components of loss in the YBCO are the hysteresis and self-field losses.

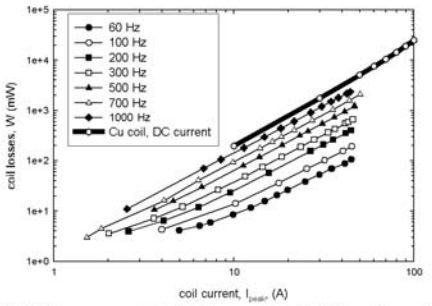

Fig.7 The measured total AC losses of the YBCO and Cu coils as a function of the coil current I_{rms} at various frequencies from 60 Hz (bottom curve) up to 1000 Hz (upper curve). The losses of Cu coil were measured with DC current.

Of particular interest are the non-sinusoidal voltages measured at higher currents, as seen in the inset in Fig.4.

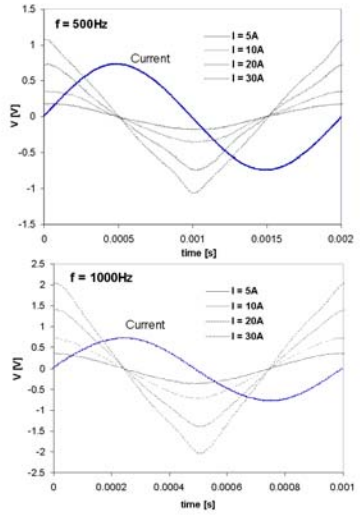

Fig. 8: Coil voltage,V, measured at 500 Hz and 1000 Hz at various currents (rms values)

The heating of the YBCO coil was monitored by a copper-constantan thermocouple installed in the winding and was negligible; at 1000 Hz and I_{peak} = 50 A, the temperature increase was below 0.2 K.

IV. Conclusions

In summary, we measured the AC losses in a small YBCO pancake coil and a similar coil using plain copper tape. Due to the magnetization currents, the YBCO coil inductance depends on the coil current. At 60 Hz, the losses of the YBCO coil were nearly two orders of magnitude lower than those in the Cu coil. With increasing frequency, this difference becomes smaller, but the YBCO coil still exhibited lower losses at 1000 Hz. The radial magnetic field component showed that the current distribution in the tape is not uniform. This indicates a need for loss calculation which is suitable for inhomogeneous fields and the need for a more ac-tolerant architecture of YBCO conductor.

References

[1] P.N. Barnes, G.L. Rhoads, J.C. Tolliver, M.D. Sumption, K.W. Schmaeman, IEEE Trans. Magn. 41, 268 (2005).
[2] K. Higashikawa, T. Nakamura, T. Hoshino, Physica C 419, 129 (2005)
[3] J. Pitel, P. Kovac, Supercond. Sci. Technol. 10, 7 (1997)
[4] J. Kvitkovic, M. Polak, Physica C 401, 146 (2004)
[5] M. W. Rupich, U. Schoop, C. Thieme, D. T. Verebelyi, W. Zhang, X. Li, T. Kodenkandath, N. Nguyen, E. Siegal, L. Civale, T. Holesinger, A. Goyal, and M. Paranthaman, IEEE Trans. Appl. Supercond. 15, 2458 (2005).
[6] U. Schoop et al, Annual DOE Peer Review, Washington DC, July 24 2004: http://www.energetics.com/supercon04.html
[7] A. O. Ijaduola, J. R. Thompson, A. Goyal, C. L. H. Thieme, K. Marken, to be published.
[8] E. H. Brandt, M. Indenbom, Phys. Rev. B 48, 12 893 (1993)
[9] N. Amemiya, T. Nishioka, Z. Jiang, K. Yasuda, Supercond. Sci. Technol. 17, 485 (2004)
[10] W. J. Carr, C. E. Oberly, IEEE Trans. Appl. Supercond. 9, 1475 (1999)
[11] C.B. Cobb, P.N. Barnes, T.J. Haugan, J. Tolliver, E. Lee, M. Sumption, E.Collings, and C.E. Oberly, Physica C, 382, 52 (2002).
[12] M. D. Sumption, E. W. Collings, P. N. Barnes, Supercond. Sci. Technol. 18, 122 (2005)
[13] O. Tsukamoto, Supercond. Sci. Technol. 18, 596 (2005)
[14] P.N. Barnes, M.D. Sumption, G.L. Rhoads, "Review of High Power Density Superconducting Generators: Present State and Prospects for Incorporating YBCO Windings," Cryogenics, accepted.

17 Appendix III

Institute of Physics Publishing
doi:10.1088/1742-6596/43/1/145

Journal of Physics: Conference Series **43** (2006) 591–594
7th European Conference on Applied Superconductivity

Coupling losses and transverse resistivity of multifilament YBCO coated superconductors

M. Polak[1], E. Usak[1,4], L. Jansak[1], E. Demencik[1], G. A. Levin[2], P. N. Barnes[2], D. Wehler[3], B. Moenter[3]

[1]Institute of Electrical Engineering, Slovak Academy of Sciences, Bratislava, Slovakia, [2]Air Force Research Laboratory, Wright-Patterson Air Force Base, USA, [3]University of Wuppertal, Germany, [4]Slovak Technical University, Faculty of Electrical Engineering and Information Technology, Bratislava, Slovakia

The corresponding author: M. Polak, elekpola@savba.sk

Abstract. We studied the magnetization losses of four different types of filamentary YBCO coated conductors. A 10 mm wide YBCO coated conductor was subdivided into 20 filaments by laser ablation. We measured the frequency dependence of the total losses in the frequency range 0.1 Hz < f < 608 Hz. The coupling loss was obtained from the total by subtracting the hysteresis loss. The latter was measured at low frequencies since only hysteresis loss is non-negligible at frequencies below 1 Hz. The transverse resistivity, ρ_{tr}, was determined from the coupling losses; it was assumed that the sample length is equal to half of the twist pitch. The values of ρ_{tr} deduced from the loss data were compared with those obtained by the four-point measurements with current flowing perpendicular to the filaments. Preliminary results indicate the existence of electrical contacts between the superconducting filaments and the substrate in some areas of the samples. This was also confirmed by the Hall probe mapping of the magnetic field in the vicinity of the tape. The measured transverse resistivity was close to the resistivity of the substrate (Hastelloy).

1. Introduction

A sufficiently ac-tolerant YBCO coated conductor can enable the fully-superconducting version for motors and generators in which both the field and armature windings are superconducting [1]. To reduce hysteresis losses in tapes several millimetres wide, subdividing of the tape into narrow parallel stripes is necessary [2,3]. The resulting conductor is a multifilamentary tape with parallel thin strips (filaments) separated by narrow gaps. The striation can be done using various technologies such as photolithography and wet etching [4] or laser micromachining [5].

The striated (filamentary) tapes become vulnerable to localized defects. This problem can be solved either by covering the filaments by a sufficiently thick normal metal layer with low resistivity metal/YBCO boundary, or by making a network of superconducting bridges, which allow the current sharing between filaments [6]. As shown by Amemyia et al. [7], in filamentary tapes prepared by laser micromachining the total losses contain also a coupling loss component due to the presence of electrically conductive path between the filaments and the metallic substrate [5].

The goal of this work is to determine the frequency dependence of losses in 3 different types of filamentary tapes with multiply connected filaments, prepared from YBCO coated conductors. We

also compare the obtained results with the loss behavior of a non-striated tape and a sample prepared on $LaAlO_3$ substrate with electrically insulated filaments.

2. Loss components in a filamentary YBCO coated conductor

In samples of filamentary YBCO coated conductors the total losses have several components, as described in [8]. For tapes with relatively wide filaments the main loss components are the hysteresis losses, W_{hyst}, and the coupling losses, W_{coupl}. The hysteresis loss per unit length, P [W/m], in a tape consisting of N_f isolated filaments, can be calculated using the formula of Brandt and Indenbom [9], if we neglect the interaction between the filaments:

$$P = 2\, f\, w_f\, I_{fc}\, B_0\, [2B_c/B_0 \ln \cosh(B_0/B_c) - \tanh(B_0/B_c)]\; N_f\,, \qquad (1)$$

where f is the frequency, w_f is the half filament width, $I_{f,c}$ is the critical current in the filament [A/m]. I_{fc} is supposed to be constant, independent on the local flux density and on the local electric field. The consequence of this assumption is the independence of the per cycle hysteresis loss on the frequency. Herrmann et al.[10] measured the frequency independent hysteresis losses in 0.1 mm wide YBCO strips. However, numerous measurements of E(I) curves in YBCO samples showed that the slope of these curves can be described by the equation $I = I_0(E/E_0)^n$, where n can have values about 30 [11]. The reduction of the filament width below ~100 μm causes the reduction of $J_{f,c}$ and n [12]. The effect of the sample length is analyzed in [13].

3. Experimental

Sample W/1 has 7 filaments 0.5 mm wide on $LaAlO_3$ substrate, the width and length of the substrate are 4.8 mm and 40 mm. The striation was made by photolithography and wet etching. The following samples were prepared from coated conductor produced by the IBAD method on approximately 100 μm thick, 10 mm wide buffered Hastelloy substrate with a YBCO layer subsequently covered by a ~3μm thick Ag layer. Laser micromachining was used to striate the samples. The samples are 100 mm long and were cut from 2 longer pieces of coated conductor. The samples B/0, B/1 and B/2 were cut from a tape with the nominal critical current before striation I_c = 160 A. The samples B/3 and B/4 were cut from a tape with I_c in the range from 120 A to 140 A. The sample B/0 is non striated and B/1 is fully striated with 20 filaments (without superconducting bridges). Samples B/2, B/3 and B/4 are also divided into 20 filaments (approximately 0.5 mm wide each) that are interconnected by superconducting bridges, as shown in Fig.1

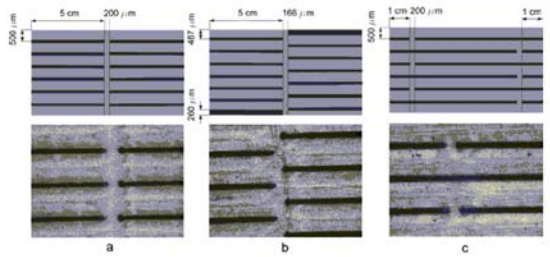

Figure 1. (a) – the sketch and microphotograph of sample B/2, (b) - sample B/3, and (c) -sample B /4.

The losses were measured in a copper dipole coil with the working space with diameter of 40 mm and the field/current constant of 0.97 mT/A at 77 K. At low frequencies (below 0.5 Hz) the losses were measured using pick-up coils and an analog integrator. Above 15 Hz we measured the time

dependence of the pick-up coil difference voltage and the losses were determined using the first harmonics obtained by Fourier analysis of the signal.

4. Results and discussion

Fig. 2 shows the measured dependence of the loss per cycle in samples W/1 and W/2. They are pure hysteresis losses. The increase of A_1 per the change of f by a factor of 10 is ~14% and ~15% for W/1 and W/2, respectively.

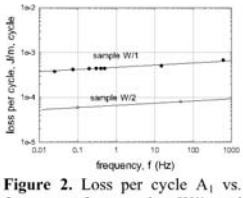

Figure 2. Loss per cycle A_1 vs. frequency for samples W/1 and W/2 at B_m = 54 mT

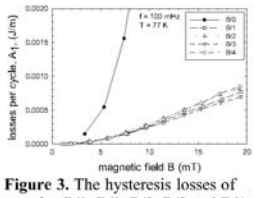

Figure 3. The hysteresis losses of samples B/0, B/1, B/2, B/3 and B/4 measured at low frequency (100 mHz) and 77 K

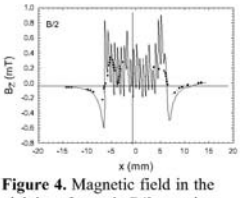

Figure 4. Magnetic field in the vicinity of sample B/2 carrying magnetization currents

In Fig.3 we plotted the loss per cycle, A_1, measured at frequency 100 mHz, when coupling loss is negligible. As expected, the largest loss is in sample B/0, the difference of losses in the filamentary samples is relatively small. The smallest hysteresis loss at 20 mT (~7.2 x10^{-4} J/m) is in sample B/3, losses in sample B/4 are larger by about 25% than those of B/3 (~9 x10^{-4} J/m).

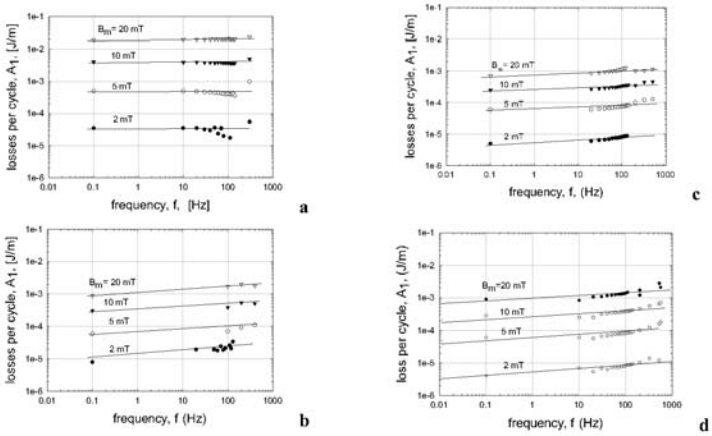

Figure 5. The dependence of losses per cycle on the frequency of the magnetic field at various field amplitudes: a- sample B/0, b – sample B/2, c- sample B/3, d – sample B/4

We mapped the magnetic field in the vicinity of all samples carrying magnetization currents. The measurements showed that the filament separation in some parts of samples B/2 and B/4 is not perfect, so that the effective sample width is a multiple of the filament width 0.5 mm (see Fig.4).

In Fig.5 a, b, c and d we show the losses per cycle of samples B/0, B/2, B/3 and B/4, as a function of the frequency changing from 0.1 Hz to 608 Hz. The largest loss increase has sample B/2 followed by B/4 and B/3. Sample B/0 showed very small increase of losses with increasing frequency (~5 % only). The hysteresis losses, A, are proportional to the critical current, I_c, which increases with increasing frequency, f, as it is controlled by the electric field E ~ f. According to the experiments with W/1 and W/2, the hysteresis losses in samples B/2, B/3 and B/4 at 500 Hz were determined by multiplying the losses determined at 0.5 Hz by the factor 3 x 12% =1.36 (the value 14 % per the decade of f measured at 54 mT was reduced due to smaller B_m = 20 mT to 12 %). The coupling losses at 500 Hz, W_{coupl}, were determined by subtracting the hysteresis losses determined at 500 Hz from the measured total losses. The transverse resistivity ρ_{tr} was calculated using the expression for the coupling losses per unit volume

$$W_{coupl} = (1/4\rho_{tr})(f\, B_m\, 2\, L)^2 \qquad (2)$$

where L is the sample length and f is frequency. The values of ρ_{tr} obtained for samples B/2, B/3 and B/4 are2.5 x 10^{-6}, 1.05 x 10^{-5}, 3.17 x10^{-6} Ωm, respectively. As seen, the values of ρ_{tr} for B/2 and B/4 are close to the resistivity of the substrate (~1.3 x 10^{-6} Ωm).

5. Conclusions

The per cycle losses measured in the filamentary YBCO samples with filaments 0.1 mm and 0.5 mm wide at frequencies from ~0.1 Hz up to ~500 Hz were not frequency independent. They increased with increasing frequency by 10 to 15 % per decade of the frequency. The total loss in our samples of filamentary YBCO coated conductors on Hastelloy substrate is affected by finite interfilamentary resistance. This translates into measurable frequency dependence of per cycle loss. Substantial coupling losses were found in all filamentary samples prepared from YBCO coated conductors.

Acknowledgements

The financial support from AFOSR, grant number FA8655-03-1-3082 is gratefully acknowledged. We also acknowledge the support of the Center of Excellence CENG, Slovak Academy of Sciences. M.P. thanks the Alexander von Humboldt Foundation for the support of the work.

References

[1] P. N. Barnes, G. L. Rhoads, J. C. Tolliver, M. D. Sumption, K. W. Schmaeman, IEEE Trans. Mag. 41, 268 (2005)
[2] W. J. Carr, C. E. Oberly, IEEE Trans. Appl. Supercond. **9,** 1475 (1999)
[3] C. B. Cobb, P. N. Barnes, T. J. Haugan, J. Tolliver, E. Lee, M. Sumption, E. Collings, and C. E. Oberly, Physica C, **382**, 52 (2002).
[4] M. Polak, L. Krempasky, S. Chromik, D. Wehler, and B. Moenter, Physica C **372-376** (2002) 1830-1834.
[5] K. E. Hix, M. C. Rendina, J. L. Blackshire, G. A. Levin, cond-mat/0406311
[6] G. A. Levin, P. N. Barnes, IEEE Trans.on Appl.Superc. 15 (2005) 2158
[7] N. Amemyia, S. Kasai, K. Yoda, Z. Jiang, G. A. Levin, P. N. Barnes, C. E. Oberly, Supercond. Sci. Technol. 17 (2004) 1464-1471
[8] Ch. E. Oberly, L. Long, G. L. Rhoads, W. J. Carr Jr., Cryogenics 41 (2001) 117-124
[9] E. H. Brandt, M. Indenbom, Phys. Rev. B 48 (1993) 12893
[10] J. Hermann, K.-H. Muller, N. Savvides, S. Gnanarajan, A. Thorley, A. Katsaros, Physica C 341-348 (2000) 2493-2494
[11] U. Scoop, M. W. Rupich, C. Thieme, D. T. Verebelyi, W. Zhang, X. Li, T. Kodenkandath, N. Nguyen, E. Siegal, L. Civale, T. Holesinger, B. Maiorov, A. Goyal, M. Paranthaman, IEEE Trans. On Appl. Supec. 15 (2005) 2611
[12] S.I. Kim, D. M. Feldmann, D. C. Larbalestier, D. T. Verebelyi, W. Zhang, C. Thieme, AFOSR HTS Coated Conductor Review, St. Petersburg, FL, January 19-21, 2004
[13] S. Takacs, F. Gomory, Inst. Phys. Conf. Ser. No. 167 2000 IOP Publishing Ltd., 611-614

18 Appendix IV

APPLIED PHYSICS LETTERS **88**, 232501 (2006)

ac losses in a $YBa_2Cu_3O_{7-x}$ coil

M. Polak, E. Demencik, L. Jansak, and P. Mozola
Institute of Electrical Engineering, 841 04 Bratislava, Slovakia

D. Aized and C. L. H. Thieme
American Superconductor Corporation, Westborough, Massachusetts 01581

G. A. Levin and P. N. Barnes[a)]
Air Force Research Laboratory, Wright-Patterson Air Force Base, Ohio 45433

(Received 2 March 2006; accepted 1 May 2006; published online 6 June 2006)

The properties of a small pancake coil made with a 10 mm wide copper-stabilized $YBa_2Cu_3O_{7-x}$ (YBCO) coated conductor were investigated. The radial component of the magnetic field was mapped at the coil edge in both the dc and ac regimes and differs significantly from that calculated assuming a uniform current distribution. The observed hysteresis indicates the strong influence of the ferromagnetic properties of the substrate. The ac losses of the coil were measured for ac frequencies between 60 and 1000 Hz. The differences in properties of the YBCO coil and a similarly prepared copper coil are discussed. © *2006 American Institute of Physics.*
[DOI: 10.1063/1.2207837]

Second generation high temperature superconductors (2G HTSs), or $YBa_2Cu_3O_{7-x}$ (YBCO) coated conductors, are now seen as the preferred candidate for high energy density HTS applications.[1] The present focus for commercialization is the scaling of the 2G HTS production to levels that allow the construction and testing of prototype coils and cables, for both dc and ac applications. Stacks of pancake or double pancake coils are a popular way of magnet construction for winding technology reasons. However, the calculation and measurement of losses and critical currents in such coils is complicated by several factors. The magnetic anisotropy of these tapes strongly affects the distribution of the current density in intricate ways.[2] The critical current of a coil wound with 2G HTS is limited by the largest magnetic field component perpendicular to the tape plane.[3] Also, the HTS tape located near the axial ends of the solenoidal configuration is exposed to an inhomogeneous magnetic field and the determination of the critical current is not straightforward.[4]

According to Brandt and Indenbom,[5] the hysteresis loss in a homogeneous YBCO tape is directly proportional to the tape width when exposed to a uniform transverse magnetic field applied perpendicular to the tape plane. Amemiya *et al.* have shown that for an arbitrary orientation of a uniform magnetic field, ac losses are proportional to the perpendicular component of the field.[6] To reduce hysteretic losses, subdividing the tape into narrow filaments is necessary.[7,8] Sumption *et al.* published experimental data on losses of unstriped and striped YBCO coated conductors in external magnetic fields with frequencies of 50–200 Hz demonstrating the effectiveness of striated 2G HTS.[9] Finally, Tsukamoto showed that the nonuniform current distribution in YBCO tapes can cause a deviation of the measured losses from calculated results.[10] As such, ac losses in windings made of YBCO coated conductor are expected to be quite high and difficult to assess.[11] This work provides initial characterization of a small pancake coil made with YBCO conductor and compares the results with those obtained on a coil made from pure copper tape with dimensions similar to the YBCO conductor.

The 2G YBCO coil was made using a 1.2 m length of copper-stabilized YBCO coated conductor. It was cowound with wet, epoxy-saturated fiberglass cloth on a G10 coil form, and had an inner and outer diameter of 25.8 and 33.8 mm after completion. The n value was ~29 and the number of turns in the winding was 13. The conductor was made using a RABiTs type Ni-5 at % W substrate with a sputtered Y_2O_3 seed layer, a yttrai-stabilized zirconia (YSZ) barrier layer, and a CeO_2 cap layer.[12] The substrate had a Curie temperature of ~60 °C and is ferromagnetic at 77 K.[13] This ferromagnetism is expected to contribute to the coil's inductance, as observed in experiments with superconducting cables.[14] The 0.8 μm YBCO layer was deposited using a Trifluoroacetate (TFA)-based solution process and subsequently capped with a 3 μm Ag layer to which a 50 μm thick Cu 110 foil was laminated. The copper coil was made using a ~110 μm thick, 1.26 m long copper tape, 10 mm wide, with a resistivity of 1.8×10^{-7} Ω cm at 77 K. The number of turns, the inner and outer coil diameter, and insulation were the same as those of the YBCO coil. The ac losses of both coils were measured by a NORMA Power Analyzer 4000D.

The dc critical current of the YBCO coil with a slowly increasing transport current was 154 A, at 0.1 μV/cm. The corresponding current density calculated for the winding cross section was $\sim5\times10^3$ A/cm^2 and for the 2G conductor cross section was $\sim7.7\times10^3$ A/cm^2. Assuming a homogeneous current distribution in the winding cross section, the calculated axial field in the coil center ($z=0$, $r=0$) is $B_z(z=0, r=0)=80.4$ mT and at the center of the inner turn of the coil is $B_z(z=0, r=20\text{ mm})=145$ mT at 154 A.

The YBCO tape used in the pancake tape coil is exposed to a strongly inhomogeneous magnetic self-field.[4] Using a small active area Hall probe we measured B_r in the radial direction at a small distance of ~0.5 mm from the coil just outside the windings ($z=5.5$ mm). The radial distribution of $B_r(z=5.5)=f(r)$ measured at room temperature and 77 K for several values of dc currents is shown in Fig. 1. For com-

a)Electronic mail: paul.barnes@wpafb.af.mil

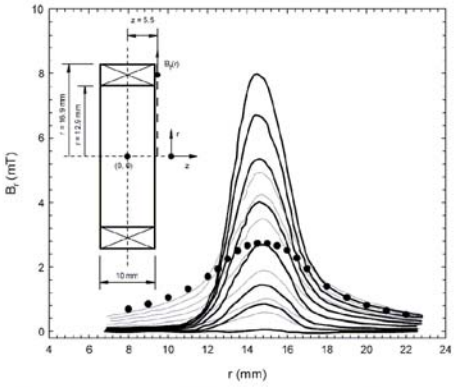

FIG. 1. The field component B_r vs the radial coordinate, r, in the distance of 0.5 mm from the coil: at 300 K (gray lines), measured at coil currents of 6, 5, 4, 3, 2, 1, 0.5, and 0 A (from the top to the bottom), at 77 K (black lines), measured at the same coil currents. (●) calculated values at 5 A assuming uniform current distribution. Inset: the winding geometry.

parison, the distribution of $B_r(z=5.5)$ calculated for a current of 5 A which assumes a uniform current density in the windings is also shown in Fig. 1. The radial component $B_r(r)$ reaches a maximum, $B_{r,\max}$, in the middle of the winding at $r=15$ mm. Experiments with larger coil currents and also with ac currents showed that the position of this maximum does not depend on the amplitude and frequency of the current. At 77 K the values for $B_{r,\max}$ are much larger than those measured at room temperature, as well as the calculated value. This is a clear indication of the nonuniform current density caused by the induced screening currents.

The variation of $B_{r,\max}$ with the triangular shaped current wave $I=0\rightarrow I_m\rightarrow 0\rightarrow -I_m\rightarrow 0$ at 77 K is shown in Fig. 2. In the inset we show $B_{r,\max}(I)$ measured at room temperature

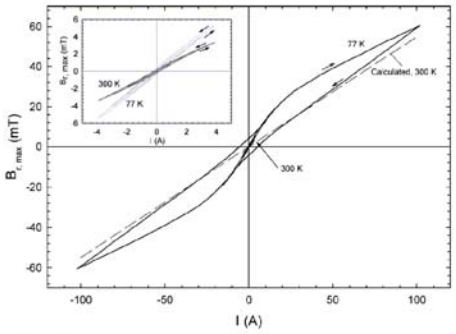

FIG. 2. The maximum of the radial field component, $B_{r,\max}$, measured at 77 K for the full dc current waves $0\rightarrow 100$ A $\rightarrow 0\rightarrow -100$ A, $\rightarrow 0$. The dashed line shows the calculated values assuming the uniform current distribution. The rate of change for dI/dt is ~5 A/s. The inset shows the shape and hysteresis of the curves $B_{r,\max}=f(I)$ measured at 300 and 77 K. Note the change of the character of the hysteresis observed at 77 K and at small currents compared with that for the large current (the curve branch down is below the curve branch up).

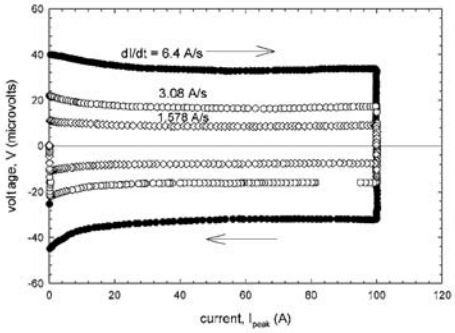

FIG. 3. Coil voltage measured vs coil current for triangular current waves with $dI/dt=6.4$ A/s (●), 3.08 A/s (○), and 1.578 A/s (◇).

and 77 K with several smaller current amplitudes (the small current amplitudes were chosen to avoid the coil heating). The curves at room temperature as well as at 77 K have a clearly visible nonlinear and hysteretic feature. The calculated $B_{r,\max}$ values are lower than the measured ones. The character of the hysteresis of $B_{r,\max}(I)$ curves at 300 K is different from that at 77 K. This indicates the influence of the ferromagnetism of Ni+4%W substrate on the magnetic field in the coil winding. According to Ijaduola *et al.*,[13] the substrate material has a Curie temperature of ~360 K and the magnetization in parallel field saturates at $H\cong 1000$ Oe, which is above the values reached with our coil.

To determine the coil inductance, L, we recorded the coil voltage, V, while applying triangular transport current waves with the amplitude of 50 A at frequencies of 50, 100, and 200 mHz (Fig. 3). With $V=LdI/dt$, the shape of the curves shows that L depends on the current at low current values, ranging from ~7 μH at $I=0$ to ~5 μH with increasing currents. At higher currents, L is current independent which independence tends to shift to higher current levels as dI/dt increases. The decrease of the inductance with increasing current indicates again an influence of the magnetic properties of the substrate material.

Loss measurements for the YBCO coil at frequencies from 60 to 1000 Hz are shown in Fig. 4. Also shown are the losses in the Cu coil with dc currents and ac currents at frequencies of 100 and 1000 Hz. There is a little difference in losses in the Cu coil between the dc and ac at 100 Hz. At 1000 Hz, the losses in the copper coil also contain a measurable eddy current contribution. The total losses of the YBCO coil increase proportional to I^n, where $n\cong 1.7$ at a frequency of 60 Hz and $n\cong 1.9$ at 1000 Hz. The losses of the copper coil are proportional to I^2 as predicted by theory. However, considerable heating of the Cu coil was observed at larger currents as deduced from the V-I curve, 8.9 K at $I=100$ A.

At 60 Hz, the losses in the YBCO coil are nearly two orders of magnitude lower than the Cu coil. With increasing frequency, the YBCO coil losses increase and approach the Cu coil losses, but are still smaller at 1000 Hz. The main components of loss in the YBCO are the hysteresis and self-field losses. Of particular interest are the nonsinusoidal voltages measured at higher currents, as seen in the inset in Fig. 4. The heating of the YBCO coil was monitored by a

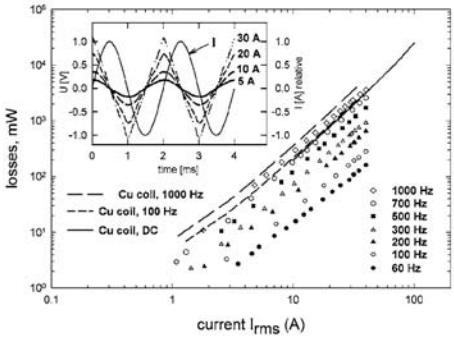

FIG. 4. The measured total ac losses of the YBCO and Cu coils as a function of the coil current I_{rms} at various frequencies from 60 Hz (bottom curve) up to 1000 Hz (upper curve). The losses of Cu coil were measured with dc current (—) and with ac current at 100 Hz (- -) and 1000 Hz (— —). The inset shows the coil voltage, V, vs time measured at various current I_{rms} at 500 Hz.

copper-Constantan thermocouple installed in the winding and was negligible; at 1000 Hz and I_{peak}=50 A, the temperature increase was below 0.2 K.

In summary, we measured the ac losses in a small YBCO pancake coil and a similar coil made of plain copper tape. We have found that the ferromagnetic substrate significantly influences the coil's magnetic field. As a consequence of the substrate and the induced magnetization currents, the YBCO coil inductance depends on the coil current. At 60 Hz, the losses of the YBCO coil were nearly two orders of magnitude lower than those in the Cu coil. With increasing frequency, this difference becomes smaller, but the YBCO coil still exhibited lower losses at 1000 Hz although indicates the need for a more ac tolerant architecture for the YBCO conductor. At a rms current of 40 A and 1000 Hz the coil showed a stable operation, the losses were ~4 W at 77 K. The measured radial component of the magnetic field showed that the transport current distribution in the windings is highly nonuniform. This indicates a need for the development of ac loss models more suitable for inhomogeneous fields.

Effort sponsored by the Air Force Office of Scientific Research under Grant No. FA8655-05-1-3062.

[1]P. N. Barnes, G. L. Rhoads, J. C. Tolliver, M. D. Sumption, and K. W. Schmaeman, IEEE Trans. Magn. **41**, 268 (2005).
[2]K. Higashikawa, T. Nakamura, and T. Hoshino, Physica C **419**, 129 (2005).
[3]J. Pitel and P. Kovac, Supercond. Sci. Technol. **10**, 7 (1997).
[4]Y. Wolfus, Y. Adanny, A. Friedman, F. Kopansky, and Y. Yeshurun, Proceedings of the EUCAS, Vienna, 11–15 September 2005, Paper No. TH-P4-20
[5]E. H. Brandt and M. Indenbom, Phys. Rev. B **48**, 12 893 (1993).
[6]N. Amemiya, T. Nishioka, Z. Jiang, and K. Yasuda, Supercond. Sci. Technol. **17**, 485 (2004).
[7]W. J. Carr and C. E. Oberly, IEEE Trans. Appl. Supercond. **9**, 1475 (1999).
[8]C. B. Cobb, P. N. Barnes, T. J. Haugan, J. Tolliver, E. Lee, M. Sumption, E. Collings, and C. E. Oberly, Physica C **382**, 52 (2002).
[9]M. D. Sumption, E. W. Collings, and P. N. Barnes, Supercond. Sci. Technol. **18**, 122 (2005).
[10]O. Tsukamoto, Supercond. Sci. Technol. **18**, 596 (2005).
[11]P. N. Barnes, M. D. Sumption, and G. L. Rhoads, Cryogenics **45**, 670 (2005).
[12]M. W. Rupich, U. Schoop, C. Thieme, D. T. Verebelyi, W. Zhang, X. Li, T. Kodenkandath, N. Nguyen, E. Siegal, L. Civale, T. Holesinger, A. Goyal, and M. Paranthaman, IEEE Trans. Appl. Supercond. **15**, 2458 (2005).
[13]A. O. Ijaduola, J. R. Thompson, A. Goyal, C. L. H. Thieme, and K. Marken, Physica C **403**, 163 (2004).
[14]R. C. Duckworth, M. J. Gouge, J. Caughman, J. W. Lue, J. A. Demko, J. Tolbert, C. L. H. Thieme, and D. T. Verebelyi, IEEE Trans. Appl. Supercond. **15**, 1578 (2005).

19 Appendix V

Characterization of Individual Filaments in a Multifilamentary YBCO Coated Conductor

M. Polak, J. Kvitkovic, P. Mozola, P. N. Barnes, G. A. Levin

Abstract— **Striation of wide YBCO coated conductor tapes is necessary to reduce the hysteresis losses. However, the processes used to striate the films may adversely affect the overall critical current of the tape not only by simple removal of superconducting material, but by introducing additional defects. We studied the transport properties of individual filaments of a filamentary YBCO tape on Hastelloy substrate striated by laser ablation. The tape consisted of 24 parallel filaments 0.5 mm wide, covered by thin Ag layer. I-V curves on 9 cm long filament sections as well as the changes of the critical current along the filament were measured at 77 K in magnetic fields up to 70 mT. 8 of 24 filaments were experimentally characterized by the mean value of the critical current and the associated n-value. The best filament had a critical current of ~ 7 A at 1 microvolt/cm and B=0.**

Index Terms—**critical current, Hall probe, multifilament YBCO coated conductor.**

I. Introduction

IN AC power applications the superconductor is exposed to time-varying magnetic field, which may induce large AC losses. Hysteresis loss is proportional to the width of the tape [1], [2]. In order to reduce this loss component, tape is striated to form narrow YBCO filaments [3].

Uniformity of the properties of individual filaments are very important for a good performance of multifilamentary YBCO tapes. A localized defect in one filament can impede the flow of the transport current through the whole length of this filament. A sufficiently thick normal metal layer covering the filament, which takes over a part of the filament current in the defect section, is one of possible solution of the problem. Another solution represents the concept of multiply connected filaments [4]. Scanning laser microscopy was used to investigate the transport properties and the current distribution in multifilamentary YBCO-coated sample with zipper area [5]. The authors have found that in the superconducting state the main dissipation in the sample occurs at the zipper area but also in neighbouring filaments near the zipper, which is a sign of lower local J_c.

Manuscript received August 23, 2006.

M. Polak, J. Kvitkovic and P. Mozola are with the Institute of Electrical Engineering, Slovak Academy of Sciences, Bratislava, Slovak Republic (e-mail: elekpola@savba.sk, elekkvit@savba.sk, elekpamo@savba.sk).

P. N. Barnes and G. A. Levin are with the Air Force Research Laboratory, WPAFB, OH 45433-7919 USA (e-mail: paul.barnes@wpafb.af.mil; george.levin@wpafb.af.mil).

The variation of the local critical current in the individual filaments can have several reasons. The first one is the non-uniformity of the original tape, from which the filamentary tape is prepared. The striation technology can cause an additional non-uniformity. The laser ablation [6] could affect the local critical current density by overheating the filament during the cutting process. Degradation due to laser ablation and the effective filament width evaluation is discussed in [7]. The results presented in this paper lead us to conclusion that there is no evidence of significant degradation of the critical current I_c in YBCO-coated conductors by laser ablation.

We studied the non-uniformity of the critical currents of filaments in a sample of filamentary YBCO tape. We measured the uniformity of the transport critical current in an YBCO coated conductor, which was used to prepare the filamentary sample. The non-uniformity of current distribution was determined from the map of the magnetic field above measured samples. Measurement of magnetic field in the filamentary sample, in which the current contacts were attached to one filament only, were used to detect the possible electrical contacts between the filaments. In the filamentary sample we measured I-V curves and determined the critical currents of various filaments supplied separately. Also the longitudinal uniformity of filament critical current was investigated. In several filaments we measured the dependence of the filament critical current and n-factor on magnetic field.

II. Experimental

A. Samples

12 mm wide non-striated YBCO-coated conductors manufactured by SuperPower Inc. [8] were used for sample preparation. In these conductors the 1.2 μm thick YBCO film was deposited on 50 μm thick buffered Hastelloy substrate and covered by 3 μm thick silver protective layer.

A control sample denoted as P6 was the virgin, nonstriated YBCO tape with dimensions of 12 mm x 100 mm. The striated sample, P5, was made from the same piece of tape as P6 and had the same linear dimensions. It consisted of 24 filaments 0.48 mm wide, one stripe at the edge is about 1.5 times wider than the rest. The striation of sample P5 was done using the laser ablation technique as described in [6]. The grooves segregating the superconducting filaments are about 30 μm wide. The critical current before striation was ~ 160 A.

B. Experiments

The properties of the virgin tape were investigated by measuring the magnetic field of the sample P6 produced by magnetization currents. They were induced by cycling the external field B_e from 0 to ~ 0.2T and back to zero. The sample magnetic field component B_z, perpendicular to tape plane, was measured by a micro Hall probe with the active area of 20 μm x 20 μm. We measured the profiles $B_z = f(x)$ at various positions of y along the whole sample length at external magnetic field $B_e = 0$, Fig.1.

The following properties of the filamentary sample P5 were investigated: possible electrical connections between the filaments, the I-V curves of the individual filaments and the effect of the external magnetic field on the filament critical currents.

For the measurement of I-V curves of individual filaments it is very important to know whether there are electrical contacts between the measured filament and neighbouring ones or contacts of filaments with the substrate. To answer this question we supplied only one filament (in the center) with a small current at 300K and measured the magnetic field profile across the width of the tape. Similar measurements were performed at 77 K with higher current. If the current flows in the supplied filament only the width of the field profile corresponds to the filament width. If the filaments are interconnected or there is an electrical contact to the substrate the profile width corresponds to the whole tape width.

To measure I-V curves of individual filaments we soldered the current contacts to the chosen filament using In-solder and attached 4 potential taps distanced by 30 mm, see Fig.2.

We measured the voltages between potential taps 1 and 2, 2 and 3 and 3and 4 of the contacted filament as a function of filament current. After the measurement of this filament the current contacts and the potential taps were removed and attached to another filament and the same measurements were repeated. From these measurements we determined the mean value of the filament critical current in 3 sections, each 30 mm wide. We also measured I-V curves at various external fields in one chosen section of each filament.

The described measurements of individual filaments using transport current and 4 potential taps reveal only the differences of the mean values of filament critical current I_{fc} in 30 mm long sections. To study the change of local I_{fc} variation along the filaments we used measurement of magnetic field due to magnetization currents. We measured the field profiles $B_z = f(x)$ at various y position with 1 mm step. Sample P5 was measured in a similar way as sample P6. The measurements at various positions along the sample (y-direction) allow us to get information on the uniformity of the critical current. The variation of maxima of $B_z = f(x)$ curves corresponding to individual filaments is proportional to the variation of magnetization current in y-direction.

The I-V curves were also measured in various external magnetic fields up to 70 mT at 77 K. From these curves we determined $I_c(B)$ and n(B) characteristics. The slope of I-V curves characterized by n-factor reflects also the homogeneity of J_c in the filament. We also determined "n" from the measured I-V curves for various filaments.

III. Results and discussion

The magnetic field in the vicinity of the nonstriated sample P6 carrying persistent magnetization currents at 77 K measured by a probe located at a distance z_o=0.8 mm, is shown in Fig.3. From the shape of magnetic field map it is seen that the left side of the tape (x=-1.7 up to –4 mm) has a deformed triangle profile and has also lower I_c than that the right side along the whole measured length (y=+-40 mm). From this measurement we can deduce that the tape, was inhomogeneous before the striation and can affect the filament homogeneity accordingly. The $B_z(x)$ maxima varied by ± 9 % from the mean value. Similar variation of the critical current in the tape is expected.

The magnetic field profile was measured above the striated sample P5 at 300K with only one filament (No.12) connected to the current source. We found that the profile width was much larger than the tape width, which is a sign that the current from 12th filament is distributed by metallic connections throughout the whole width of the sample.

In the next step we cooled the sample P5 to 77 K and measured the magnetic field profile at the same position. The results are in Fig.4. At 77 K the width of the profile corresponds to the filament width, it means that the current is flowing in the 12th filament only. The grooves are not superconducting at 77 K.

The measured I-V curves of 8 filaments from sample P5, on taps 1-4, Δl = 9 cm, into which the current was fed separately, at the external field B_e = 50 mT are shown in Fig.5. The shapes of I-V curves of filaments, 15, 19 and 21 are very similar and these filaments have similar value of I_{fc} = 4.1 A. In the rest of filaments we see that the I_{fc} of the filaments are quite different. The maximum and minimum of I_{fc} is ~ 2.4 A and 6 A, respectively. These figures clearly demonstrate that each filament has different I_{fc}. For precise evaluation of tape I_c it is necessary to measure all filaments separately.

From the I-V curves at 39.2 mT measured between the taps 1-2, 2-3 and 3-4 we determined the mean value of I_{fc} (1 μV/cm) between these taps and displayed these results in Fig.6. As seen the I_{fc} values vary from 2.55 A (filament 8) up to 5.76 A (filament 19). The smallest steps has 21st filament and we could say that it is most homogeneous filament in this sample on 9 cm length.

The maxima of the magnetic field profiles $B_z(x)$ measured at the distance of z_o = 0.45 mm above filaments of sample P5 in various longitudinal positions y are shown in Fig.7. It is seen that the maxima of $B_z(x)$ vary along the y axis, i.e. the filaments are inhomogeneous also in the longitudinal direction (y). Filaments 8-11 are inhomogeneous, mainly at y = 6 mm (filaments 8 and 9) and at y = 4 mm (filament 10) where the defects are present.

In Fig.8. we present normalized $I_c(B)$ curves for various filaments of sample P5 at 77 K in magnetic field interval 0 – 70 mT. It is seen that all curves have the same shape. In the magnetic field interval (30 -70 mT) they have the same slope 0.004 mT^{-1}. Critical current of filament was reduced to < 50 % of $I_{fc}(0)$ at magnetic field > 70 mT.

The dependence of n-factor for various filaments of sample P5 on magnetic field at 77 K is presented in Fig.9. It changes

in zero magnetic field from 18 to 31. These values also indicate that the J_{fc} in individual filaments is quite non-uniform.

IV. CONCLUSIONS

Both transport and magnetic measurements of individual filaments of the striated sample show that the filament critical current, I_{fc} and n-factor differ significantly from filament to filament. We also detected the variations of local critical current along their lenght. On the basis of our experiments we conclude that both inhomogeneity of the critical current of the virgin YBCO tape and the striation procedure cause the nonuniformities of the critical current of individual filaments. At this moment we cannot evaluate, which of these factors have larger impact on the filament critical current. We have also found that the electrical contacts between the filaments and between filaments and substrate have a resistive character and are not superconducting at 77 K.

ACKNOWLEDGMENT

This work was supported by the AFOSR, grant number FA8655-05-1-3062. The authors acknowledge the support of the Center of Excellence CENG, Slovak Academy of Sciences.

REFERENCES

[1] M. Polák , L. Krempaský, Š. Chromik, D. Wehler, and B. Moenter, "Magnetic field in the vicinity of YBCO thin film strip and strip with filamentary structure," *Physica C* , vol. 372-376, pp. 1830-1834, 2002.

[2] M. Majoroš, R. I. Tomov, B.A. Glowacki, A.M. Campbell, C.E. Oberly, "Hysteretic losses in YBCO coated conductors on textured metallic substrates," *IEEE Trans. Applied Supercond.*,,vol. 13, pp.3626-3629, 2003.

[3] W.J. Carr and C.E. Oberly, "Filamentary YBCO Conductors For AC Applications," *IEEE Transactions on applied superconductivity*, vol. 9, No. 2, pp. 1475-1478, June 1999.

[4] G.A. Levin and P.N. Barnes, "Concept of multiply connected Superconducting tapes," *IEEE Transactions on applied Superconductivity*, Volume 15, Issue 2, pp.2158 – 2161, June 2005.

[5] L. B. Wang, P. Selby, C. Khanal, G. Levin, T.J. Haugan, P. N. Barnes and C. Kwon, "The distribution of transport current in YBCO coated conductor with zipper striation," *IEEE Trans. on Appll. Superc.* Vol 15, No2, pp. 2950, June 2005.

[6] K.E. Hix, M. C. Rendina, J. L. Blackshire and G. A. Levin, "Laser Micromachining of Coated YBa2Cu3O6+x Superconducting Thin Films," to be published.

[7] C. B. Cobb, P. N. Barnes, T. J. Haugan, J. Tolliver, E. Lee, M. Sumption, E. Collings and Ch. E. Oberly, "Hysteretic loss reduction in striated YBCO," *Physica C*, Volume 382, Issue 1, pp. 52-56, October 2002.

[8] Y.-Y. Xie et al. *Physica C*, "Progress in scale-up of second-generation high-temperature superconductors at SuperPower Inc," 426-431, 849-857 (2005).

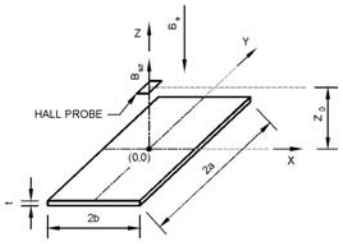

Fig. 1. Measurement arrangement in the coordinate system, z_e-sample to probe distance, 2a-length of the sample, 2b-width of the sample, t-sample thickness, B_e-external magnetic field, B_{ez}- perpendicular component of measured magnetic field.

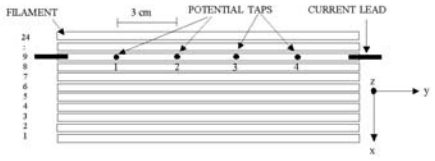

Fig. 2. Position of current leads and potential taps on YBCO filamentary tape.

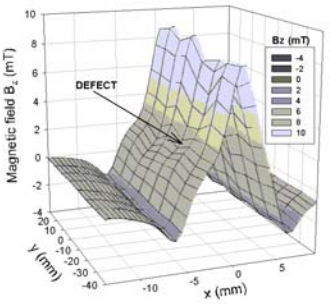

Fig. 3. Magnetic field map above sample P6, z_e = 0.8 mm.

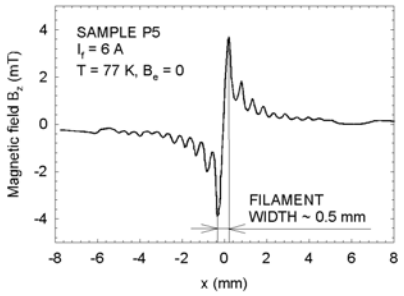

Fig. 4. Magnetic field profile of the tape P5. One filament was supplied by DC transport current 6A at 77 K, z_e = 0.33 mm.

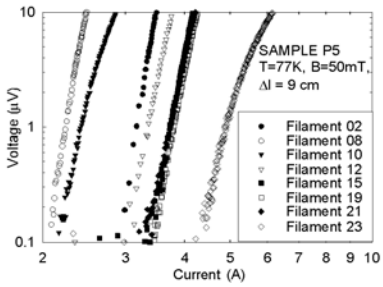

Fig. 5. Current-voltage characteristics of individual filaments of sample P5 measured on potential taps 1-4, at B = 50 mT.

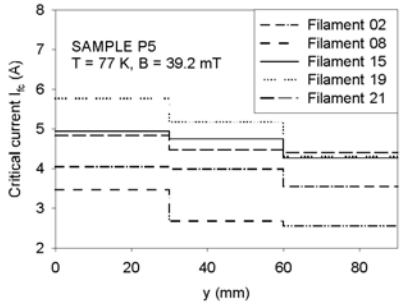

Fig. 6. Longitudinal homogeneity of filaments on 3 cm sections evaluated from transport current measurements.

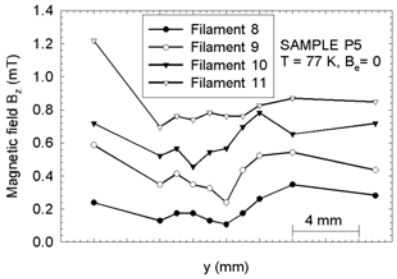

Fig. 7. Longitudinal homogeneity of filaments evaluated from magnetic measurements, z_e = 0.45 mm.

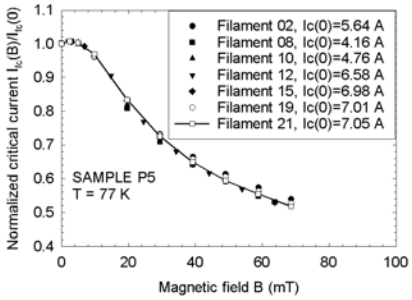

Fig. 8. Normalized critical current dependence on magnetic field for various filaments.

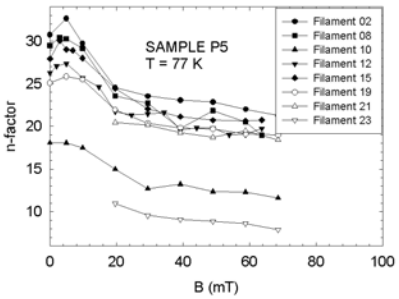

Fig. 9. n-factor as a function of magnetic field for various filaments.

20 Appendix VI

INSTITUTE OF PHYSICS PUBLISHING SUPERCONDUCTOR SCIENCE AND TECHNOLOGY
Supercond. Sci. Technol. **19** (2006) 817–820 doi:10.1088/0953-2048/19/8/022

YBCO/Ag boundary resistivity in YBCO tapes with metallic substrates

M Polak[1], P N Barnes[2] and G A Levin[2]

[1] Institute of Electrical Engineering, Slovak Academy of Sciences, Dubravska 9, 84104 Bratislava, Slovak Republic
[2] Air Force Research Laboratory, Wright-Patterson Air Force Base, OH 45433, USA

E-mail: elekpola@savba.sk

Received 25 April 2006, in final form 30 May 2006
Published 3 July 2006
Online at stacks.iop.org/SUST/19/817

Abstract

The quality of the contact between a YBCO layer and the protective silver coating is an important parameter affecting the current transfer between YBCO and the normal metal. We studied experimentally the quality of this contact in 6 mm wide YBCO-coated conductor with a critical current of ~60 A at 77 K. The measured current transfer length for the original sample of a YBCO-coated conductor covered by ~3 μm thick silver and for the same sample additionally laminated by a 25 μm thin copper layer was 0.19 and 0.47 mm, respectively. The contact resistivity determined from these experiments was between 3.7×10^{-11} and 7.0×10^{-12} Ω m^2. A direct measurement of the resistance between two overlapped tapes soldered by indium yielded values between 2.5×10^{-12} and 5×10^{-12} Ω m^2. The boundary resistance and current transfer length are important parameters for the design of the optimal tape architecture for coils and windings, especially for stability issues.

(Some figures in this article are in colour only in the electronic version)

1. Introduction

In the $YBa_2Cu_3O_{7-x}$ (YBCO)-coated conductor architecture, the YBCO layer is often covered by a thin Ag or Au protecting layer. Adjacent to this Ag protection layer is a metallic stabilizing layer, typically Cu with thickness of 25–100 μm, which is either soldered on (copper foil) or electroplated on [1, 2]. The intent of the stabilizing layer is to temporarily carry a substantial part of the total current in the coated conductor sections with hot spots, thus improving the electrical stability of the tape. The thickness of stabilizer to be added should be sufficient to allow for proper protection. The addition of excess stabilizer is undesirable since it will decrease the engineering current density of the overall conductor. Further, more Cu will lower the voltage produced in a quench, and it makes detection more difficult or slower [3]. Another advantage of the Ag protective layer and Cu stabilizer is that it facilitates electrical connection to the YBCO conductor, since the current leads can simply be soldered to the copper surface over a sufficient length.

With good conductivity and an appropriate thickness for the metallic layer, the contact resistance of the YBCO/silver boundary layer becomes very important for the tape stability. For comparison, in Bi-2223/Ag monocore tapes the boundary contact resistivity between the superconducting core and the surrounding silver at 77 K is about 10^{-12} Ω m^2 and the current transfer length is $\lambda < 0.3$ mm [4]. In YBCO-coated conductors covered by a 0.3–0.5 μm Au layer, the resistivity of the YBCO/Au interface was about 10^{-9}–10^{-10} Ω m^2 [5]. In this case the Au was deposited by thermal evaporation onto the YBCO. It has been reported that YBCO ceramic low resistivity contacts of 10^{-11} Ω m^2 were prepared by soldering on a copper layer prepared by an electrochemical route [6].

In this work, we determined the boundary resistivity, R_b, in samples from YBCO tape covered by a thin Ag protection layer using two different measurements. The first one is the measurement of the current transfer length, λ. We measured the decrease of the current flowing in the Ag layer with increasing distance from a short current contact with the sample as received, sample A. In this sample, λ was approximately the same length as that of the current contact. An additional Cu metallic layer was soldered to the Ag layer to increase λ, sample B. The second measurement method was based on the measurement of the voltage drop across a soldered

0953-2048/06/080817+04$30.00

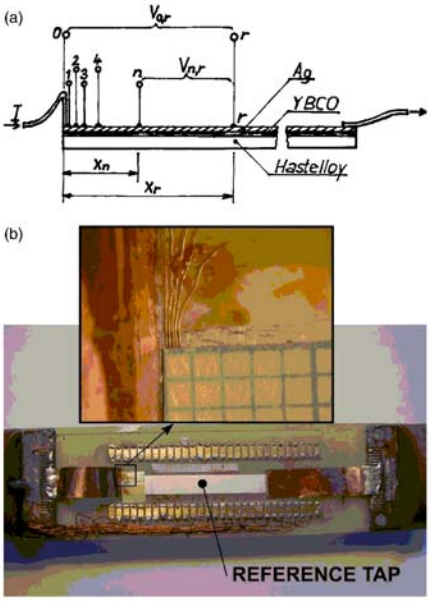

Figure 1. (a) A sketch of sample 1 with the current contacts and the potential taps. (b) A photograph of sample 1 with the position of the reference tap, r. The detail shows the positions of the potential taps close to the current contact.

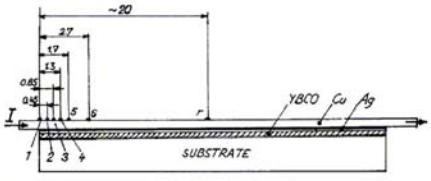

Figure 2. A sketch of sample 2 with the positions of the potential taps.

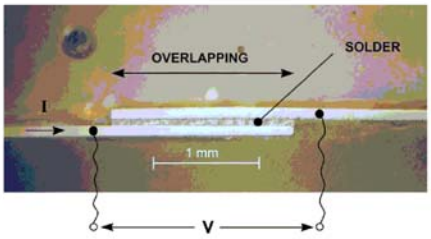

Figure 3. A microphotograph of sample 3 with the overlapped tapes and the position of the potential taps.

joint of two overlapped tapes with the assumption that each tape has a constant potential over the joined area.

2. Methods of measurement

The samples were prepared from 6 mm wide YBCO tape covered by a ~3 μm thick Ag layer. The substrate was ~90 μm Hastelloy with the YBCO layer slightly less than 1.5 μm. Two different methods were used to determine the contact resistivity of the boundary YBCO/Ag layer, R_b. The first method was based on the measurement on the current transfer length as previously used in experiments with BSCCO tapes [4]. For this technique, a current lead is soldered to one end of the sample over a small length (sample 1). The current lead was a copper foil that was 0.05 mm thick and 6 mm wide, as shown in the sketch in figure 1(a). The length of the soldered tape section is less than 0.15 mm. Several potential taps (labelled as $1, 2, 3, \ldots, n$) were attached to the silver-coated surface of the sample at increasing intervals from the end. A reference tap (labelled as r) is attached far from the sample ends, roughly in the middle of the sample, where all current flows in YBCO. A photograph of sample 1 is shown in figure 1(b). The inset in figure 1(b) displays the potential taps for sample 1 with a 1 mm grid overlay. I–V curves were obtained between the taps 1 and r, 2 and r, etc, at 77 K, as described in detail in [4]. The current transfer voltages between potential tap n and r ($V_{n,r}$) was plotted versus the distance (x) at a constant current to obtain information on the current flowing in the upper metallic layer.

For the sample of the as-received tape with a silver protective layer only (sample 1), the potential taps had a spacing of 0.15 mm. To increase the current transfer length, a second sample (sample 2) was prepared by adding a copper stabilizing layer to a sample very similar to sample 1. Using pure indium with an electrical resistivity at 77 K of 1.4×10^{-8} Ω m, a 25 μm thick copper foil was soldered to the face of the tape on the Ag side of the YBCO-coated conductor. The spacing of the potential taps for sample 2 are given in figure 2. An additional potential tap and different spacing is used on sample 2 since the thicker metallic layer will result in a longer current transfer length.

The second method used to determine the transverse resistivity directly is quite simple. Two tapes are overlapped over a distance l_0 and soldered together using pure indium. The cross-section of one of the joints prepared in this fashion is shown in figure 3. Samples 3, 4, 5, and 6 for these joints have the length of their overlapped ends 1, 2, 3, and 5 mm, respectively.

3. Results and discussion

I–V curves were measured between taps with various distances from the end of the current contact and the reference tap r for sample 1 and 2 as shown in figures 4 and 5, respectively. The dependence of the current transfer voltages $V_{n,r}$ versus the distance x for sample 1 at $I = 1$ A and for sample 2 at $I = 10$ A is shown in figure 6.

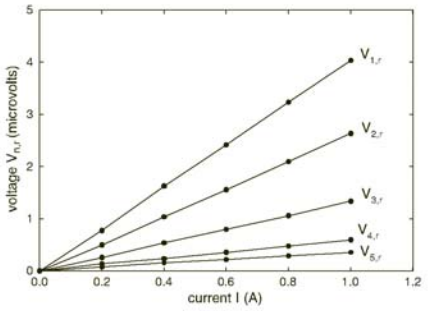

Figure 4. The current transfer voltage measured between tap n and the reference tap r, $V_{n,r}$, versus current I for sample 1 at 77 K.

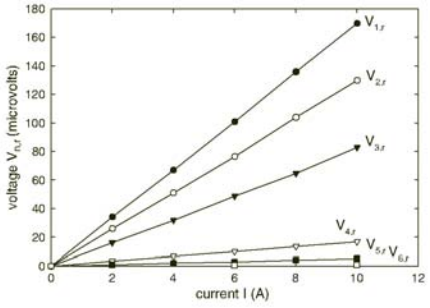

Figure 5. The current transfer voltage measured between tap n and the reference tap r, $V_{n,r}$, versus current I for sample 2 at 77 K.

The current transfer length λ, characterizing the drop of the current flowing in the normal metal layer (Ag), is defined by

$$I_{\mathrm{Ag}}(x) = I_0 \exp(-x/\lambda) \tag{1}$$

where $I_{\mathrm{Ag}}(x)$ is the current flowing in the normal metal (silver) layer at the distance x from the sample end (see figure 1(a)) and I_0 is the total sample current.

As shown in [4],

$$I_{\mathrm{Ag}}(x)/I_0 = V_{x,r}/V_{0,r} = \exp^{-x/\lambda} \tag{2}$$

and λ can be determined using the measured values $V_{x,r}$ and $V_{0,r}$ as

$$\lambda = x/\ln(V_{0,r}/V_{0,x}). \tag{3}$$

By applying linear regression to the $\ln V_{n,r}(x)$ data of figure 6 and using equation (3) we determined $\lambda \sim 0.19$ mm for sample 1 (Ag only overlayer) and $\lambda \sim 0.47$ mm for sample 2 (with added Cu). The coefficients of variation of the parameters characterizing the straight lines $\ln V_{\mathrm{nr}} = f(x)$ for samples 1 and 2 are from 11% to 25%, approximately. Thus, in spite of the experimental errors (in particular errors in the determination of the distances x) it is possible to extract λ quite precisely. We note that the measured $V_{n,r}$ versus x curves

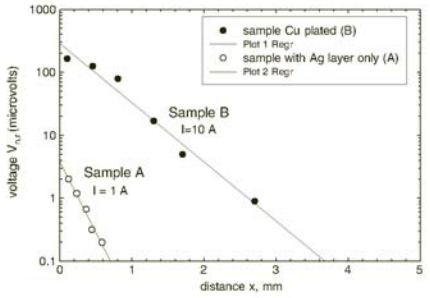

Figure 6. The current transfer voltage versus the distance of the measuring potential tap from the tape end for sample 1 (at 1 A) and for sample 2 (at 10 A). The straight lines are fits using linear regression.

could be affected by the sample preparation. The quality of the YBCO/Ag contact at the sample end could be lowered by the cutting procedure, which results in a longer current transfer length and, consequently, in a higher value of the boundary resistivity. This is probably valid for sample 1. Sample 2 has a longer current transfer length and the effect of the cutting is smaller.

Using the values of the current transfer length λ determined experimentally we can calculate the contact resistance of the boundary between the YBCO and Ag metal. This contact resistance per unit length of the sample (1 m) for the given width can be determined from the relation [4]

$$R_{\mathrm{b1}} = \lambda^2 R_{\mathrm{nm},1}(77\ \mathrm{K}) \tag{4}$$

where $R_{\mathrm{nm},1}(77\ \mathrm{K})$ is the resistance of the normal metal covering the sample per unit sample length (1 m). This parameter was determined experimentally for the Ag overlayer from the measurements of the sample resistance at room temperature and at a temperature slightly above T_c. We obtained for $R_{\mathrm{nm},1}(77\ \mathrm{K})$ the value of 0.17 Ω m^{-1} for sample 1 and 5.3×10^{-3} Ω m^{-1} for sample 2. Using equation (4), we obtain $R_{\mathrm{b1}} = 6.14 \times 10^{-9}$ Ω m^2 for sample 1 and 1.17×10^{-9} Ω m^2 for sample 2.

The contact resistivity of the YBCO/Ag boundary is given by [4]

$$R_{\mathrm{b}} = A_{b,1} R_{b,1} \tag{5}$$

where $A_{b,1}$ is the area of the boundary per unit sample length (1 m). Inserting for $A_{b,1}$ the value 6×10^{-3} m, we obtain for $R_{\mathrm{b}} = 3.7 \times 10^{-11}$ Ω m^2 and 7.02×10^{-12} Ω m^2 for samples 1 and 2, respectively. Both values are smaller than the values given in [2], which is likely the result of improvement in the lamination process of applying metallic layers to the YBCO, which is expected as technology improves over time.

The measurements of the resistance R_j of the overlapped joints with the different overlapping lengths were carried out on samples 3, 4, 5, and 6. The contact resistivity of the boundary YBCO/Ag was calculated as (neglecting the effect of the indium solder)

$$R_{\mathrm{b}} = R_j w L_j \tag{6}$$

where L_j is the length of the overlapping region of the adjoined

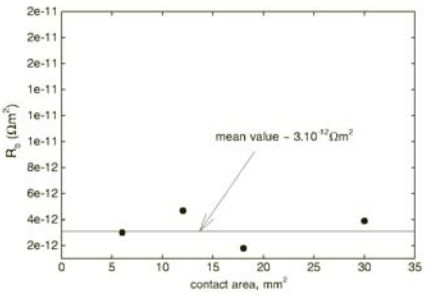

Figure 7. The values of the contact resistivity of the YBCO/Ag boundary measured with samples 3, 4, 5, and 6, plotted versus the contact area.

tapes. The results are shown in figure 7. The mean value of R_b is $\sim 3 \times 10^{-12}$ Ω m^2.

The largest and the smallest values of the boundary resistivity obtained from our experiments are 3.7×10^{-11} Ω m^2 and 2×10^{-12} Ω m^2, respectively. As shown, R_b decreased by a factor of $\sim$5 for sample 2 in comparison with sample 1. As shown by Dreuth and Dederichs [7], after annealing of already finished Ag contacts with contact resistivity of $\sim 10^{-10}$ Ω m^2 in flowing oxygen at a temperature of 250 °C, the contact resistivity dropped by two orders of magnitude. In our sample the copper foil was soldered to YBCO/Ag at a temperature of $\sim$220 °C, which might be high enough to cause a certain degree of diffusion between Ag and the YBCO layer and to improve the electrical contacts between them.

An interesting consequence of the values obtained for λ is related to the interfilament connections (bridges) in multifilament coated conductors [8, 9]. A bridge includes the superconducting film and the stabilizer on top of it. The size of the bridges is substantially smaller than λ. Therefore there will be practically no current exchange between the superconductor and stabilizer along the bridge. This has to be taken into account in future work on the optimization of multifilament, multiply connected conductors for power applications.

4. Conclusions

The contact resistivity between the protecting Ag layer and the YBCO layer in a sample of YBCO-coated conductor was determined from the measurement of the current transfer length to be $R_b = 3.7 \times 10^{-11}$ Ω m^2. An alternate determination of R_b, likely more precise, using the same sample laminated by an additional layer of copper yielded a value of $R_b = 7.02 \times 10^{-12}$ Ω m^2. Very similar values of $R_b = 3 \times 10^{-12}$ Ω m^2 were obtained from the direct measurement of the resistance of the joint of two overlapped tapes. Knowledge regarding the boundary resistivity and the current transfer length is important in order to design the optimal tape architecture for coil windings and magnets which can experience quenches [10]. This information is especially relevant to conductor stability issues.

Acknowledgments

This work was supported by AFOSR, grant FA8655-05-1-3062. The authors thank J Talapa for the careful preparation of samples.

References

[1] Xie Y Y *et al* 2005 *Physica* C **426–431** 849
[2] Schoop U *et al* 2005 *Proc. Electrochem. Soc.* **PV 2003-29** 254
[3] Barnes P N, Sumption M D and Rhoads G L 2005 *Cryogenics* **45** 670
[4] Polak M, Parrell W J, Cai X Y, Polyanskii A, Hellstrom E E, Larbalestier D C and Majoros M 1997 *Supercond. Sci. Technol.* **10** 769
[5] Usoskin A, Issaev A, Freyhardt H C, Leghissa M, Oomen M P and Neumueller H-W 2002 *Physica* C **372–376** 857
[6] Ueltzen M, Martinek I, Syrowatka F, Floegel-Delor U and Riedel T 2002 *Physica* C **372–376** 1653
[7] Dreuth H and Dederichs H 1993 *Supercond. Sci. Technol.* **6** 464
[8] Levin G A, Barnes P N, Amemiya N, Kasai S, Yoda K, Jiang Z and Polyanskii A 2005 *J. Appl. Phys.* **98** 113909
[9] Majoros M, Glowacki B A, Campbell A M, Levin G A, Barnes P N and Polak M 2005 *IEEE Trans. Appl. Supercond.* **15** 2819
[10] Fu Y, Tsukamoto O and Furuse M 2003 *IEEE Trans. Appl. Supercond.* **13** 1780